ADDIS ABABA UNIVERSITY

School of Graduate Studies

VOLCANOLOGY, PETROLOGY AND GEOCHEMISTRY OF THE GEDEMSA VOLCANO (Nazreth area)

A THESIS

Presented to
The School of Graduate Studies
Addis Ababa University

In partial fulfillment
of the Requirements for the Degree
Master of Science in Geology

by

DEREJE AYALEW

January, 1994

ADDIS ABABA UNIVERSITY

SCHOOL OF GRADUATE STUDIES

A STUDY ON ERROR SIZES AND REQUIRED SAMPLE SIZE IN SEQUENTIAL PROBABILITY RATIO TEST

By

Gemechis Dilba
Statistics Department
Addis Ababa University

Approved by the Examining Board

Prof. Asmerom Kidane
Chairman, Department
Graduate Committee

Dr. Abebe Tessera
Advisor

Dr. Desta Hamito
Examiner

Dr. Eshetu Woncheko
Examiner

Addis Ababa University

School of Graduate Studies

VOLCANOLOGY, PETROLOGY AND GEOCHEMISTRY OF GEDEMSA VOLCANO

by

DEREJE AYALEW

Approved by:

Dr. Tilahun Mammo
Chairman

Dr. Gezahegn Yirgu
Advisor

Prof. Angelo Peccerillo
Examiner

Dr. Bekele Megersa
Examiner

Dr. Endale Ketefo
Examiner

This thesis has been submitted with my approval as University Advidor

Name: Gezahegn Yirgu

Signature: _____

Place of submission: Addis Ababa

Date: January 1994

ABSTRACT

The Gedemsa volcano lies on the floor of the northern sector of the Main Ethiopian Rift. It is characterized by a polygenic caldera resulting from large pyroclastic eruptions. K/Ar dating performed by previous studies indicates an age of 0.8 to 0.1 Ma for the exposed volcanic products.

Volcanologic and stratigraphic studies allowed recognition of several phases of activity during the evolution of Gedemsa. The lowest exposed products are represented by acidic lavas, which are covered by thick plinian fall pumice deposits. This are followed by an ignimbrite deposit and by intra-caldera lava flows and interbedded pyroclastic products. The caldera, is clearly a composite structure resulting from several collapses which occurred after plinian and ignimbritic eruptions. A separate stage of volcanic activity connected to the Wonji Fault System (basaltic volcanism) formed surge deposits and numerous basaltic cinder cones and lavas, both within and outside the caldera depression.

The volcanic products from Gedemsa volcano are petrologically and geochemically diverse. Alkaline and peralkaline silicic lavas and pyroclastics (trachytes and rhyolites) are by far the most abundant products. The mafic rocks are only represented by the mafic inclusions occurring within some of the post-caldera products. The younger rift-related activity is, instead, represented by Na-transitional basalt. On the whole, the rocks occurring in the area have a very marked bimodal distribution, a situation which is typical of almost all the young volcanism of the Ethiopian Rift Valley.

Major and trace element variations of peralkaline silicic volcanic rocks from Gedemsa volcano support an origin by crystal/liquid fractionation starting from mafic parental liquids, with separation of olivine, plagioclase, clinopyroxene and opaques during the early to intermediate stages and of alkalifeldspar and a few mafic phases (alkali amphiboles and pyroxenes) during the late stages of evolution. These processes generated strong enrichments in incompatible trace elements and depletion in compatible elements in the acidic magmas. Consequently, rhyolites display extremely high values of Zr, Y, Rb and F and low to very low abundances of ferromagnesian trace elements, Sr and Ba. Some rhyolites, however, have low Na and fluorine, most probably due to interaction with groundwaters. Such a process may represent an explanattion of the high F contents in the groundwaters of the Wonji area and of other zones inside the rift. Although, crystal fractionation best fits the geochemical variations, field and petrographic observations indicate that mixing processes were also active during the magma evolution.

A model is presented for the evolution of the internal structure of the Gedemsa volcano, based on volcanological, stratigraphic and geochemical evidence. According to this model, extensive fractional crystallization of parent mantle-derived basaltic magmas occurred in a huge shallow level magma chamber. This process, possibly accompanied by some mixing and assimilation of wall rocks, generated a zoned magma chamber whose upper part was occupied by silicic magmas. The presence of this silicic magma effectively acted as a density barrier to the mafic magma ponding on the bottom of the reservoir. This explains why the Gedemsa eruptions were invariably characterized by emission of acid material. Huge plinian and ignimbritic eruptions generated the caldera collapse. This resulted in strong decrease in the size of the magma chamber. The post caldera eruptions tapped a smaller, still zoned reservoir. However, due to the small volumes of acidic magma standing in the upper part of the chamber, in some cases also mafic magma was brought to the surface intermingled with the acid material. The final basaltic eruptions are not related to the Gedemsa volcanic activity but represent liquids arising along regional faults which cut the rift floor, and the Gedemsa volcano itself.

Contents

Figures

Tables

Plates

ACKNOWLEDGEMENTS

The present thesis benefited from the help of a number of people to whom I express my deepest gratitude. Prof. Mauro Rosi introduced me to volcanological studies and led me in the field during several trips helping in recognition of various deposits, description of stratigraphic sections, collection of samples and all the other activities which are traditionally carried out in the field. Prof. Dario Visonà kindly provided F and Cl analyses of selected samples. Prof. Alberto Marini helped with interpretation of satellite images which allowed to recognize structural features which were invisible in the field. Dr. Gezahegn Yirgu gave precious help during various phases of the field and interpretation work. Dr. Abebaw Endeshaw of the Geothermal Exploration Project of the Ethiopian Ministry of Mines kindly provided access to boreholes stratigraphy and made available some core samples. Prof. Angelo Peccerillo provided major and trace element analyses on rock samples and assisted during field work, data discussion and editing. My colleagues and friends Warash Getaneh, Tamiru Alemayehu, Berhanu Temesgen and Tasfaye Kydane were of much assistance and encouragement. The kind assistance of Prof. Anatoli Sliouniaev during field work and printing of the thesis is gratefully acknowledged. The Italian Technical Cooperation, the DAAD and SAREC are gratefully acknowledged for allowing use of cars and other facilities and for providing financial support.

1. INTRODUCTION

The Gedemsa volcano is located in the central sector of the Ethiopian Rift Valley about 25km southwest of Nazret town considerably close to the eastern Rift margin (fig. 1). The study area lies within 39°6'E and 39°14'E longitude and 8°17'N and 8°28'N latitude. The area is bounded to the north by the Awash river, to the west by the Koka lake and to the east by Wonji sugar plantation.

The area is characterized by the presence of large volcanic depression (caldera) about 8km in diameter and with the rims reaching a maximum altitude of 1950m. The central part of the caldera is occupied by an irregular chain of hills, locally named Ittisa, which result from the coalescence of several volcanic edifices. One of these volcanoes, sited at the eastern edge of the chain, contains an explosion crater (Kore crater) with a diameter of about 1km and a depth of about 100m.

Gedemsa volcano is accessible by vehicle through two dry-weather roads. One of this road starts from the Wonji sugar factory and rises to the northeast rim of the caldera (the northeast road), while the other runs from Wonji town to the western side of the caldera.

The climate of the study area is designated as warm temperate, with a mean annual rainfall of 800mm and a mean annual temperature of 20.9°c (National Meteorological Service Agency, 1970). The vegetation is sparse and mostly of thickets and wood plants, and scattered small shrubs and low acacia trees in a ground cover of annual and perennial grasses and herbs (National Meteorological Service Agency, 1970).

Previous studies demonstrated that the Gedemsa volcano was built up during various phases of explosive and effusive activity, all characterized by the emission of acidic lavas or, more commonly, pyroclastics. These characteristics are typical of many other volcanoes along the Ethiopian Rift Valley. However, in spite of the large interest regarding the various aspects of the evolution of the rift and of the associated volcanism, detailed geological, stratigraphic, volcanological and petrological investigations on single volcanic districts are still in their infancy. Consequently, the evolution of a large number of volcanoes, their relationships with the main phases of the opening of the rift and the magmatological processes occurring in these volcanoes remain poorly understood.

The present work is aimed to take a step toward a better understanding of

the evolutionary processes of rift volcanism by an integrated volcanological, stratigraphic and geochemical investigation of the Gedemsa volcano. In order to reach this goal, the following steps have been followed:

1. geological mapping at a scale 1:25,000 of the area;
2. recognition of the eruptive events;
3. description of the various effusive and explosive units which built up the Gedemsa volcano;
4. petrographic, petrological and geochemical study of representative samples from various stratigrahpic unit;
5. integrated use of geological, volcanological and geochemical evidence to work out models for the internal structure of the volcano, the main processes of magmatic evolution and the way the volcano has been working during the various phases of its activity.

A total of five weeks of field work has been carried out. The geological map of 1:25,000, has been compiled, by combined field observations and aerial photographs interpretation. A volcanological and structural map at a scale 1:50,000 (approx) is also presented. Geochemical and petrographic studies have been done for unaltered samples collected along representative sections during several field trips. Some samples of strongly hydrated pumices have been analyzed and the implications for the mechanisms of interaction between rock and ground waters have been discussed. Computer based processing of analytical data has been carried out.

2. REGIONAL GEOLOGICAL AND TECTONIC SETTING

2.1 General

The Ethiopian Rift Valley, which cuts the uplifted Ethio-Somali plateau is one of the most important structures of the Great East Africa Rift System. The Ethiopian Rift Valley is connected via the Afar triple junction with the Red sea-Gulf of Aden constructive plate boundary. The rift system runs in a north-northeast direction.

The pre-rift rocks consist of extremely folded and foliated basement of Precambrian age overlain by sub-horizontal Mesozoic transgressive and regressive sedimentary strata separated by a marked Paleozoic unconformity, and covered by Tertiary volcanics. The whole series has been uplifted since Eocene as part of the Afro-Arabian swell across which large scale faulting has later taken place to form the eastern and western margins of the rift.

2 .2 The Ethiopian Rift Valley volcanism

2.2.1 Tectonics of the Ethiopian Rift Valley

The Ethiopian Rift Valley is a huge graben that resulted from extensional tectonics. Tensional faults are the dominant structural features and arranged in an "en echelon" pattern. Some transversal structures of probable transform or transcurrent nature, apparently connecting adjacent sectors of the offset axial zones of the rift have also been described (Di Paola, 1972; EIGS-Elc, 1987). The eastern margin of the Main Ethiopian Rift is morphologically well expressed as compared to the western one, which at places is so subdued that boundary between the rift floor and the plateau is hard to define.

Geographic distribution and compositional diversity among volcanic units of the Ethiopian volcanic province indicate that there has been a relationship between magma composition and rifting processes (Barberi et al., 1980; Betton and Civetta, 1984; Hart et al., 1989). According to Woldegabriel et al. (1990) the Ethiopian Rift Valley is a consequence of the initial mantle upwelling, which produced both the crustal doming and the volcanicity. The anomalously thin Mesozoic sequence

along the Guraghe western rift margin suggests a doming stage in the Mesozoic that preceeded Tertiary volcanism and rifting.

It is possible to divide the Ethiopian rift system into: the Southwestern Rift Zone, the Main Ethiopian Rift, and the Afar.

In the Afar, the timing of continental rifting is debated (Barberi et al., 1975, 1982; Kasmin et al., 1980); however, it appears likely that rifting commenced in Late Oligocene-Early Miocene time (Barberi et al., 1975,1982). Chemical and isotopic data from the Afar rocks suggests that hybrid mantle sources were initially tapped whereas depleted mantle sources successively melted (Barberi et al., 1980,1982; Betton and Civetta, 1984; Hart et al., 1989). Makris and Ginzburg (1987) explain that in Afar the crust has been thinned by tensional stresses caused by an updoming of high temperature-low density upper mantle material and has a thickness between a true oceanic crust (Tadjura) and a continental one (20-14km).

Structural and stratigraphic relationship in the Main Ethiopian Rift indicates a two stage rift development. During the early phase (Late Oligocene-Early Miocene), a series of alternating opposed half grabens formed along the rift with major border faults. These succesively evolved to symmetrical rifts in late Miocene-early Pliocene time. Basaltic volcanism associated to early rifting (Kella Basalts) have a transitional to alkaline affinity, and are believed to be generated by lithospheric mantle melting (Woldegabriel, 1987; Hart et al., 1989). By late Miocene times, when definite block faulting ensued, elemental and isotopic signatures of Guraghe Basalt show the addition of an asthenospheric mantle source to a lithosphere mantle source (Hart et al., 1989).

The floor of the Main Ethiopian Rift is marked by a persistent belt of intense fresh faulting which has been termed as the Wonji Fault Belt (Mohr, 1960). The faults are short arranged in "en echelon" fashion, normal type and oriented in north-northeast direction (Gibson and Tazief, 1970). The faulting is clearly not all contemporaneous and is in general younger along the medial line of the rift valley, becoming progressively older as one approaches the rift margins (Gibson and Tazief, 1970). The more recent faults are associated with recent basalt fissure eruptions. The faults show a right stepping and "en echelon" arrangement (Damte, 1990), suggesting that a left lateral component of movement has taken place. These results show that oblique extension direction (east-northeast, west-southwest direction) with respect to the main displacement zone and a strike-slip system has played a mojor role in the development of the Main

Ethiopian Rift (Damte, 1990).

The Wonji Faults also cut the Gedemsa volcano. These faults have normal character with NNE trend and dip at moderate to steep angles (approximately >60°). The faults have variable throws ranging from 20m to 35m, the average being about 25m. Bigazzi et al (1981) presumed that the age of these faults are younger than 0.1Ma. In the eastern margin of Gedemsa caldera, in the vicinity of Cheka village, these faults seem to have a sinistral component motion (Damte, 1990).

Gravimetric and seismic refraction data suggest that the continental crust of the Main Ethiopian Rift has a thickness ranging from 30km in the northern most sector to 40km in the southern one (Makris and Ginzburg,1987).

Another similar set of north-northeast oriented normal faults in "en echelon" arrangement which correspond to the Wonji Fault Belt was identified by Di Paola (1972) in the Siliti-Butajira area.

Rifting in the southwest Ethiopia developed between Late Miocene and Middle Pliocene times (Moore and Davidson, 1987), probably later than when definite faulted rift margins had formed in the Main Ethiopian Rift in late Miocene time.

2.2.2 Petrology and Volcanology of the Ethiopian Rift Valley Volcanism

The Ethiopian rift is associated with Pliocene to Present volcanism. The more salient features of the rift volcanites are the transitional nature of the basaltic sequence, the abundance of peralkaline ignimbrites, and the dearth of rocks of intermediate composition (Mohr, 1967; Di Paola, 1972; Zanettin et al., 1978; Merla et al.,1979).

Most of the geologic sections exposed along the rift margins are dominated by Tertiary volcanic rocks except for a few locations (Eastern, Southern and Western Afar margins; the Western rift margin along Guraghe Mountain of the central sector of the Main Ethiopian Rift, and in the Amaro Horst of the southern sector of the Main Ethiopian Rift) where crystalline basement is unconformably overlain by Mesozoic sedimentary and/or Tertiary volcanic rocks.

The distribution of rock units and the alignment of volcanic ranges are parallel to the NNE rift trend.

Di Paola (1972) assigns the volcanic activities within the rift to the following succession of events:

Fig. 1. Location map of Gedemsa area.

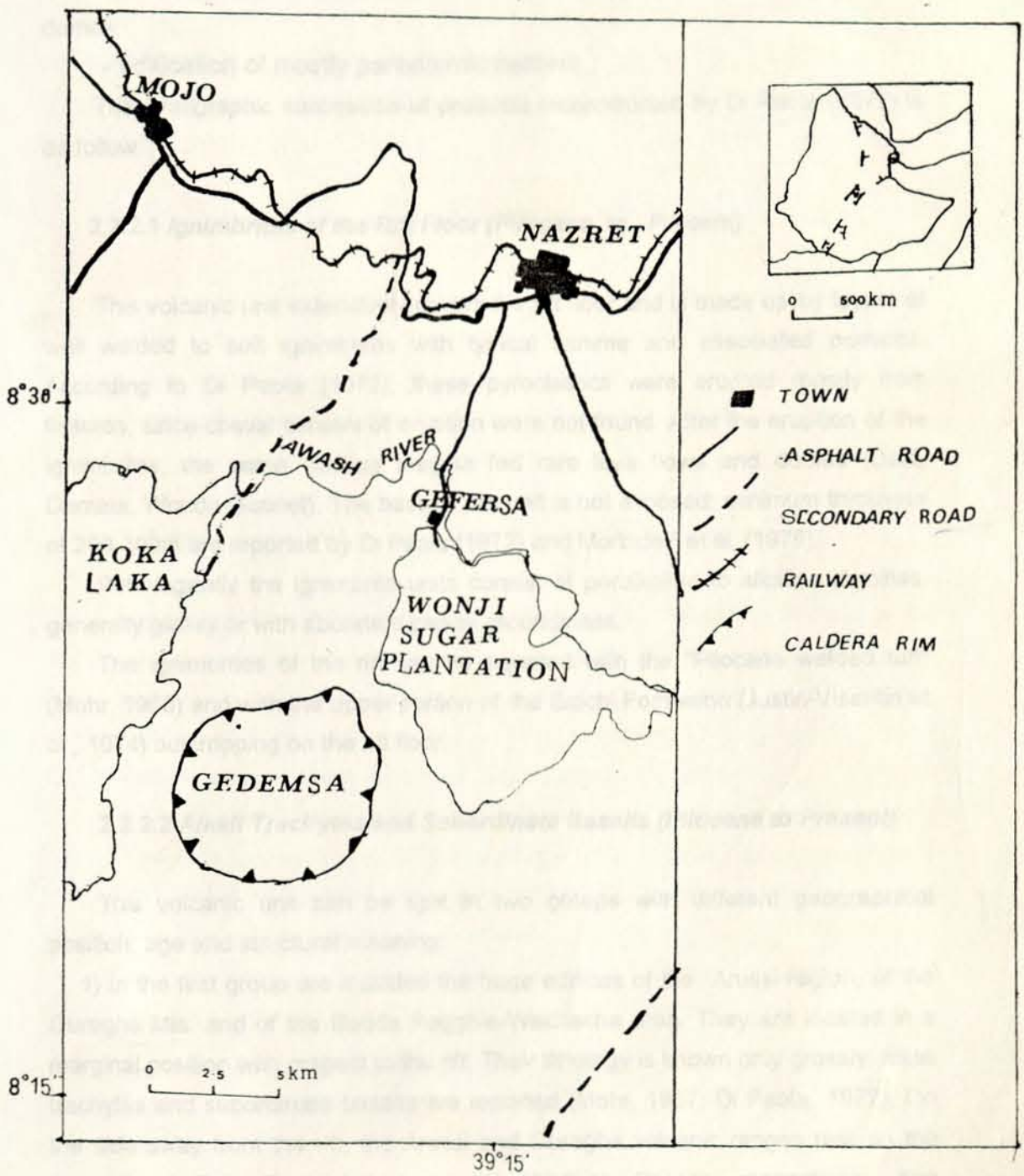

- fissure eruptions with emplacement of ignimbrite products followed by volcano-tectonic collapses, and successive building of rare silicic central volcanoes;

- basaltic fissure eruptions with subsequent alkali trachytic lava flows and domes;

- edification of mostly pantelleritic centers.

The stratigraphic succession of products reconstructed by Di Paola (1972) is as follow:

2.2.2.1 *Ignimbrites of the Rift Floor (Pliocene to Present)*

This volcanic unit extensively covers the rift floor and is made up by layers of well welded to soft ignimbrites with typical fiamme and associated pumices. According to Di Paola (1972), these pyroclastics were erupted mostly from fissures, since coeval centers of eruption were not found. After the eruption of the ignimbrites, the same viscous magma fed rare lava flows and domes (Data, Damata, Wondo Guenet). The base of the unit is not exposed: minimum thickness of 200-300m are reported by Di Paola (1972) and Morbidelli et al. (1975).

Petrologically the ignimbrite units consist of peralkaline to alkaline rhyolites, generally glassy or with abundant glassy groundmass.

The ignimbrites of the rift can be equated with the "Pliocene welded tuff" (Mohr, 1968) and with the upper portion of the Balchi Formation (Justin-Visentin et al., 1974) outcropping on the rift floor.

2.2.2.2 *Alkali Trachytes and Subordinate Basalts (Pliocene to Present)*

This volcanic unit can be split in two groups with different geographical position, age and structural meaning.

1) In the first group are included the huge edifices of the Arussi region, of the Guraghe Mts. and of the Badda Rogghie-Wachacha area. They are located in a marginal position with respect to the rift. Their lithology is known only grossly: alkali trachytes and subordinate basalts are reported (Mohr, 1967; Di Paola, 1972). On the side away from the rift, the Arussi and Guraghe volcanic ranges rest on the Arussi and Bale Basalts and on the Wollega Basalts, respectively. Age determinations from samples collected from the Wachacha and in the Arussi

volcanoes range from 4.6 to 2.5Ma (Miller and Mohr, 1966; Kunz et al., 1975).

2) The second group includes the alkali trachytic lavas and domes connected to the basaltic alignments within the rift. The Zuqwala, the Bosetti-Gudda and the Fantale volcanoes are the more significant edifices referable to this unit. They have top calderas more or less preserved (Mohr, 1967; Di Paola, 1972; Gibson, 1974; Morbidelli et al., 1975). Two K/Ar datings from the Bosetti-Gudda gave ages of 1.5 and 1.6Ma (Morbidelli et al., 1975). An age of 1.3 to 0.9 has been reported for Zuqwala (Morton et al., 1979.)

2.2.2.3 *Pantelleritic Lavas and Pumice Flows (Pleistocene to Present)*

These rocks are found on the slopes of individual volcanoes, such as Boseti, Ittisa, Bericcio, Bora, Alutu, Urji and Chabbi volcanoes. They consist of unwelded pumice flows, pumice falls and ashes. Some obsidian lava flows are also present and generally mark the final stages of activity of some centers (Di Paola, 1972). Obsidians appear as generally porphyritic.

2.2.2.4 *Basalt Lava Flows and Cinder Cones (Pleistocene to Present)*

Three distinct lava fields of aligned spatter cones, sometimes filled by small lakes, can be recognized in the northern portion of the rift: one extends from Lake Zwai to the Fantale, the second lies close to the Gurage escarpment (Buttajira-Goggetti), the third is located SE of Addis Ababa (Debre Zeit) (Di Paola, 1972). The lavas are basaltic, generally aphyric to poorly porphyritic.

The thickness of the formation, which is intensely faulted, does not exceed 100m. The age is very young as indicated by the discovery of human artifacts amidst the tephra of Bishoftu tuff cones (Mohr, 1961) and historical records of some effusive eruptions (Metahara lava flow).

This unit corresponds to the Bishoftu Basalts of Zanettin and Justin-Visentin (1974) and to the "Basaltoid volcanites" of Morbidelli et al. (1975).

3. STRATIGRAPHY AND VOLCANOLOGY OF THE GEDEMSA VOLCANO

3.1 Generals and Previous Investigations

The Gedemsa volcano is found in extensional tectonic setting in rift where voluminous volcanism occurs. The volcanic history of the center has been dominated by the eruptions, in the form of both lavas and pyroclastics, of silicic magmas (Fig. 2, attached).

The lowest exposed products are represented by acidic lavas, which are covered by thick plinian fall pumice deposits. These are followed by an ignimbrite deposit and by intra-caldera lava flows and interbedded pyroclastic products. The formation of the caldera, is clearly a composite structure resulting from the occurrence of several collapses. A separate stage of volcanic activity (basaltic volcanism) formed surge deposits and numerous basaltic cinder cones and lavas, both within and outside the caldera depression. Interbedded oxidized soil horizons (red boles) occur in several places within the volcanic sequence and record repose periods between eruptions.

In the Gedemsa caldera, extensive sediment successions developed within and outside the depression. These are typical continental sediments (fluvial, alluvial fan and lacustrine).

From the knowledge of the stratigraphy, it is clear that eruptions from the rhyolitic centers of Gedemsa are separated by relatively long repose period. On the other hand, the basaltic volcanoes show a common progression from phreatomagmatic to a strombolian phase. This reflects a decrease in the water-magma interaction during the eruption.

A primary account on the geology of the Gedemsa caldera has already been given by a few author.

Di Paola (1972) mentioned briefly the geology of some of the major units of the center and showed the presence of dextral dislocation associated with the normal movement.

Thrall (1973) described and classified the volcanic products on the basis of field characteristics and analytical (major element) data. According to this author the caldera collapse was not associated with outpourings of ignimbrite or pumice fall but collapse was caused by foundering of a large part of the cone along a

cylindrical fault.

A geo-volcanological investigation on Gedemsa was carried out as part of a geothermal reconnaissance study of selected sites of the Ethiopian rift system by EIGS and Elc (1987). They suggested that the caldera was formed through ignimbritic eruptions and attributed a phreatomagmatic origin to the Kore crater.

Recently, Damte (1990) provided a valuable account on the volcanotectonic features of the volcano. He presented a generalized stratigraphy of Gedemsa volcano which starts with a base of very thick pyroclastic flow and ignimbrites followed by rhyolites and obsidian lava flows of post caldera activity capped finally by pumice fall deposits.

3.2 Structural and Volcanological Outlines of Gedemsa Area

Gedemsa volcano morphology is dominated by a slightly elliptical caldera, about 8 km in diameter and minimum NNW elongation. Thus the shape of the caldera does not reflect the regional stress patterns and is purely the result of magmatic activities. The shallowest part of the structure occurs in the northeast. The central part of the caldera is occupied by cones and domes which reach an altitude of about 200m with respect to the caldera floor. There is no evidence for the occurrence of resurgent structures (i.e. later updoming of the intracalderic ignimbrite or sediments). The altitude of the caldera rim is very uneven with a maximum of 1950m on the west and maximum altitude difference with respect to the caldera floor of about 250m. This suggests the occurrence of several pre-caldera flows and domes along the flank of the volcano. The northeast part of the caldera is characterized by a younger escarpment and by a more depressed calderic floor. This suggests that the caldera has been formed by several eruptions and the most recent collapse occurred in the northeast. Cinque et al (1991) suggested that the caldera collapse occurred in two phases.

Field observations confirmed a two phase collapse for the caldera. The first phase occurred as a consequence of huge plinian explosive eruptions which produced the Lower Pumice Fallout deposits which are by far the most widespread pyroclastic unit of the Gedemsa volcano, being found over wide areas both inside and outside the caldera. The second phase of caldera formation was connected with the ignimbrite eruption and mainly affected the northern and northeastern part

of the previously formed structure.

Analyses of satellite images indicate that an older caldera almost completely covered by younger products is present just north of the Gedemsa volcano. The southern rim of this older caldera intersects the northeastern edge of the Gedemsa caldera and its presence had strong effects on the geometry of the collapse connected to the ignimbrite eruption (Fig. 3). Indeed, this explains why the northern edge of the Gedemsa caldera shows a convexity rather than a concavity toward the center of the depression.

3.3 Stratigraphy and Volcanology

On the basis of the present work and of literature data, a detailed stratigraphy of Gedemsa has been reconstructed. The recognized units, and their representative stratigraphic sections and suggested correlations are shown in Fig. 4. The various units have been named according to their positions along the volcanic succession. These units are from bottom to top:

- Basal Rhyolite Lavas
- Lower Pumice Fallouts
- Upper Obsidian Lavas
- Ignimbrites
- Upper Pumice Fallouts
- Intracalderic Lava Domes and Pyroclastics
- Intracalderic Lacustrine Sediments
- Phreatomagmatic Tuffs
- Cinder Cones and Basaltic Lavas

3.3.1 Basal Rhyolitic Lavas

This unit represents the lowest exposed products in the center and is traceable over large area. The main exposures are displayed in the south, southeast and norhtern flanks, where thick lava bodies, probably domes and associated flows, crop out.

Along the northeastern road, rhyolitic lavas underlie the lower pumice fallout, and appears strongly weathered and friable. The lava shows flow folded

structures and is aphyric. The upper part is partly vesicular. Near to the top, the lava flow contains abundant bands of dark obsidian with perlitic texture. The flows appear to continue on the flank of the volcano where they show a thickness of about 20 to 40m.

Another important outcrop occurs along the northern escarpment of the caldera. This flow tends to show upsequence succession of a variety of lithologies and textural features: a basal layer with thin and subordinate levels of unwelded pumices, interpreted as co-eruptive pumice fall deposit having an exposed thickness of 10m, followed by a steep sided and jointed flow with a thickness of 18m; at the top 5m thick obsidianaceous and perlitic bands occur. Above these, there are Lower Pumice Fallout and then the breccia of the ignimbrite.

The southeastern corner of the caldera exposes a basal aphyric lava, intermediate pumice fallouts and upper lavas. The sequence is about 30m thick, but the base is not exposed. The basal lava and the pumice fall units are separated by a red soil, whereas the pumice fall and the upper lava are separated by a brown soil. The basal lava is grey, aphyric and shows flow structures. Sometimes it grades to obsidian. It has an exposed thickness of about 10m. The upper lava contains flow-folded obsidian partly perlitised and has a thickness of 8m.

At the eastern rim of the caldera again a basal obsidian lava, intermediate pumice fall and upper obsidian lava are exposed. Here, the thickness of the sequence is about 80m.

In summary, field evidence clearly indicates that effusion of acidic obsidian was a widespread process of the pre-caldera phase of the Gedemsa volcano. Structural features of these rhyolites (e.g. thickness, columnar jointing) suggest that these forrmed endogenous domes and, in some cases, thick lava flows.

3.3.2 Lower Pumice Fallout

This unit consists of thick plinian pumices of rhyolitic composition with interbedded paleosols (Plate 1a).

The lower pumice fallout exposed at Bora Mountain represents the highest thickness (>35m) and forms the hills of Bora and Ruckecha. Two soil horizons are interbedded with the plinian fallout units. The pumices are light grey in color and show crude stratification dipping away from the caldera (30°W). The deposit is

predominantly composed of pumice with few lithic clasts. The average maximum diameters of the three largest pumice clasts and the three largest lithic clasts are 70, 60, 50 and 65, 60, 55 cm respectively. These very large dimensions indicate a close vent. Reverse grading of large pumice clasts has been observed. The deposit shows an upward increase in the proportion and size of lithic clasts and reflect vent widening by conduit wall erosion during the eruption. Towards the top, the deposit is fine grained, shows stratification and is interbedded with two soil horizons. Subsequent erosion of the pumice has resulted in uncover some of the earlier lavas which had been hidden beneath the pumice.

The same unit can be traced up to the northeastern road. Here the thickness is much lower (10 to 15m), there are no interbedded paleosols, whereas there are thin strata of pisolitic ashes which suggests that there were large fluctuations in the plinian eruption activity and these pisolitic ashes may mark small episodes of magma-water interaction. The deposit contains considerable amount of obsidian, scoria and rhyolite fragments. The pumice clasts show reverse grading.

At Jemute, along a fault scarp, plinian pumice fallout with a thickness of 12m is exposed. The base contains pumice clast up to 6cm in diameter. Lithics are scarce and mainly are obsidian fragments of lava carapaces.

In the southwestern sector the pumices represent the highest unit on the caldera rim. They show a visible thickness of 14 m. Here, as well, there are two paleosols. As in the northwestern sector, the upper unit shows large pumice clasts. The deposit is separated from the underlying lava by a paleosoil. The deposit consists of at least six size-graded layers and dips about 20°NW away from the caldera. A peculiar aspect of the deposit is the presence of a level of fallout consisting of a black, completely welded glassy rock, which mantles topography. In the middle of the deposit, there is a level which shows abnormally coarse granulometry with average maximum size of pumice clasts 28cm in diameter, indicating a drastic change in eruption conditions.

At the eastern edge of the caldera, these pumices are grey, well sorted, with reverse grading of pumice clasts and are crudely stratified dipping about 30°S away from the caldera. The deposits contain obsidian and altered ryolitic rock fragments. The maximum size of pumice and lithic clasts are 20 and 15 cm, respectively. About 20 cm thick red soil horizon is interbedded towards the lower layer.

At the section about 1 km southeast of Bogra, the lower pumice fall deposit

attains thickness about 2m and the maximum size of pumice clasts is reduced to 3 cm. Field observations suggest that the thickness and the size of clasts of the lower pumice fall deposits decrease towards the northeastern edge of the caldera.

In summary, the pumice fall deposits are by far the most voluminous formation outcropping at Gedemsa. Accordingly, it is obviuos to conclude that its emplacement was responsible for the caldera collapse. The large pumice clasts found all around the caldera, except in the northeastern edge, is an evidence for the emission for a central crater. The lower dimensions of pumice clasts on the NE border of the caldera is explained by tha fact that in this sector there was a widening of the depression as a consequence of ignimbrite eruption and, accordingly, the present rim of the depression is located in a more distal position than the original rim of the caldera.

3.3.3 Upper Obsidian Lavas

Obsidian lava flows are observed overlying the Lower Pumice Fallout only in the eastern and south-eastern sectors of the volcano. These form dome like structures, most probably formed along the rim of the caldera. They show perlitic textures and resemble very closely the obsidian of the basal flows, although the former are more porphyritic in texture than the latter.

3.3.4 Ignimbrite

This unit consists of three facies: a basal dense lithic-rich level (co-ignimbrite breccia), an intermediate spatter agglutinate and an upper densely welded ignimbrite (multiple ignimbrite). The multiple ignimbrite shows features that are typical of normal ignimbrite flow units. The spatter agglutinate resembles lava but contains abundant pockets of lithic breccia. The co-ignimbrite breccia is a lithic rich layer which overlies a meter thick paleosol. This unit is best exposed on the northern and eastern rim of the caldera. It is also found along the western rim, whereas it is completely missing on the southern sector of the volcano. Its maximum dipping angle is 25°NE. The ignimbrite has an earlier plinian phase. The overall geometry of the ignimbrite is variable depending on the underlying topography.

The type section found in the northern slope of the caldera near the Bogra

place exposes, from bottom to top:

- rhyolite lava
- lower plinian fallout
- paleosol
- loose breccia
- spatter agglutinate
- multiple welded ignimbrite

The multiple ignimbrite has a basal dark-brown and an upper green ignimbrite. Here, the ignimbrite shows a typical eutaxitic texture partially modified by rheomorphism with stretching of fiamme and flow folds. Towards the top, ignimbrite has a greenish color, an evident eutaxitic texture, a secondary vesiculation parallel to fiamme and contains black vesiculated material which resemble basaltic scoria. The base of the multiple ignimbrite is underlain by a fairly welded spatter agglutinate (Plate 1b) containing large lithic breccia, which sometimes become predominant over the agglutinate . The spatter agglutinate covers a fine depleted incoherent breccia rich in lithics (Plate 2a), probably representing proximal ignimbrite breccia. Lithics mainly consist of fresh and hydrothermally altered lavas (rhyolites). The maximum size of blocks in the breccia is about 70cm. The breccia rests over a meter thick paleosol. The breccia displays upward coarsing (reverse grading) of lithics and may be attributed to grain dispersive pressure. This breccia is the first to be ejected by initial phreatic explosions, consisting of coarse, fine depleted, angular fragments of broken country rocks.

About 1km southeast of this section a second breccia plus multiple ignimbrite outcrop on the escarpment of the caldera. In this locality the section consists of:

- rhyolite lava with obsidian at the top
- paleosol, 40cm thick
- lower fallout of very small pumices with a thickness of 2m
- paleosol 30cm
- loose breccia, fine depleted with small amount of juvenile material, having a thickness of 3m
- spatter agglutinate
- densely welded ignimbrite about 5m thick
- ash fall deposit about 2m thick
- yellow paleosol

Fig. 3. Sketch structural and volcanological map of Gedemsa. For symbols see Fig. 1 and Fig. 2.

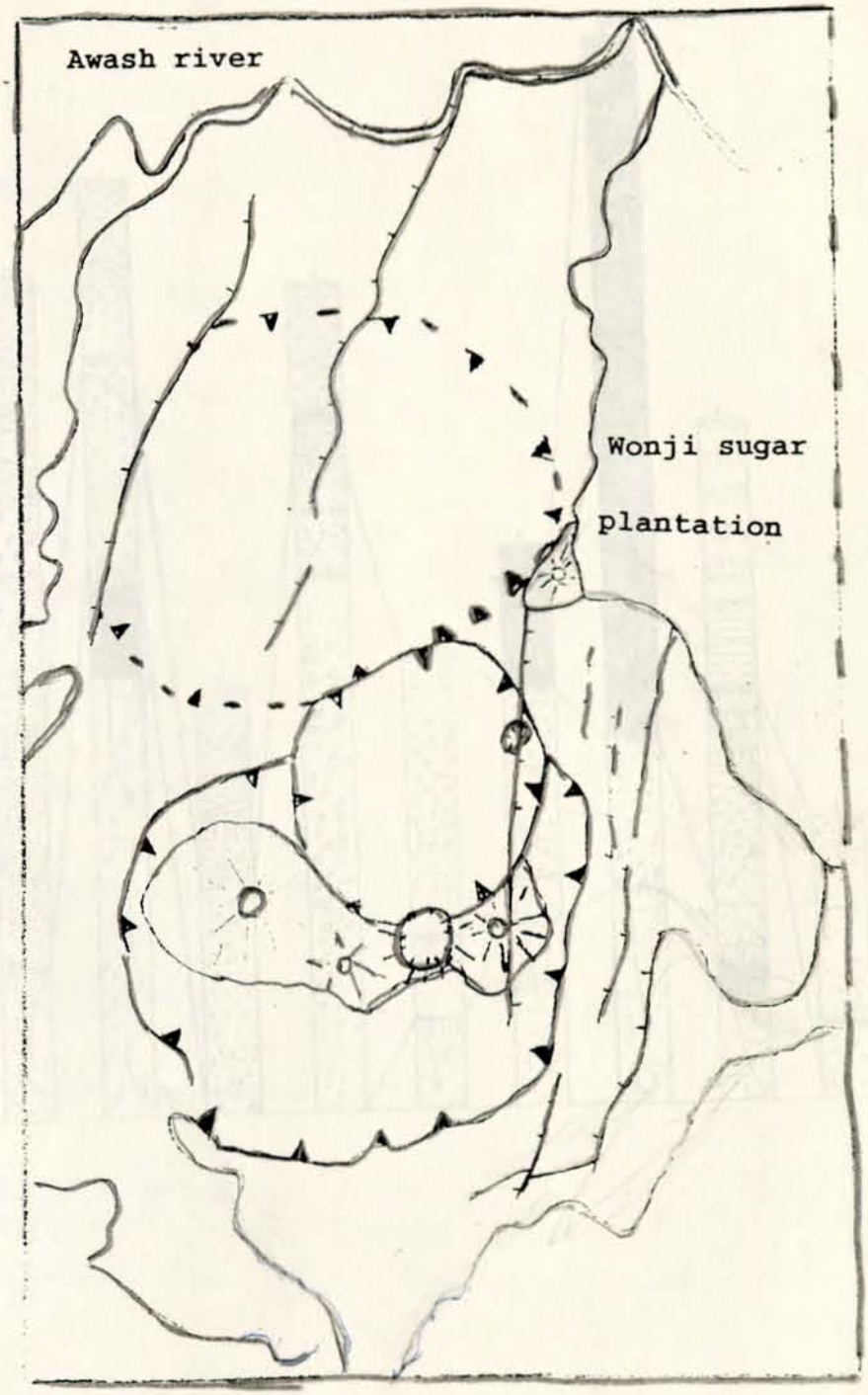

Fig. 4 Suggested correlation between stratigraphic sections of Gedemsa volcano. See Fig. 2 for location.

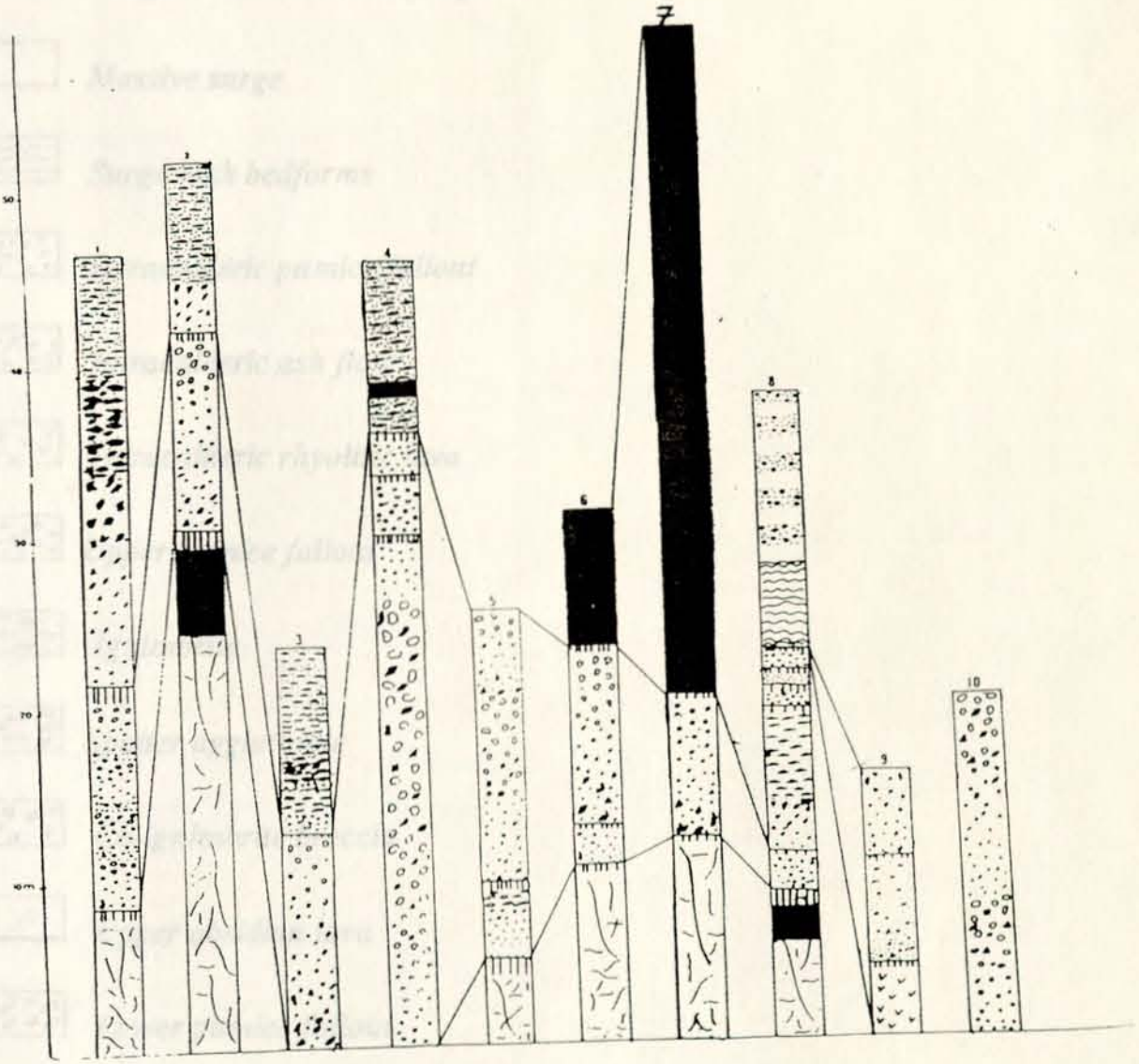

LEGEND (Fig. 4)


Surge with accretionary lapilli


Massive surge


Surge with bedforms


Intracalderic pumice fallout


Intracalderic ash flow


Intracalderic rhyolitic lava


Upper pumice fallout


Ignimbrite


Spatter agglutinate


Co-ignimbrite breccia


Upper obsidian lava


Lower pumice fallout


Basal rhyolitic lava

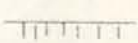
Paleosol

Fig. 4 (continued)

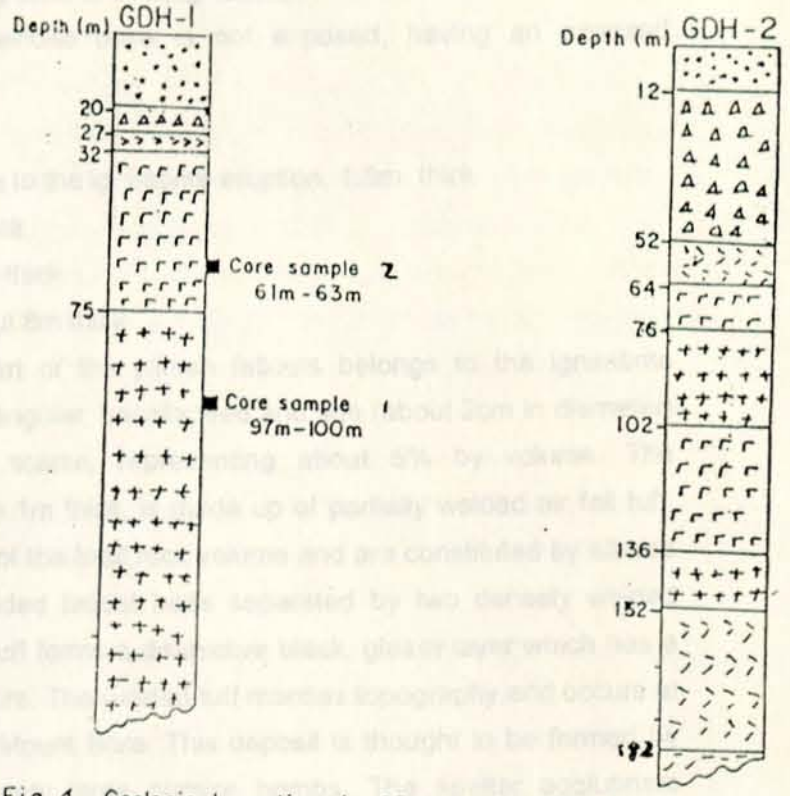

Fig. 4. Geological section in GDH-1 and GDH-2,

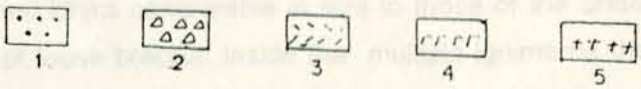

1 Alluvium

2 Pumice

3 Rhyolite lava

4 Basalt lava

5 Pumiceous ignimbrite

- surge deposit, about 15 m thick

In this outcrop the thickness of the breccia (3m) and the dimension of the blocks (20 to 30cm in diameter) are much smaller than along the northeastern road.

At Jemute, a fault scarp exposes breccia plus multiple ignimbrite (Plate 2b). From base to top the following units are recognizable:

- lower plinian fallout whose base is not exposed, having an exposed thickness of 15m
- paleosol 20m thick
- plinian fallout belonging to the ignimbrite eruption, 1.8m thick
- loose breccia, 25cm thick
- spatter agglutinate, 6m thick
- multiple ignimbrite about 8m thick

The lower 80cm thick part of the plinian fallouts belongs to the ignimbrite eruption and is made up of angular, uncollapsed and fine (about 2cm in diameter) pumice clasts. Lithics are scarse, representing about 5% by volume. The uppermost layer, as much as 1m thick, is made up of partially welded air fall tuff. Lithics represent about 10% of the total rock volume and are constituted by altered lavas. There are two unwelded fallout beds separated by two densely welded fallouts. The welded air fall tuff forms a distinictive black, glassy layer which has a well developed eutaxitic texture. The welded tuff mantles topography and occurs at a distance of 5km from the Mount Bora. This deposit is thought to be formed by the rapid accumulation of very large pumice bombs. The spatter agglutinate embeds isolated lithics comparable in size to those of the underlying breccia and also pockets of loose breccia. Inside the multiple ignimbrite there is a horizon of welded spatter about a meter thick. The thickness of the breccia (25cm) and the maximum lithic size (20cm in diameter) are limited, indicating that this section is relatively distal compared to that of the northeast escarpment of the caldera. There is no evidence of alteration, oxidation or other features which indicate a pause of activity between the ignimbrite and the plinian units.

The section at the Mount Bora is represented by a plinian fallout (thickness over 35m) overlain by the multiple ignimbrite with a thickness of 8m which covers about 50cm thick paleosol. The multiple ignimbrite lacks scoria inclusions and no breccias have been found. A zone of massive dark obsidian occurs in the lower part of the mutiple ignimbrite and may represent the ultimate degree of welding.

Field data indicate that the ignimbrite eruption was one of the main events in

the volcanological evolution of the Gedemsa volcano. However, its absence in the southwestern, south and southeastern sides of the caldera, rules out that this eruption was responsible for the collapse, although it is likely that it contributed to the widening and deepening of the north-eastern sector of the depression where maximum dimension of lithics and thickness of the breccia indicate near vent conditions.

The ignimbrite eruption started with the formation of a convective column which deposited a fallout of pumice. The convective column was followed by the emplacement of a fine rich pyroclastic flow which deposited the first ignimbrite bed. The ignimbrite was then followed by the emission of the co-ignimbrite breccia. The occurrence of lithic breccia interbedded with the overlying ignimbrite observed in some places along the caldera wall may record an increase in the magma discharge rate which accompanied the main collapse phase in the northeastern sector of the caldera.

The thickness of the multiple ignimbrite seems to increase away from the caldera rim, probably filling in valleys and ponded in local depressions. About 1km south of Shewa Alem Tena town, along a fault scarp, about 10m thick ignimbrite has been observed.

There are two K/Ar datings on ignimbrites from the caldera rim: one by Morton is 0.85Ma (green welded tuff, sample 76-10) and one by the Geothermal Exploration Project report (a feldspar from a sample northeast rim of the caldera) is 0.7Ma (sample SAG-31).

3.3.5 Upper Pumice Fallout

This unit is less extensive and composed of fallout pumice deposits with associated ashes and interbedded with paleosols.

Along the road which goes to the caldera uphill of Shewa Alem Tena, upper pumices are made up of three layers separated by paleosols, overlying the Ignimbrite and covered by the surge deposits. The section exposes a base of 40cm thick, white-grey, well sorted pumice layer containing juvenile clasts about 4cm in diameter. It is followed by 30cm thick, discrete, fine grained fall units. At the top, a 70cm thick layer consisting of poorly sorted, reversely graded pumice clasts with a fine grained basal layer occur. A 50cm thick, fine grained and thinly stratified phreatomagmatic tuffs rest on this pumice deposit. The pumice sequence

is separated from the basal ignimbrite and from the upper tuff by yellowish soils. The same sequence, but about 4m in thickness, has been observed in the northwestern outer side of the caldera rim above the ignimbrite.

The plinian deposits seem to be not very widespread and decrease rapidly in thickness away from the caldera in northeast direction. Most probably they are related to explosive activity which took place inside the caldera during the formation of the Ittisa hills.

At Didimtu, a fault scarp exposes a thick pumice fall deposit (about 20m thick) consisting of two size-graded layers. The deposit shows an upward increasing in the size and in the proportion of lithics, indicating vent widening by wall erosion which increased the mass discharge rate during the eruption. The deposit also displays a fine grained basal layer. The amount of lithics is higher in the lower layer and lithics are rhyolite, ignimbrite and plagioclase rich mafic rocks. The large size of clasts and high thickness of the deposit suggest proximity to the vent.

Along the Wonji-Nazret road near the bridge on the Awash river a pumice fallout is also exposed overlying Awash river Ignimbrite. This deposit is about 3m thick, relatively coarse grained (6cm in diameter), well sorted, stratified and shows gas segregation pipes. The ignimbrite is green, fine grained, densely welded and contains no inclusions or scoria fragments. Although pumice fall deposits overlie a green ignimbrite it appears clear that the fast attenuation of the thickness away from Gedemsa for the proximal deposit, can not fit with the characteristics of deposits cropping out near Awash bridge.

3.3.6 Intracalderic Lava Domes and Pumice Cones

These intracalderic volcanic products form coalescing cones and domes with minor lava flows (Plate 3a,b). In the eastern part there is a large crater, the Kore crater, with a diameter of about 1000m. The inner walls of this crater are nearly vertical and are constituted by rhyolitic obsidianaceous lavas overlain by pumice deposits. Di Paola (1972) suggested that these rocks are the latest volcanic products of Gedemsa and Bigazzi et al (1981) gave an age between 0.2 and 0.1Ma.

On the northern edge of the Kore crater a deposit of pumiceous breccia containing rhyolitic blocks very similar to the lavas which form the upper part of the crater rim. The lava occurring in the upper part of the crater form a continuous

outcrop all along the northern wall with a thickness of 20-40m. It consists of mingled aphyric or poorly porphyritic rhyolite and a vesicular mafic lava with abundant plagioclase phenocrysts. The mafic components are very dispersed within the rhyolite and sometimes only phenocrysts of plagioclase and olivine surrounded by a thin film of mafic lava are observed (Plate 4a,b). The maximum dimension of the mafic clasts is around 10-20cm. They are sometimes flattened and show embayed and crenulated margins at the interface with rhyolitic lava. Other times, angular blocks of mafic material is observed. This indicates the mafic material was incorporated into the rhyolitic magma both in a solid and a liquid state. Along the southern edge of the crater a partially perlitic rhyolite outcrops above the mingled lava.

The eastern cone consists of mingled mafic-rhyolitic lava overlain by a pumiceous breccia containing large juvenile clasts. Blocks of densely welded ignimbrite containing lithics and fragments of rhyolitic lavas are observed in the breccia, together with the mingled lavas. The lithology of the ejected ignimbrite blocks is similar to that observed for the ignimbrite of the NE border of the caldera.

A section located about 1km east-southeast of the Kore crater exposes the following units, from bottom to top:

- mingled mafic-rhyolitic lava.
- loose ash flow deposit with rhyolitic pumice. This is 5 to 6m thick and shows gas segregation pipes. Sillar facies are observed within these layers at places.
- pumiceous material with decimeter-sized lithics (proximal fallout). This unit seems to be the same observed on the northern edge of the Kore crater, though here lithics of mingled lavas are not observed.

The ash flow and the mingled lava are separated by a soil. This layer of mingled lava is very similar to that observed at the eastern border of Kore crater. This suggests that the eastern hill may be entirely or largely made of a highly viscous rhyolitic lava.

About 2km northwest of Kore crater (northern flank of Dima) a thick pumice deposit has been observed. This deposit is overlain by 1 to 3m thick welded perlitic material. The welded deposit forms a continuous layer which mantles the previous topography and is to be regarded as an air fall welded tuff bed.

The formation of Kore crater and associated pumice fall deposits probably represent the latest stage explosive episodes accompanying the emplacement of the eastern domes.

The western hills seem to consist of both pyroclastics and lava flows. The westernmost edge of these hills is formed of pumice and at least one homogeneous perlitic lava flows. Some outcrops on the northwest flank of the hills exhibit meter-thick pumice deposit dipping about 30NW. The pumice clasts are grey, similar to those of the lower pumice fall deposit. Slightly southwards of Dima the pumice layer is covered by perlitic lavas with evident flow lamination structures.

In the northern part of the small Kelo ridge a mingled mafic-rhyolitic lava has been observed along a ravine cut by erosion. This lava underlies a poorly sorted pumice fall containing decimeter sized pumiceous bombs. The lava consists of white-grey rhyolite containing mafic inclusions. The flow dips downhill parallel to the hill slope and with a maximum visible thickness of about 8m. In some localities the rhyolitic lava is obsidianeceous, probably representing the external part of the flow. The mafic component is formed by fairly equidimensional fragments, up to 10cm in diameter, uniformly distributed through the rhyolite (Plate 5a). The mafic fragments consist of vesiculated black lava with abundant plagioclase and minor pyroxene and olivine phenocrysts (Plate 5b). The contact between mafic and rhyolitic lava are quite sharp suggesting that the mafic fragments were solid when they were incorporated into the rhyolite. However, a few mafic blocks with crenulated and embayed edges have been also observed. The volume ratio between rhyolite and mafic lava is about constant through out the entire flow. The lava is overlain by a poorly vesiculated, poorly sorted pumice fall deposit containing large mafic clasts. These clasts occur both as separate fragments and included within the pumice clasts.

The occurrence of mingled lavas among the products of the post caldera activity indicates that uncomplete magma mixing was widespread during this phase of volcanic activity. While magma mixing within a zoned magma chamber seems a likely machanism to explain the mixed rocks of the Kore crater, the process responsible for the formation of the Kelo rocks is difficult to envisage. A simple process of magma mixing is excluded by the solid state of the largest majority of mafic components. A possibilty is that the magma was withdrawn from a stable, very shallow zoned magma chamber, which was undergoing extensive crystallization of the mafic components. Input of fresh mafic magma would have generated gas exsolution and magma vesiculation, triggering explosive eruption. This could have resulted in the intermingling between a liquid upper rhyolitic magma and a partially solidified lower mafic magma. In this frame, the presence of

abundant vesicles in the mafic clasts could be explained by the low pressure of crystallization of the mafic liquid. This process conflicts with the solid state of the mafic clasts and with their uniform distribution through the deposit.

An alternative possibility could be that the rhyolitic magma cut through a deposit of mafic scoria, possibly forming a buried cinder cone. According to this hypothesis, mixing occurred in the conduit while the acidic magmas was rising to the surface. This process is strongly supported by the well vesiculated texture of the clasts, their quite rounded shape and by the uniform distribution of the clasts. The presence of rare mafic inclusions with embayed edges which were probably incorporated in a liquid state could be explained by assuming that some mingling occurred within the magma chamber. However, there is no evidence for the occurrence of mafic eruptions during the whole evolutionary history of the Gedemsa volcano.

It is very difficult to recognize the number of centers and the stratigraphic sequence within the intracaldera hills due to the paucity of good exposures at the contact between different edifices. The pumice cone of Dima is capped by Kore products and the Kelo products seem to underlay the Dima pumice cone. At least three volcanic edifices of distinct morphology (from east to west Kore, Dima and Kelo) have been constructed.

3.3.7 Intracalderic Lacustrine Sediments

Sedimentary deposits have been found in several places within the caldera depression. Their thickness, sedimentological characteristics and origin are poorly known because of the lack of good exposures. A thickness of about 18m was measured by Kebede (1988) and testifies for an important role of accumulation of epiclastic material in the filling up of the caldera depression. The sediments are cut by the recent faults. A well evident fault in the eastern edge cuts the intracalderic material making it possible to observe a section made of a soil which covers a lahar-type deposits containing pumice clasts up to some tens cm large. Along the northwest base of Mt. Kelo, some deep cuts allow to observe that the deposits are formed of fine material containing loose grains of pumice ashes and lenses of rounded pebbles of eluvial-colluvial origin. The relationship between possible lacustrine deposits and the cinder cone are not clear. Most probably, basaltic eruptions are partly contemporaneous and partly younger than lacustrine

deposits.

3.3.8 Phreatomagmatic Tuffs

These consist of a thick series of stratified, laminated and massive deposits (Plate 6a) representing multiple surge events, emitted from a vent buried and sited very close to the eastern border of the caldera. The maximum thickness (around 30-40m) has been observed on the caldera rim, 1km south of Bonga and where the deposit forms a continuous outcrop towards Shewa Alem Tena, thinning rapidly away from the vent. Individual layers are from 1m to half meter thick near the vent to only a few centimeters in distal areas. The variation in thickness is also controlled by pre-depositional topography. The deposits drape the caldera escarpment (Plate 6b), suggesting that the pyroclastic material was sticky and plastered against the steep walls of the caldera. This clearly supports a wet surge nature for the pyroclastic cloud. Tuffs draping the caldera scarp contain several lithics and basaltic juvenile bombs with impact sags up to 50-70cm wide near the caldera rim, in proximity of the vent. Discontinuties of planar bedded deposits with penecontemporaneous slumpings are common. Some individual beds are well sorted, but the sequence as a whole is very poorly sorted owing to the pulsatory nature of particle transport and deposition. The deposit is dominated by fine-grained poorly vesicular clasts and by the occurrence of mud layers caused by the water-magma interaction. The upper part of the unit is generally fine-grained and well stratified because of the alternance of strata made of accretionary lapilli and of massive ashes, which are typical features of wet surge deposits. Here, individual strata are thin (up to 50cm thick) and locally maintain a remarkable constant thickness, indicating surges associated with plinian activities. The lower part of the deposit, generally coarse grained, shows a large areal dispersion and is characterized by the occurrence of wave-like bed forms (cross bedding and dune bedding), indicating a higher velocity of emplacement and drier conditions during transport of pyroclasts.

It is reasonable that the phreatomagmatic eruption occurred when a lake was present inside the caldera. The vent was sited along the recent fault which cuts the eastern edge of the caldera. This, together with the basaltic composition of the magma, suggests that the explosive eruption was related to the recent basaltic volcanism associated to the Wonji Faults. Early eruption of basaltic magmas inside

the caldera occurred in a lacustrine environment and generated strongly explosive surtseyan eruptions. Successively, the lake dried up, or the vent was isolated from the water, and new basaltic eruptions were characterized by strombolian activity.

3.3.9 Cinder Cones and Basaltic Lavas

They occur both inside (Plate 7) and outside the caldera. They are very young and connected with the recent Wonji fault system. The geothermal report on K/Ar dating (EIGS and Elc, 1987) gave an age of 0.41Ma for a Nagow cone, inside the Gedemsa caldera, whereas Bigazzi el at. (1981) reported a more realistic age of 0.06Ma for the mildly alkali basaltic lava flows and spatter cones around the Gedemsa volcano. The cones often have elongated forms and have an accompanying lava flow which formed when degassed magma continued to be extruded after explosive activity had terminated. The asymmetrical growth of many cones and their alignments along a northeast direction indicate that the vent were located along fissures. Lithics of country rock are uncommon, suggesting that fragmentation of magma occurred at shallow levels. Deposits of cones consist of fine to medium grained, well stratified scoria fall units, suggesting that explosion occurred at relatively long intervals. Porphyritic scoria bombs with abundant plagioclase and olivine are found near to vents. Agglutinated lava spatterns are rare. This imply that the strombolian activity was characterized by discrete, mildly explosive events with scarce or no lava fountaining. The basaltic eruptions are considered to be part of the regional recent to active rift basaltic volcanism and, accordingly, is unconnected with the history of Gedemsa.

3.4 Bore Holes Stratigraphy

Two shallow bore holes (GDH-1 and GDH-2) have been drilled in the northeastern part of the caldera floor by the Geothermal Exploration Project of the Ethiopian Ministry of Mines. The stratigraphy of the two wells, as reported by Kebede (1988), is shown in Fig. 4.

According to Kebede (1988), the borehole GDH-1 encountered alluvium, pumiceous pyroclasts, rhyolites, basalts, and pomiceous ignimbrites. Borehole GDH-2 found alluvium, pumiceous pyroclasts, rhyolites, basalts, ignimbrites,

basalts, ignimbrite and rhyolite.

Major and trace element analyses carried out on a basaltic sample coming from GDH-1 indicated a similar composition as the recent basalts associated with cinder cones. This suggests that the basaltic activity related to rifting of the Wonji fault is interfingered with the latest acidic activity of the Gedemsa caldera. However, no direct relationships between the two types of volcanism has been observed in the field.

4.SAMPLING AND PETROGRAPHY

4.1 Criteria for Sampling

The studied samples were collected from representative rock exposures with the aim to cover the entire compositional range of the volcanic sequences. The samples were selected on the basis of being fresh and unaltered. In order to detect possible vertical and lateral chemical variations, sampling has been performed at different levels and in different places for each unit. The quantity of sample was sufficiently large in order to have enough specimen for the various analytical works. Table 1 gives the location of the series and the stratigraphic position of the studied samples. Sampling localities and locations of the described sequences are shown in the attached geological map. In addition to otcropping rocks two samples coming from the borehole GDH-1 were also investigated. These samples were kindly provided by the Geothermal Project of the Ministry of Mines. For some mingled lavas, the mafic and salic portions were separated and subjected to petrographic and analytical investigation. These are labelled with the same number in Table 2, but are distinguished by "b" and "w" letters, respectively.

4.2 Petrography

The rocks from Gedemsa volcano range in composition from olivine basalt to peralkaline rhyolite, with a marked scarcity of rocks of intermediate composition. The series may be divided into the following rock types on the basis of petrography (Streckeisen, 1967) and Total Alkali vs Silica (TAS) classification grid (see fig. 5): olivine basalt, basaltic andesite, mugearite, benmoreite, trachyte and rhyolite.

4.2.1 Olivine Basalt

Olivine basalts are represented by GDCS-1 and GD-3 samples. They have a porphyritic texture (phenocryst contents about 15% of total rock volume) with phenocrysts of olivine and microphenocrysts of olivine, plagioclase and clinopyroxene set in a microcrystalline groundmass containing the same phase as

the phenocrysts. Olivine occurs as euhedral to subhedral crystals. The core sample GDCS-1 has undergone intensive alteration, and contains secondary calcite which occurs as fillings of vesicles and dispersed through the groundmass; olivine crystals are strongly altered to iddingsite. The largest olivine phenocrysts show transformation at the margins and along the fractures, whereas microphenocrysts and groundmass granules are completely transformed to iddingsite. Olivine represents about 55% of the total phenocryst assemblage.

Plagioclase (68 to 72%An determined by optical measurements on albite twinned crystals) occurs as microphenocrysts and in the groundmass. Microphenocrysts are rectangular to elongated in shape and show normal and oscillatory zoning. Sometimes reverse zoning is also observed. In the groundmass they occur as microlites. Most plagioclases are twinned according to albite law. Plagioclase contents represent about 30% of total phenocrysts. Clinopyroxene is the least abundant microphenocryst, but is widespread in the groundmass. Clinopyroxenes are colorless and comprise about 15% of total phenocrysts. They range from anhedral to acicular in shape.

4.2.2 Basaltic Andesite

Basaltic andesite (GD-13) has a porphyritic texture (phenocryst content about 20% of total rock volume) with large phenocrysts of plagioclase, clinopyroxene, olivine and opaques phenocrysts set in a microcrystalline groundmass composed of plagioclase, pyroxene and opaques. Plagioclase phenocrysts are euhedral to subhedral exhibiting normal zoning. Often they incorporate matrix, which implies very rapid growth. Opaque minerals occur as microphenocrysts, but are essentially present in the groundmass, and represent both magmatic phases and, in rare cases, exterme transformation of iddingsite. Opaques represent about 5% of total phenocrysts.

4.2.3 Mugearite

Mugearite (GD-1) is a strongly vesicular, poorly porphyritic scoria with minor plagioclase, clinopyroxene and altered olivine microphenocrysts set in a dark brown extensively oxidized glassy groundmass. The amount of phenocrysts is less than 5% of total rock volume. Plagioclase (60 to 65%An) occurs as elongated

Table 1. List and stratigraphic position of the studied samples

Bogra section
GD 28 Top of the ignimbrite
GD 27 Ignimbrite two meters below GD 28
GD 26 Ignimbrite below GD 27
GD 25 Base of the ignimbrite
GD 24 Top of the lower pumice fall deposit below GD 25
GD 23 Pumice clast below GD 24
GD 22 Pumice clast below GD 23
GD 21 Base of the lower pumice fall deposit
GD 20 Top of the rhyolite (obsidian)
GD 19 Vesicular rhyolite lava below GD 20
GD 5 Obsidian below GD 20
GD 4 Obsidian below GD 5

Northern caldera rim section
GD 37 Top of the ignimbrite
GD 38 Porphyritic obsidian at the top of the rhyolite lava
GD 48 Obsidian below GD 38
GD 36 Rhyolite lava below GD 48

Jemute fault scarp section
GD 29 Top of the ignimbrite
GD 30 Scoria below GD 29
GD 32 Ignimbrite below GD 29
GD 33 Base of the ignimbrite
GD 31 Top of the lower pumice fall deposit

Mt. Bora section
GD 34 Middle of the ignimbrite
GD 35 Middle of the lower pumice fall deposit

Southeastern caldera rim section
GD 59 Top of the obsidian
GD 17 Middle of the lower pumice fall deposit
GD 51 Top of the rhyolite

Eastern caldera rim section
GD 60 Top of the upper obsidian lava
GD 61 Obsidian below GD 60

Section about 1km SE of Bogra
GD 1 Middle of eastern phreatomagmatic ash
GD 62 Top of the ignimbrite
GD 63 Top of the rhyolite

Intra caldera cinder cone
GD 3 Basalt from the inner cinder cone

Table 1 (continued)

Kore crater
GD 2 Mixed rhyolitic-mafic lava
GD 6 Pumice fall clast
GD 7 Mixed rhyolite-mafic lava
GD 8 Aphyric rhyolite
GD 9 Aphyric rhyolite
GD 10 Mafic inclusion from the mixed lava
GD 11 Mixed rhyolite-mafic lava
GD 12 Perlitic obsidian
GD 13 Mafic inclusion from the mingled lava
GD 14 Mixed lava
GD 15 Mafic inclusion from the mingled lava

Kelo ridge
GD 18 Pumice fall clast
GD 16 Perlitic lava below GD 18
GD 47 Mingled mafic - rhyolitic lava

Core samples
GDCS 1 Basalt at 61-63m depth
GDCS 2 Ignimbrite at 97-100m depth

Other samples
GD 39 Lava from Bora hill
GD 41 Rhyolitic lava from Didimtu
GD 43 Lava from Mt. Cheka
GD 46 Ignimbrite from Jumute
GD 49 Ignimbrite along Awash river
GD 54 Obsidian near Cheka

crystal, poorly zoned with typical albite twinning. Plagioclase is estimated to represent about 60% of total phenocryst volume. Olivine is also slightly elongated and partially transformed to iddingsite. Olivine forms about 25% of total phenocrysts. Clinopyroxene is present in small amounts as microphenocryst and as fine grained granules in the groundmass.

4.2.4 Benmoreite

Benmoreites GD10 and GD15 represent mafic inclusions within post caldera acid lavas. They have scarcely porphyritic (with phenocrysts content about 5% of total rock volume) and porphyritic (with phenocrysts content around 20% of total rock volume) texture, respectively. GD10 contains clinopyroxene phenocrysts and clinopyroxene and plagioclase microphenocrysts set in a fine microcrystalline matrix composed of plagioclase, clinopyroxene and opaques. This sample also contains secondary fluorite filling vesicles.

GD15 is dominated by large phenocrysts of plagioclase, some clinopyroxene and altered olivine (iddingsitized) phenocrysts set in a microcrystalline groundmass containing acicular clinopyroxene, plagioclase lath and opaques. Plagioclase (15 to 17%An) phenocrysts are large, subhedral, exhibiting normal zoning and are generally poorly twinned. Plagioclase content is about 50% of phenocrysts. Olivine occurs as phenocryst, microphenocryst and in the groundmass as euhedral to subhedral crystal. Olivine represents about 20% of total phenocrysts. Clinopyroxene phenocrysts are pale yellow in color, sometimes show twinning. They are subhedral to euhedral, unzoned and contain inclusions of opaques.

GD15 shows clear petrographic evidenced of mingling in thin section where a portion of salic material is observed in contact with the mafic benmoreite. The salic material contains alkali feldspar and plagioclase set in a microcrystalline groundmass composed of alkali feldspar, quartz and opaques. The contact between the mafic and the salic portions forms a convoluted pattern, indicating mingling in a molten stage.

4.2.5 Trachyte

Trachytes are represented by GD2, 4, 7, 8, 11, 14, 25, 26, 27, 28, 29, 30, 32, 33, 37 and 47 samples, and, for the largest part, are characterized by mingled

textures, with the exception of three samples (GD4, 8 and 25). The mingled rocks consist of different proportions of two lithologies, respectively salic and mafic in composition. The mafic materials are present in a subordinate amount with respect to salic ones. They generally occur as elongated shards sometimes in an advanced stage of disaggregation. In some cases (e.g. GD7) the mafic material is totally dispersed within the salic rock and its presence is revealed by large xenocrysts of plagioclase and olivine still surrounded by a mafic fine graine matrix. When present in discrete fragments, the mafic materials show a porphyritic texture with phenocrysts of plagioclase and altered mafic minerals (generally olivine) set in a cryptocrystalline mafic matrix (e.g. GD2, 14). Finally, in a few cases the salic and the mafic materials are intimately intermingled, indicating advanced stage of mechanical interaction (e.g. GD47). Textural evidence clearly indicates that mafic material interacted with salic magma when it was in a liquid state. This may have happened during eruption, possibly by tapping of a small volume zoned reservoir.

Trachytes include lavas and ignimbrites, and both contain the mafic material described above. Lavas are represented by GD2, 7, 11, 14 and 47 samples. They have a porphyritic texture (with phenocryst contents about 10% of total rock volume) with phenocrysts of sanidine, plagioclase, alkali pyroxene, aenigmatite, quartz and opaques set in a partially devitrified microcrystalline groundmass containing alkali feldspar, quartz and opaques. Sanidine phenocrysts are large, euhedral to subhedral with rounded edges indicating resorption and are commonly twinned according to Carlsbad law. Plagioclase (oligoclase) phenocrysts are euhedral to subhedral and exhibit oscillatory zoning. Clinopyroxene phenocrysts are small, subhedral, yellowish green to green in color and most are twinned. Sometimes green clinopyroxene crystals are enclosed by sanidine phenocrysts. Quartz grains are always small and frequently occur as anhedral rounded crystals.

Trachytic ignimbrites include GD26, 27, 28, 29, 30, 32, 33 and 37 samples. They show evident eutaxitic texture (especially samples GD27, 28, 33 and 37), with crystals of dominant sanidine (70% of total phenocrysts) and subordinate alkali pyroxene, aenigmatite, quartz, biotite and opaques set in a glassy matrix made up of glass shards accompanied by tiny crystals of alkali feldspar and quartz. The amount of phenocrysts ranges from 10 to 20% of total rock volume. They also contain angular fragments of dark salic rocks, probably representing another ignimbrite. Sanidine phenocrysts are large, euhedral to subhedral and always have rounded edges; most of them are twinned according to Carlsbad law.

Sometimes sanidine phenocrysts are enclosed by dark scoria-like material, which, in spite of the color, have only slightly less acidic composition than the salic portion. In the groundmass, sanidine occurs as elongated microlites. Clinopyroxene phenocrysts are green, subhedral, unzonned and rarely show twinning. Biotite microphenocrysts are small and euhedral.

Trachytes GD4, 8 and 25 are not mingled rocks. GD4 and 25 are obsidians, containing sanidine, alkali pyroxene and aenigmatite set in an oxidized glassy matrix. GD8 is a scarcely porphyritic lava with microphenocrysts of sanidine, alkali pyroxene and aenigmatite set in a partially devitrified hypocrystalline groundmass containing alkali feldspar, quartz and opaques.

4.2.6 Rhyolite

Rhyolites are represented by GDCS2, GD5, 6, 9, 12, 16, 17, 18, 19, 20, 21, 22, 23, 24, 31, 34, 35, 36, 38, 51, 59, 60, 61, 63 samples. They have variable textures. A group of samples (GD5, 20, 38) is holoyaline with accessory amounts of sanidine microphenocrysts. Other rocks (GD12,16,34, 59, 60) are hypocrystalline and consist of phenocrysts of sanidine, biotite, green clinopyroxene, brown amphibole and aenigmatite set in a glassy groundmass which shows flow textures. GD59 and GD60 samples appear different, in that they show a slightly recrystallized glassy matrix. Samples GDCS2, GD6, 17, 18, 21, 22, 23, 24, 31, 35 are pumices and show highly vesicular glassy textures (pumiceous texture) with very few crystals of sanidine, alkali pyroxene, aenigmatite and brown amphibole (or biotite?). Some samples (e.g GD-18) show devitrification features. Finally, samples GD9, 19, 36, 51, 62, 63 are scarcely porphyritic with a few sanidine and rare aenigmatite and alkali pyroxene phenocrysts. The groundmass is composed of microlitic feldspars, quartz and opaques set in a partially devitrified matrix.

5. GEOCHEMISTRY AND PETROLOGY

5.1 Analytical Methods

Major and trace element abundances have been determined at the Istituto di Scienze della Terra, University of Messina, Italy, by combined wet chemical methods and X-ray fluorescence spectroscopy. Rock samples have been crushed in a steel jaw-crusher, quarted and reduced to a fine powder before analyses.

Na_2O and MgO have been determined by Atomic Absorption Spectrophotometry after attack of the powdered samples by Hf-HCl. Loss on Ignition (LOI) has been determined by heating 500 mg of sample at 950° C and measuring the loss of weight. No correction for oxidation of Fe^{2+} has been done. The other major elements have been determined by X-ray fluorescence on pure powder pellets, using routinary full matrix correction methods. Trace elements have been determined by X-ray fluorescence on the same pellets used for major elements using several international rock standards for curve calibration and applying mathematical corrections for matrix effects .

Errors on trace elements are lower than 10% for Ba, Nb, Y, and Cr and lower than 5% for Rb, Sr, Zr and Ni.

F and Cl have been determined at the Dipartimento di Mineralogia e Petrologia, University of Padua, Italy, by specific electrode methods. Precision expressed as relative standard deviation is lower than 5% for F and lower than 10% for Cl.

5.2 Results and Classification

Major and trace element data together with CIPW norms are reported in Table 2. Total iron is expressed as FeO_t. Major element data have been recalculated and normalized to 100% on a water-free basis.

A combination of chemical classification schemes has been followed for volcanic rocks of Gedemsa caldera to discriminate the rock series and as a basis for the nomenclature of the rocks.

The products of Gedemsa volcano cover a compositional range from basalt to rhyolite. The series is dominated by evolved silica-rich rocks with intermediate

rocks being very scarce. The rocks represent a saturated series in which basic samples are Hy-normative and silicic ones are invariably Q-normative. Most of the silicic rocks contain modal aenigmatite. Acmite is present in the norm showing the peralkaline character of these samples. However, only a few samples have Na_2O+K_2O/Al_2O_3 ratios higher than unity. Five pumiceous rhyolites (GD-17, 21, 22, 23, 24) do not contain normative acmite, in spite of their compositional resemblance for many major elements to the rest of the rhyolitic samples. Note, however, that these samples have much lower Na_2O and higher H_2O contents than other rhyolitic rocks, which suggest modification by secondary alteration processes.

On the basis of the TAS classification scheme (Le Bas, 1986), the analyzed rocks appear to belong to the Na-transitional series, since they plot approximately on the boundary between subalkaline and alkaline field (Fig. 5). A transitional nature for basic rocks is also indicated by the classification scheme of Piccirillo et al (1979).

The acidic samples have been further classified according to the scheme of Mc Donald and Bailey (1972) on the normative quartz versus normative femics diagram (Fig. 6), which indicates the predominance of pantellerites over comendites.

The pattern of iron enrichment shown by the series on the AFM diagram (Fig. 7) is also indicative of a transitional character with a tholeiitic affinity, inasmuch as the mafic and intermediate samples plot on the line typical of Hawaian tholeiites. Note also that there is some enrichment in Fe in the most acidic rocks, a feature which has been observed in other alkaline and peralkaline rhyolites.

All these classification schemes allow to establish the following observations:

1) A transitional nature between alkali basalts and tholeiites is shown by the available chemical analyses for the basalts.

2) Intermediate rocks are very scarce.

3) The silicic rocks are largely peralkaline, with predominance of pantellerites over comendites. Mohr (1970) attributed the scarcity of comendites to the degree of rifting. The proportion of comendites has been observed to decrease as the rift evolves, and in a well developed rift system where crustal attenuation is more intensive comendites are virtually absent.

5.3 Major and Trace Element Variation

5.3.1 Major Elements

The analyzed samples have a large range of SiO_2 contents (49.54 to 76.32 wt%). TiO_2 is invariably low (< 0.85%), except for basic and intermediate samples which show values from 1.31 to 2.72%. The content of Al_2O_3 is relatively low (7.41 - 14.60%) with the exception of sample CD13 which has 20.19% Al_2O_3, most probably indicating plagioclase accumulation. CaO and MgO range between 0.21- 10.20 and 0.01 - 8.73%, respectively, the highest value being registered in the basalt samples. FeO_{tot} is less variable and all the rocks, including the most acidic ones, are relatively enriched in FeO_{tot} (5.94 - 11.70). Most of the rocks contain substantial amounts of Na_2O (1.52 - 7.46%) and K_2O (1.13 - 5.37%). P_2O_5 is relatively low (< 0.39%) and only samples GD-10 and GD-1 have values of 0.88 and 1.51%, respectively.

Fig. 8 reports the variations of major elements against SiO_2. The rocks display well defined negative trends of MgO, CaO, FeO_t, TiO_2 and to a lesser extent P_2O_5 versus SiO_2, and positive correlation for K_2O. Na_2O increases up to 70%wt SiO_2 and then decreases sharply with ia further increase of SiO_2 content. Al_2O_3 maintains a constant value up to 60%wt SiO_2 and then decreases with increasing SiO_2 contents.

Within the general variation trends, considerable dispersions are also observed, partly due to secondary alteration processes and partly to crystal accumulation, but also due to some petrological processes which must be investigated. Samples or group of samples which show significant deviations from the main trends include:

1. GD6,17,18,21,24,31,35 and GD4,25,29,32,33 are rich in K_2O. These rocks also display an enrichment in alkali feldspar phenocrysts which may indicate that the high potassium derives from feldspar accumulation.

2. GD5,12,16,20,34,38 are rich in Na_2O and represent a rock rich in alkali pyroxene, alkali amphibole and alkali feldspar. Again alkali feldspar accumulation may account for the high sodium abundance of these rocks.

3. GD13 shows anomalous high CaO, Al_2O_3 and and low FeO_t, which are explained by accumulation of plagioclase in this highly porphyritic rock.

4. GD1, 10 show high P_2O_5 and TiO_2 contents as compared to other mafic-

Table 2. Chemical analyses (major elements as wt%, trace element in ppm) and CIPW norms of Gedemsa volcanics.

	GDCS1	GD3	GD1	GD13	GD10	GD15	GD30
SiO_2	49.54	49.89	52.17	53:43	56.84	61.35	63.41
TiO_2	1.97	1.98	2.72	1.31	2.22	1.19	0.84
Al_2O_3	15.02	14.75	15.02	20.19	13.90	15.57	14.08
FeO	10.43	10.47	10.93	6.97	10.23	7.82	8.08
MnO	0.19	0.19	0.26	0.15	0.28	0.34	0.51
MgO	7.76	8.82	3.73	3.22	2.64	1.36	0.26
CaO	10.64	9.51	7.98	9.65	5.58	3.85	1.89
Na_2O	2.90	2.87	4.11	3.45	5.16	5.30	6.09
K_2O	1.20	1.14	1.56	1.33	2.28	2.98	4.70
P_2O_5	0.38	0.39	1.51	0.32	0.88	0.25	0.14
Total	100.00	100.00	100.00	100.00	100.00	100.00	100.00
LOI	3.05	0.10	1.65	0.80	0.85	0.80	1.90
Cl	---	272	---	447	319	194	---
F	---	488	---	469	2216	817	---
Rb	30	25	28	57	49	46	50
Ba	319	332	599	458	2395	1713	2597
Sr	429	410	568	576	360	201	53
Nb	28	26	39	31	54	47	43
Zr	158	158	235	225	328	293	244
Y	20	23	47	33	133	43	54
Ni	141	143	1	16	15	9	1
Cr	321	312	1	1	1	1	1
AN	49.89	49.81	34.13	55.04	15.53	18.05	0.00
Q	0.00	0.00	3.83	4.05	4.70	8.18	4.35
Or	6.80	6.68	8.86	7.68	13.18	17.32	26.65
Ab	23.52	24.03	33.51	28.60	42.73	44.09	44.33
An	23.42	23.75	17.36	35.02	7.86	9.71	0.00
Di	19.97	16.39	9.15	8.00	11.25	6.26	7.18
Hy	5.70	12.29	9.77	7.82	7.03	6.33	6.18
Ol	7.48	6.57	0.00	0.00	0.00	0.00	0.00
Ac	0.00	0.00	0.00	0.00	0.00	0.00	4.48
Mt	4.92	5.02	5.97	4.03	5.32	3.87	1.10
Il	3.59	3.72	4.98	2.43	4.12	2.22	1.54
Ap	0.83	0.90	3.38	0.72	1.99	0.58	0.30
NMS	0.00	0.00	0.00	0.00	0.00	0.00	0.00
Rb/Sr	0.070	0.061	0.049	0.057	0.158	0.244	0.868
K/Rb	332	379	461	333	332	505	849
K/Ba	31.2	28.5	21.6	24.0	7.9	14.4	15.1
den	2.69	2.69	2.64	2.58	2.57	2.49	2.45

Continued: Table 2

	GD26	GD25	GD37	GD33	GD27	GD32	GD14
SiO_2	63.85	64.13	65.21	66.16	65.57	66.47	67.69
TiO_2	0.85	0.78	0.83	0.69	0.85	0.67	0.74
Al_2O_3	12.96	13.89	13.04	13.23	12.81	12.87	12.38
FeO	8.29	7.88	8.09	6.86	7.79	7.07	6.18
MnO	0.53	0.49	0.45	0.39	0.44	0.41	0.21
MgO	0.36	0.32	0.42	0.35	0.50	0.32	1.04
CaO	3.05	1.71	1.90	1.37	2.11	1.62	2.44
Na_2O	5.76	6.15	5.78	5.99	5.76	5.87	5.50
K_2O	4.18	4.55	4.16	4.85	4.01	4.62	3.68
P_2O_5	0.16	0.12	0.14	0.10	0.17	0.09	0.14
Total	100.00	100.00	100.00	100.00	100.00	100.00	100.00
LOI	1.10	1.00	0.95	1.15	0.65	1.25	0.60
Rb	50	52	55	66	68	74	109
Ba	2898	2137	2451	1074	2597	791	362
Sr	33	25	31	87	55	54	144
Nb	47	48	56	64	70	72	99
Zr	268	261	323	367	394	407	698
Y	42	41	49	68	57	57	86
Ni	1	1	1	1	1	1	13
Cr	1	1	1	1	1	1	1
AN	0.00	0.00	0.00	0.00	0.00	0.00	0.00
Q	7.15	5.57	9.77	9.70	10.82	11.04	15.34
Or	24.05	26.36	24.11	27.72	23.28	26.71	21.10
Ab	42.15	45.13	43.13	39.73	42.88	39.65	41.85
An	0.00	0.00	0.00	0.00	0.00	0.00	0.00
Di	12.05	6.61	7.30	5.22	8.05	6.42	9.17
Hy	4.47	6.94	6.73	6.30	5.96	6.17	3.34
Ac	4.61	5.12	4.27	6.28	4.49	6.25	2.86
Mt	1.07	0.71	1.21	0.00	1.14	0.00	1.78
Il	1.58	1.44	1.54	1.27	1.60	1.25	1.37
Ap	0.37	0.28	0.32	0.23	0.39	0.21	0.32
NMS	0.00	0.00	0.00	0.50	0.00	0.45	0.00
Rb/Sr	1.515	2.080	1.774	0.759	1.236	1.370	0.757
K/Rb	695	727	627	610	489	518	280
K/Ba	12.0	17.7	14.1	37.5	12.8	48.4	84.5
den	2.46	2.44	2.45	2.42	2.45	2.42	2.42

Continued: Table 2

	GD2	GD4	GD17	GD29	GD28b	GD28w	GD21
SiO_2	67.86	67.17	72.68	68.71	68.70	69.06	74.58
TiO_2	0.64	0.54	0.41	0.68	0.60	0.62	0.44
Al_2O_3	12.31	13.64	11.88	10.89	11.13	10.85	10.66
FeO	6.04	5.78	6.26	7.21	7.00	6.91	5.82
MnO	0.22	0.31	0.24	0.35	0.35	0.33	0.21
MgO	0.80	0.09	0.16	0.27	0.32	0.30	0.22
CaO	2.11	1.00	0.54	1.29	1.46	1.36	1.02
Na_2O	5.68	6.52	2.84	6.08	6.04	6.08	1.67
K_2O	4.22	4.90	4.95	4.42	4.34	4.42	5.36
P_2O_5	0.13	0.06	0.03	0.11	0.08	0.08	0.03
Total	100.00	100.00	100.00	100.00	100.00	100.00	100.00
LOI	1.60	0.40	7.70	0.90	1.20	1.15	8.05
Cl	---	730	---	---	365	113	---
F	---	922	---	---	1291	1096	---
Rb	112	64	123	92	90	91	126
Ba	272	362	111	962	612	606	76
Sr	83	1	18	28	28	28	10
Nb	101	60	117	87	94	92	126
Zr	735	335	801	538	567	569	817
Y	95	47	95	77	78	75	109
Ni	12	1	7	8	8	6	11
Cr	1	1	1	1	1	1	1
AN	0.00	0.00	9.37	0.00	0.00	0.00	25.57
Q	14.07	10.84	30.35	19.13	18.49	19.75	36.09
Or	24.11	28.66	26.82	25.41	25.12	25.53	28.90
Ab	38.50	42.44	22.09	30.58	32.41	30.47	12.86
An	0.00	0.00	2.28	0.00	0.00	0.00	4.42
Di	7.98	4.01	0.00	4.88	5.78	5.35	0.00
Hy	4.38	4.94	6.04	6.93	6.51	6.41	5.22
Ac	6.13	5.87	0.00	6.25	6.05	6.10	0.00
Mt	0.00	0.00	2.73	0.00	0.00	0.00	0.00
Il	1.18	1.01	0.72	1.25	1.12	1.16	0.76
Ap	0.30	0.14	0.07	0.25	0.19	0.19	0.07
NMS	0.23	1.29	0.00	2.89	2.52	2.99	0.00
Rb/Sr	1.349	64.000	6.833	3.286	3.214	3.250	12.600
K/Rb	313	635	334	398	400	403	353
K/Ba	128.8	112.3	369.9	38.1	58.8	60.5	585.7
den	2.41	2.40	2.39	2.41	2.41	2.41	2.38

Continued: Table 2

	GD7	GD35	GD31	GD11b	GD8	GD6	GD18
SiO_2	69.43	73.17	72.15	69.83	70.37	72.88	73.49
TiO_2	0.59	0.39	0.42	0.60	0.44	0.21	0.21
Al_2O_3	11.95	11.03	9.22	11.06	10.59	8.03	7.85
FeO	5.86	5.71	6.50	6.25	6.06	7.44	7.65
MnO	0.21	0.20	0.27	0.23	0.29	0.31	0.31
MgO	0.77	0.16	0.20	0.76	0.10	0.07	0.13
CaO	1.82	0.37	0.59	1.50	1.31	0.27	0.77
Na_2O	5.36	3.69	5.29	5.63	6.24	5.16	3.89
K_2O	3.93	5.25	5.32	4.04	4.58	5.60	5.69
P_2O_5	0.09	0.03	0.04	0.10	0.03	0.03	0.03
Total	100.00	100.00	100.00	100.00	100.00	100.00	100.00
LOI	0.40	5.85	3.45	0.60	1.35	4.45	5.00
Cl	---	---	---	149	---	2950	2487
F	---	---	---	1526	---	2470	2301
Rb	115	140	122	115	117	222	162
Ba	283	95	99	311	335	120	131
Sr	96	2	11	71	64	1	67
Nb	97	125	127	108	98	216	160
Zr	704	863	778	799	663	1508	1059
Y	83	103	113	105	91	208	156
Ni	10	11	10	14	7	21	12
Cr	1	1	1	1	1	1	1
AN	0.00	0.00	0.00	0.00	0.00	0.00	0.00
Q	18.29	27.12	27.96	20.52	22.54	31.63	32.89
Or	22.75	28.96	29.79	23.52	26.59	31.44	31.74
Ab	38.75	25.70	16.90	33.91	28.44	9.58	8.22
An	0.00	0.00	0.00	0.00	0.00	0.00	0.00
C	0.00	0.00	0.00	0.00	0.00	0.00	0.00
Di	7.09	1.36	2.22	5.77	5.50	0.97	3.04
Hy	4.45	5.45	7.29	6.17	4.87	10.01	9.34
Ac	5.00	3.00	5.50	6.05	5.58	4.92	4.92
Mt	0.51	1.19	0.00	0.00	0.00	0.00	0.00
Il	1.10	0.68	0.76	1.12	0.82	0.38	0.38
Ap	0.21	0.07	0.09	0.23	0.07	0.07	0.07
NMS	0.00	0.00	4.48	1.44	3.98	6.12	4.02
Rb/Sr	1.198	70.000	11.091	1.620	1.828	222.000	2.418
K/Rb	284	311	362	292	325	209	291
K/Ba	115.3	458.6	445.7	107.8	113.5	387.6	360.3
den	2.40	2.38	2.38	2.40	2.39	2.39	2.39

Continued: Table 2

	GD23	GD22	GD9	GDCS2	GD34	GD24	GD16
SiO_2	75.81	75.33	71.08	73.36	72.16	76.32	72.63
TiO_2	0.38	0.39	0.47	0.29	0.16	0.36	0.14
Al_2O_3	10.51	10.68	10.82	9.63	8.10	9.76	7.87
FeO	5.86	5.69	6.24	6.78	7.61	5.19	7.40
MnO	0.24	0.23	0.29	0.28	0.26	0.19	0.26
MgO	0.19	0.19	0.12	0.14	0.01	0.20	0.13
CaO	0.38	0.51	0.70	0.37	0.24	1.01	0.25
Na_2O	2.32	2.46	5.67	4.57	7.09	1.78	6.95
K_2O	4.29	4.50	4.59	4.56	4.33	5.16	4.33
P_2O_5	0.03	0.03	0.03	0.03	0.04	0.03	0.03
Total	100.00	100.00	100.00	100.00	100.00	100.00	100.00
LOI	7.80	7.30	0.60	3.10	0.50	6.50	0.89
Cl	---	1521	---	---	---	---	1512
F	---	160	---	---	---	---	3138
Rb	142	128	124	188	150	124	159
Ba	61	70	349	238	149	82	125
Sr	15	27	10	5	4	27	6
Nb	134	127	98	179	172	117	182
Zr	885	822	658	1220	1136	754	1216
Y	115	109	75	176	153	100	183
Ni	7	7	7	19	13	10	20
Cr	1	1	1	1	1	1	1
AN	7.87	9.97	0.00	0.00	0.00	18.55	0.00
Q	38.88	37.12	23.77	29.53	30.95	39.33	31.99
Or	23.28	24.58	26.83	25.88	25.23	28.49	25.12
Ab	18.02	19.29	29.76	23.20	17.33	14.05	16.10
An	1.54	2.14	0.00	0.00	0.00	3.20	0.00
C	1.32	0.84	0.00	0.00	0.00	0.00	0.00
Di	0.00	0.00	2.86	1.41	0.83	1.11	0.93
Hy	5.54	5.29	6.65	8.62	10.83	4.11	10.71
Ac	0.00	0.00	5.67	5.15	4.80	0.00	4.74
Mt	2.68	2.70	0.00	0.00	0.00	2.60	0.00
Il	0.66	0.68	0.87	0.53	0.30	0.65	0.27
Ap	0.07	0.07	0.07	0.07	0.09	0.07	0.07
NMS	0.00	0.00	2.62	1.89	8.48	0.00	8.45
Rb/Sr	9.467	4.741	12.400	37.600	37.500	4.593	26.500
K/Rb	251	292	307	201	239	345	226
K/Ba	583.9	533.1	109.2	159.0	241.0	522.2	287.3
den	2.38	2.38	2.39	2.39	2.39	2.37	2.39

Continued: Table 2

	GD19	GD11w	GD12	GD36	GD5	GD38	GD20
SiO_2	72.94	73.06	72.47	73.19	72.79	72.82	73.20
TiO_2	0.37	0.44	0.16	0.42	0.35	0.33	0.30
Al_2O_3	10.17	10.29	8.18	9.46	8.98	9.11	9.40
FeO	6.21	5.45	6.92	6.70	6.32	6.32	5.77
MnO	0.27	0.21	0.25	0.28	0.23	0.25	0.20
MgO	0.20	0.28	0.01	0.20	0.02	0.01	0.08
CaO	0.35	0.53	0.21	0.47	0.24	0.24	0.23
Na_2O	4.81	5.38	7.51	4.63	6.63	6.47	6.40
K_2O	4.65	4.32	4.27	4.62	4.43	4.44	4.41
P_2O_5	0.04	0.04	0.02	0.03	0.01	0.01	0.01
Total	100.00	100.00	100.00	100.00	100.00	100.00	100.00
LOI	1.50	0.85	0.30	1.25	0.30	0.20	0.10
Cl	---	189	---	---	1963	---	1348
F	---	1135	---	---	2268	---	2102
Rb	95	126	205	133	134	131	135
Ba	82	217	138	101	66	90	74
Sr	39	13	1	9	1	1	1
Nb	142	122	207	133	136	132	134
Zr	897	878	1450	817	836	816	853
Y	141	107	201	108	117	114	118
Ni	7	10	16	10	10	10	8
Cr	1	1	1	1	1	1	1
AN	0.00	0.00	0.00	0.00	0.00	0.00	0.00
Q	28.25	28.16	31.42	30.40	30.64	30.50	30.48
Or	26.89	25.06	25.06	26.89	25.94	26.12	25.88
Ab	25.90	28.35	18.16	22.61	21.39	22.00	23.61
An	0.00	0.00	0.00	0.00	0.00	0.00	0.00
Di	1.26	2.04	0.81	1.84	1.00	1.00	0.96
Hy	7.81	5.91	9.66	8.33	7.81	7.92	7.11
Ac	5.38	5.58	4.80	5.53	5.35	5.29	5.21
Mt	0.00	0.00	0.00	0.00	0.00	0.00	0.00
Il	0.68	0.82	0.30	0.78	0.66	0.63	0.57
Ap	0.09	0.09	0.05	0.07	0.02	0.02	0.02
NMS	1.83	2.33	9.20	2.26	6.57	6.15	5.64
Rb/Sr	2.436	9.692	205.000	14.778	134.000	131.000	135.000
K/Rb	406	285	173	288	274	282	271
K/Ba	470.5	165.3	256.8	379.6	556.5	409.9	494.8
den	2.38	2.37	2.38	2.39	2.37	2.37	2.37

intermediate samples. It is unlikely that these features are derive from any kind of accumulation of mineral phases. Rather, it seems likely that the abundances of these two oxides indicate that there are two distinct trends in the mafic rocks, which could indicate different types of mafic magmas.

5. Five pumiceous rhyolites (GD17, 21, 22, 23, 24) have low Na_2O and high LOI which reflect secondary alteration of pumices as a result of interactions with water.

5.3.2 Trace Elements

The large ion lithophile elements (LILE) display variable values. Rb has variable but generally high abundances. Ba and Sr are very depleted in acid rocks and show medium to high abundances in the intermediate and basic samples. The primitive members of Gedemsa have the lowest Rb/Sr ratios and the highest ratios are observed in pantellerites, corresponding to the lowest content of Sr and the highest content in Rb. K/Rb and K/Ba ratios also increase strongly from mafic to acidic rocks.

The high field strength elements (HFSE) Nb and Zr but also Y have very variable but generally high values in the analyzed samples.

A strong depletion is observed for the ferromagnesian trace elements Cr and Ni in all the samples, except for the two basalts.

Fig. 9 shows variation diagrams of trace elements against silica. Rb, Nb, Zr and Y increase slightly passing from mafic to intermediate samples, whereas they show a very steep increase in the most acidic composition where they reach extremely high abundances. Sample GD-10 is the only intermediate rock which shows anomalously high Y content, comparable to some rhyolites. Ba and Sr increase from basalt to mugearite and benmoreite displaying a strong decrease in the trachytes and rhyolites. Variation diagrams of Nb and Rb vs silica also show that a group of acidic rocks fall outside the trends defined by the bulk of the samples. This deviation is due to anomalous high silica of these samples. Inspection of Table 2 indicates that these samples are represented by the pumices with etremely high LOI and low Na_2O. The most likely possibility is that the silica contents of these samples has been overestimated after calculation on a water-free basis. This makes these samples to fall outside the main trends. The volatile elements F and Cl also show highly variable contents. Variation diagrams against silica clearly indicate that both these elements increase sharply passing from

intermediate to acid rocks where they reach concentration of some thousand ppm. One sample (GD10) has anomalously high F content, for its intermediate major element composition. This is related to the secondary enrichment processes evidenced by the presence of fluorite filling vesicles. Since this sample has also shown high Y, it must be concluded that secondary processes also produced an enrichment in this element which, most probably, is present in the fluorite as isomorphic substitute for Ca (see Deer et al., 1978).

Figure 10 reports the abundance of incompatible trace elements normalized to a primordial mantle composition for selected samples. The various samples exhibit different patterns and trends. The trends for the basic samples are those typical of transitional within plate volcanics. They show poorly fractionated patterns with a slight upward convexity. The acid samples all show more complicated patterns with positive spikes of Rb, K, Nb, Zr and Y, and negative anomalies of Ba, Sr, P, Ti. Both these characteristics become most striking with increasing acidity of the rocks.

Fig. 5 Alkali (wt.%) vs silica (wt.%) classification diagram for the Gedemsa volcanics (after Le Bas et al., 1986)

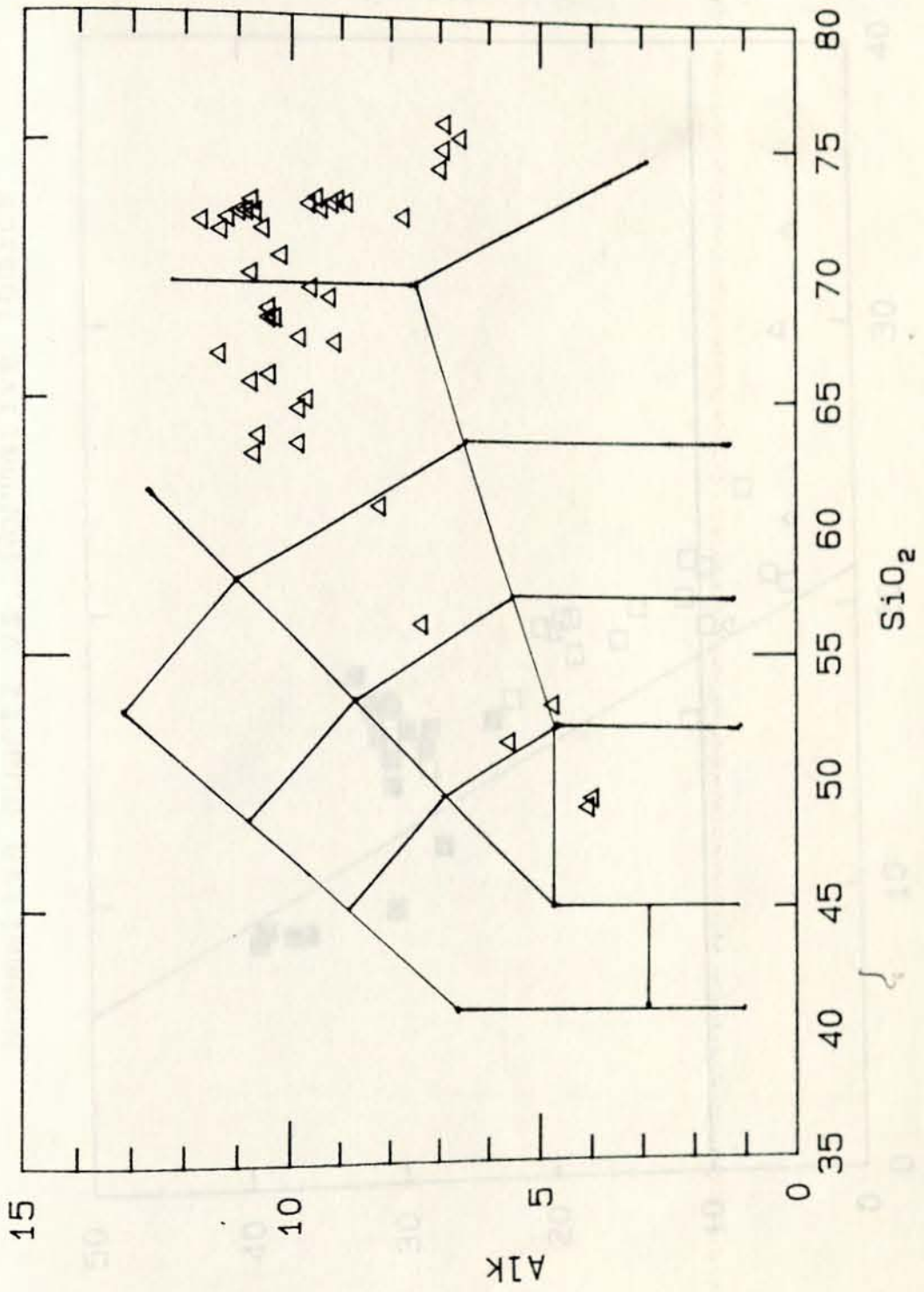

Fig. 6 Classification of the analyzed peralkaline trachytes and rhyolites (after Mc Donald and Bailey, 1972). open triangles: intermediate rocks: open

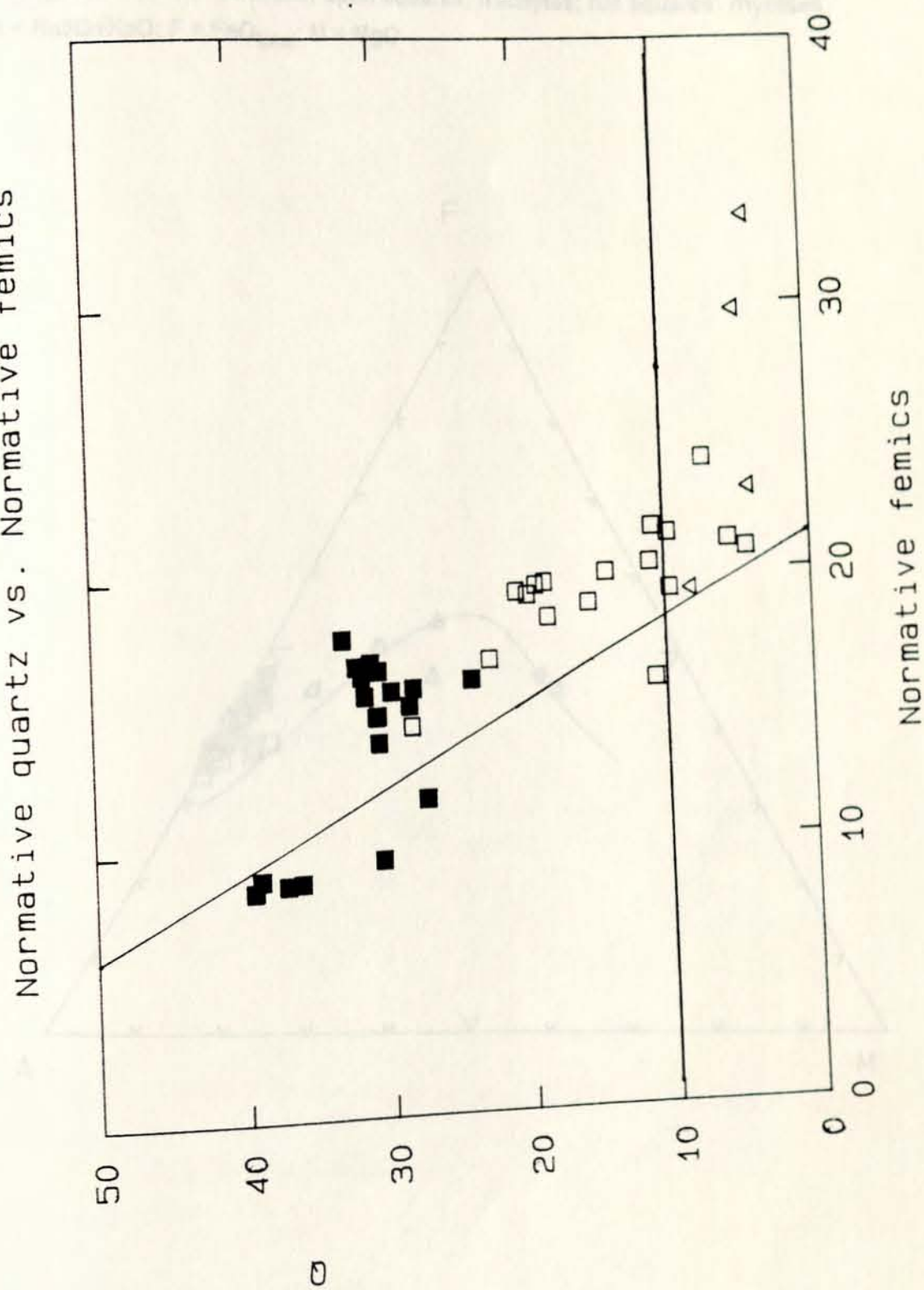

Fig. 7 AFM Diagram for the Gedemsa volcanics. Full circles: basalts; open triangles: intermediate rocks; open squares: trachytes; full squares: rhyolites. A = Na_2O+K_2O; F = FeO_{total}; M = MgO

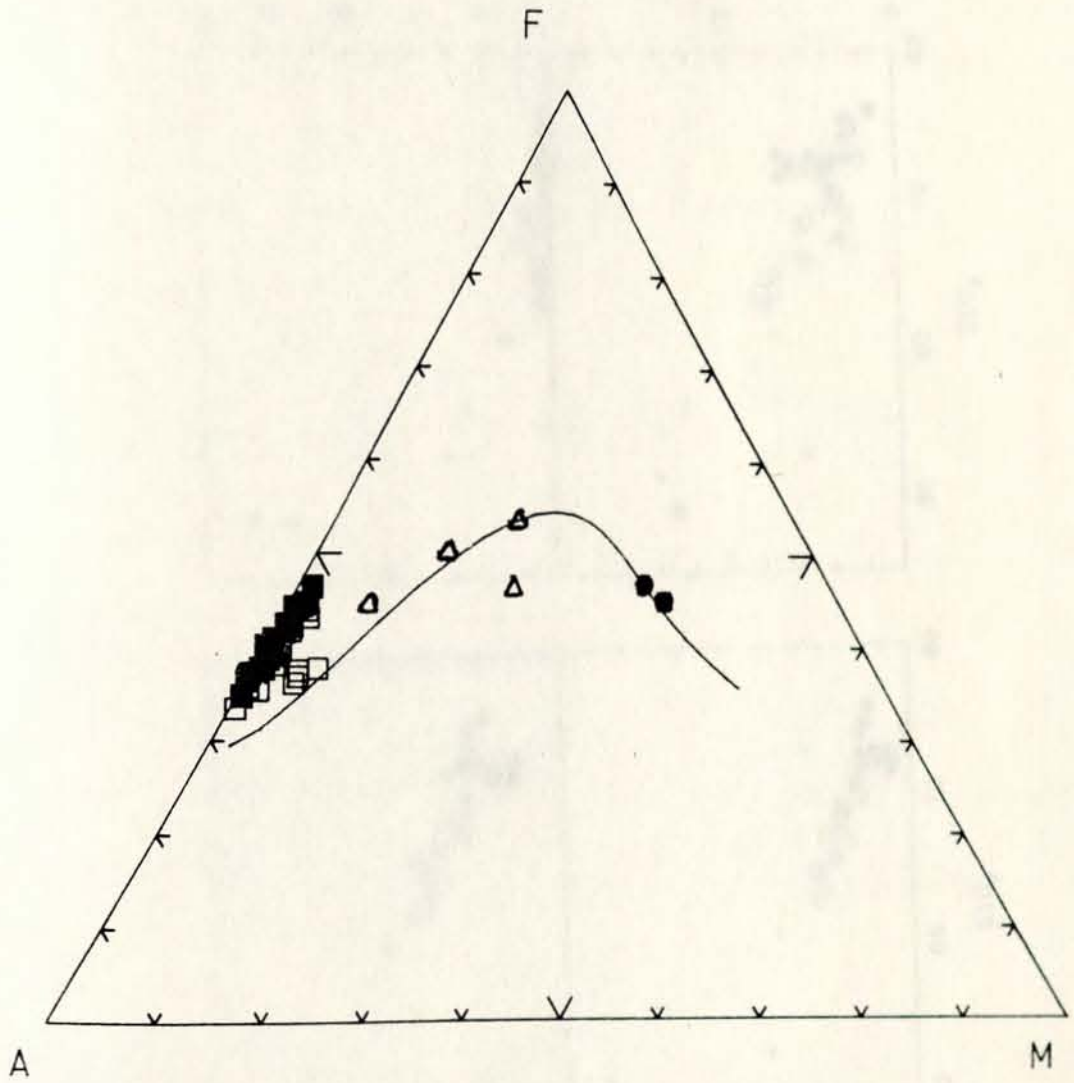

Fig. 8 Variation diagrams of major elements (wt.%) vs. SiO_2 (wt.%). Symbols as in Fig. 7.

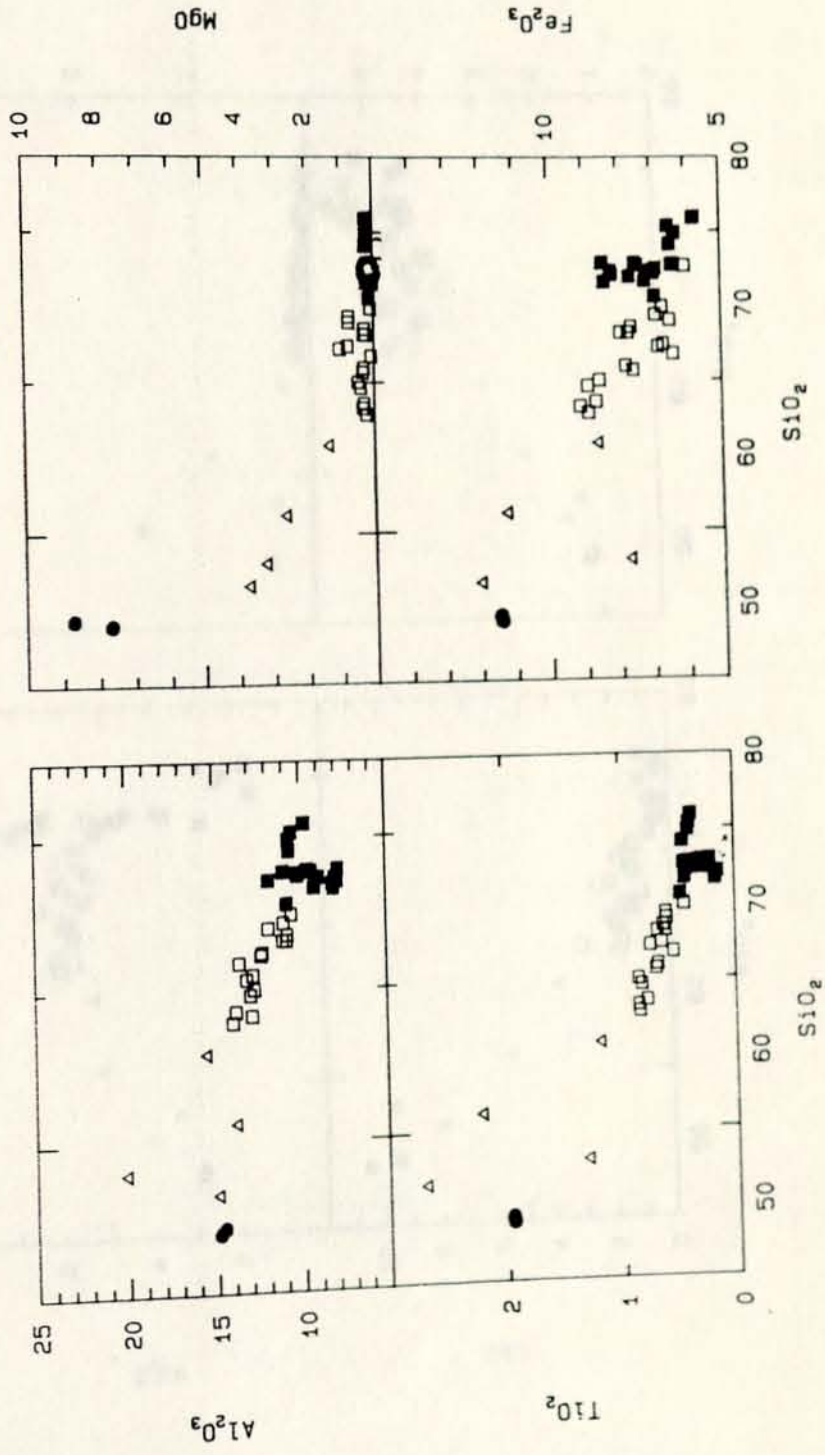

Fig. 8. (Continued)

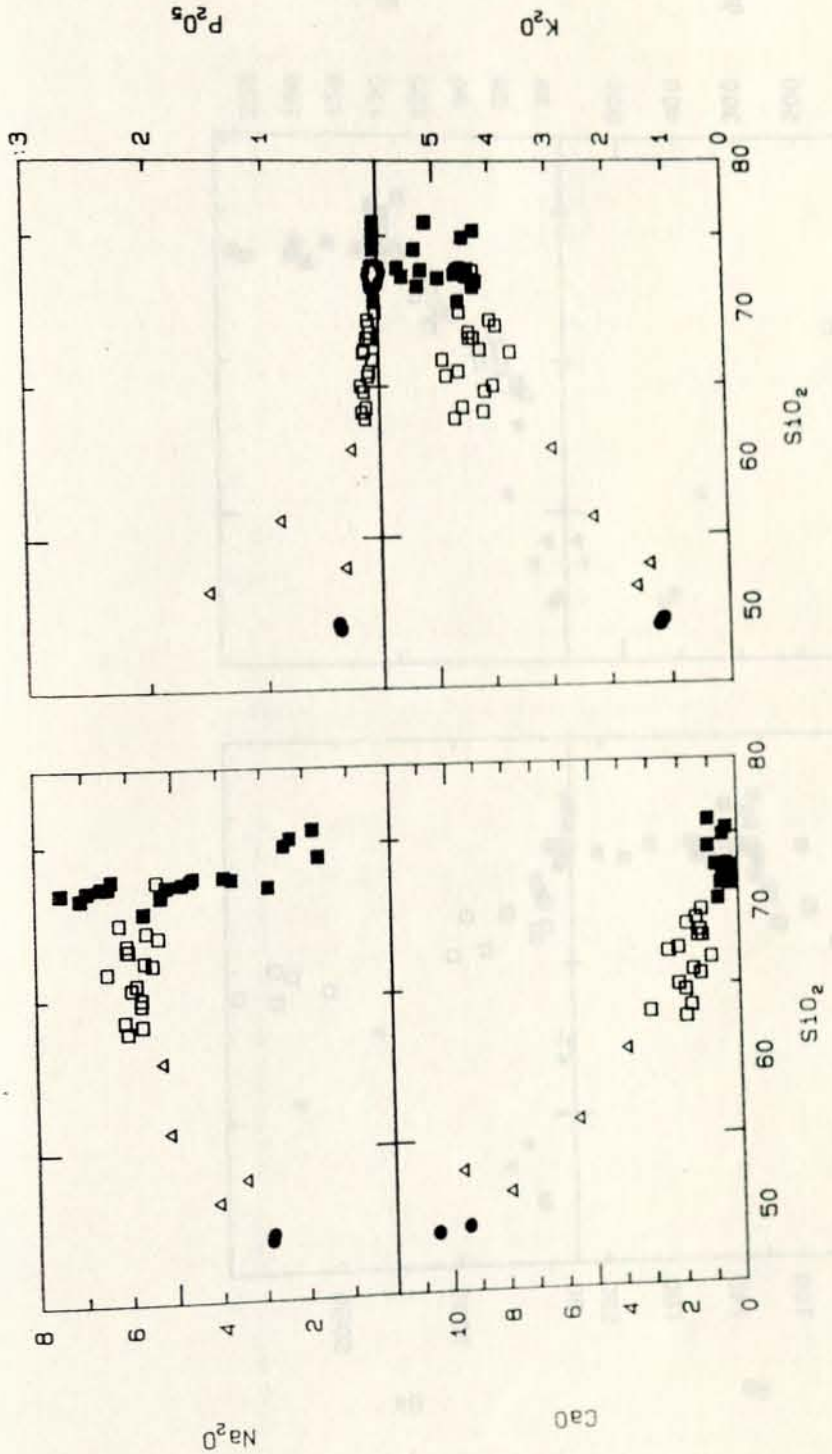

Fig. 9. Variation diagrams of trace elements (ppm) vs. SiO_2 (wt.%). Symbols as in Fig. 7.

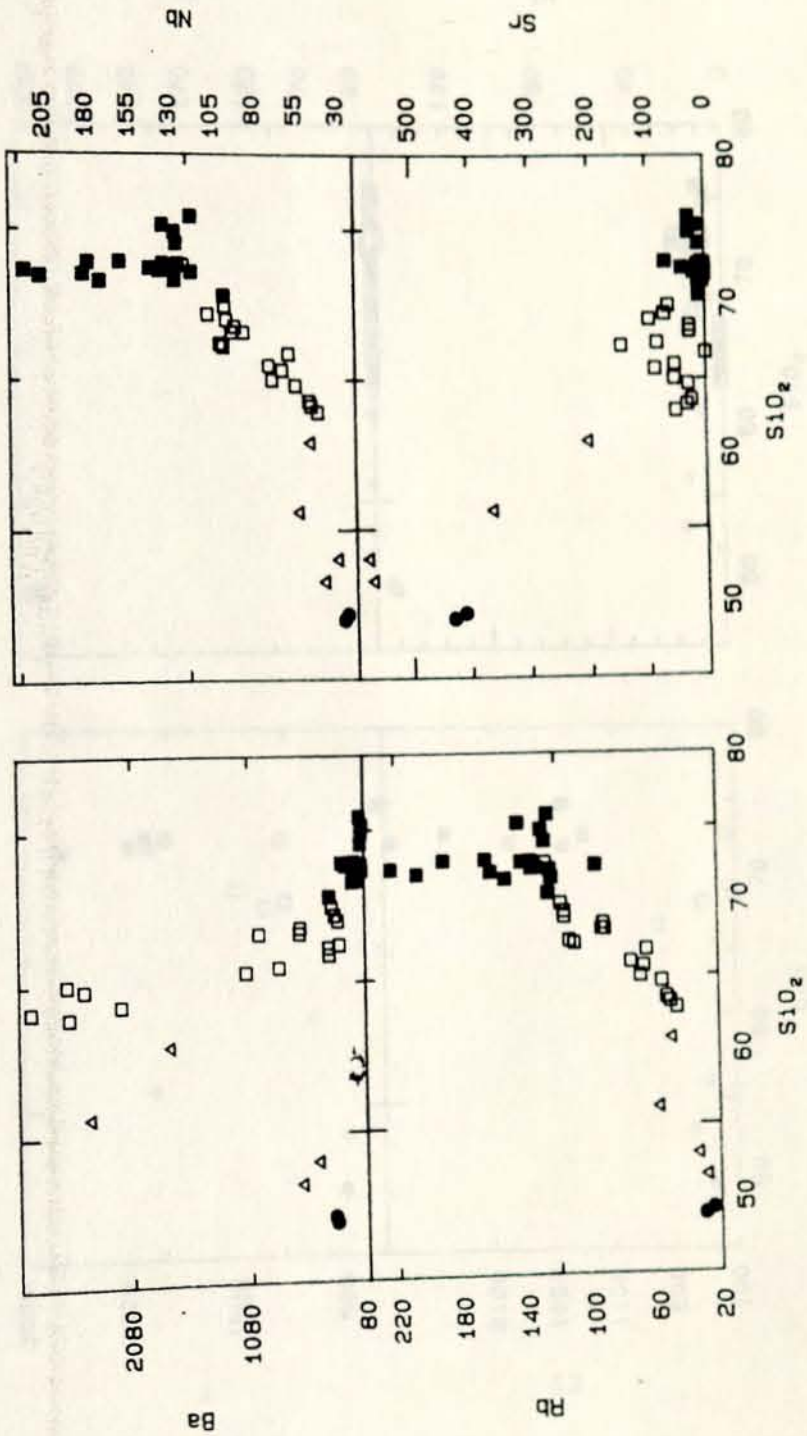

Fig. 9. (continued)

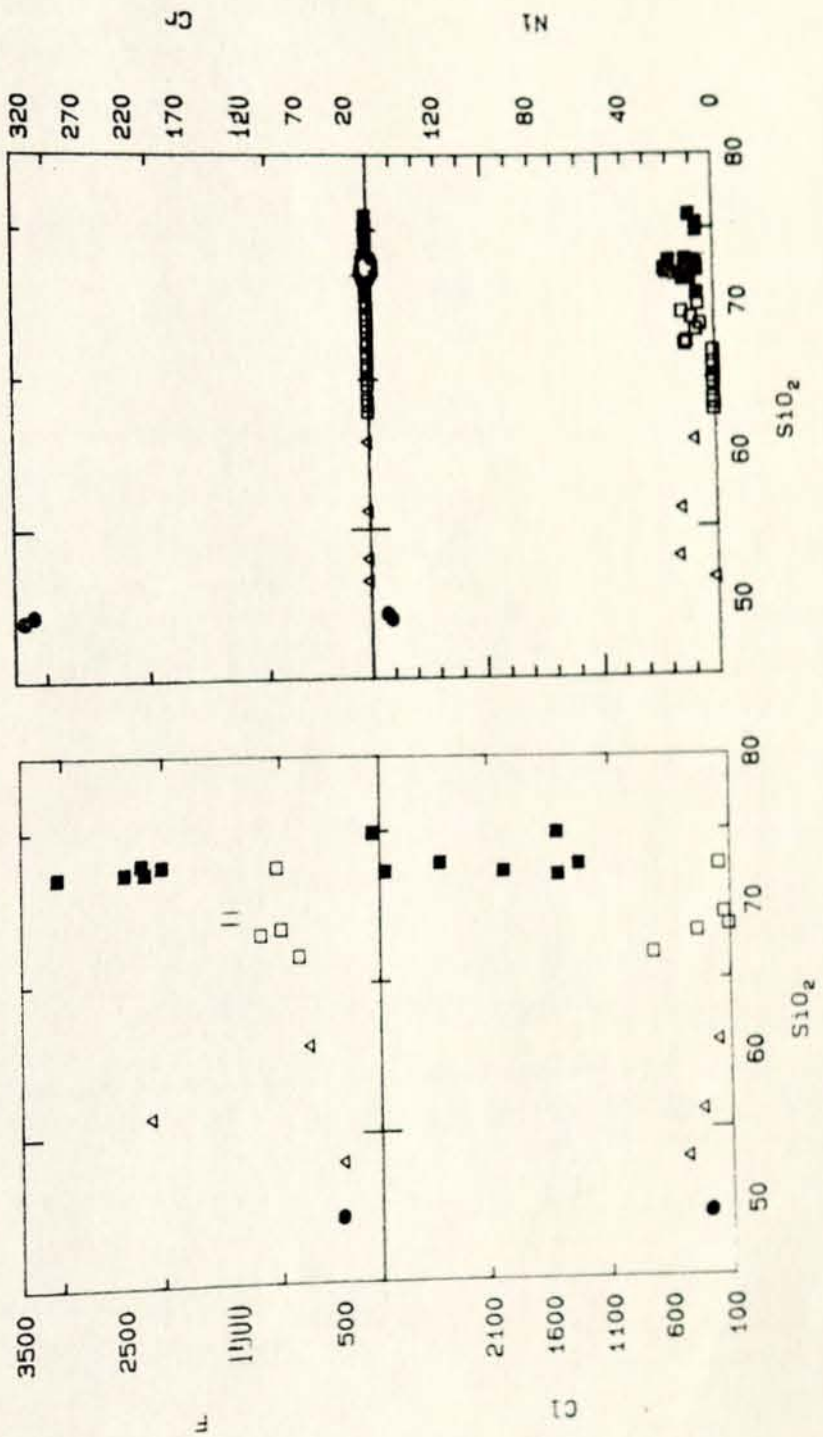

Fig. 9. (continued)

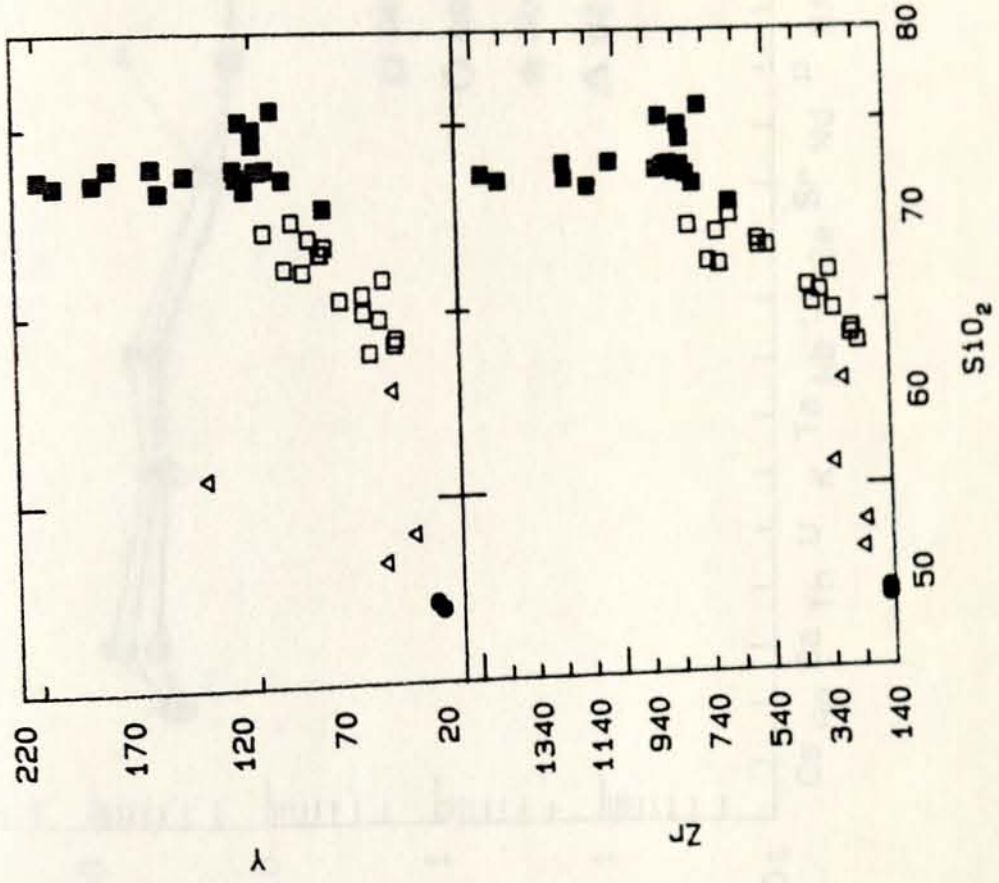

Fig. 10. Incompatible element patterns normalyzed to a primordial mantle composition (spidergrams) of the analyzed rocks.

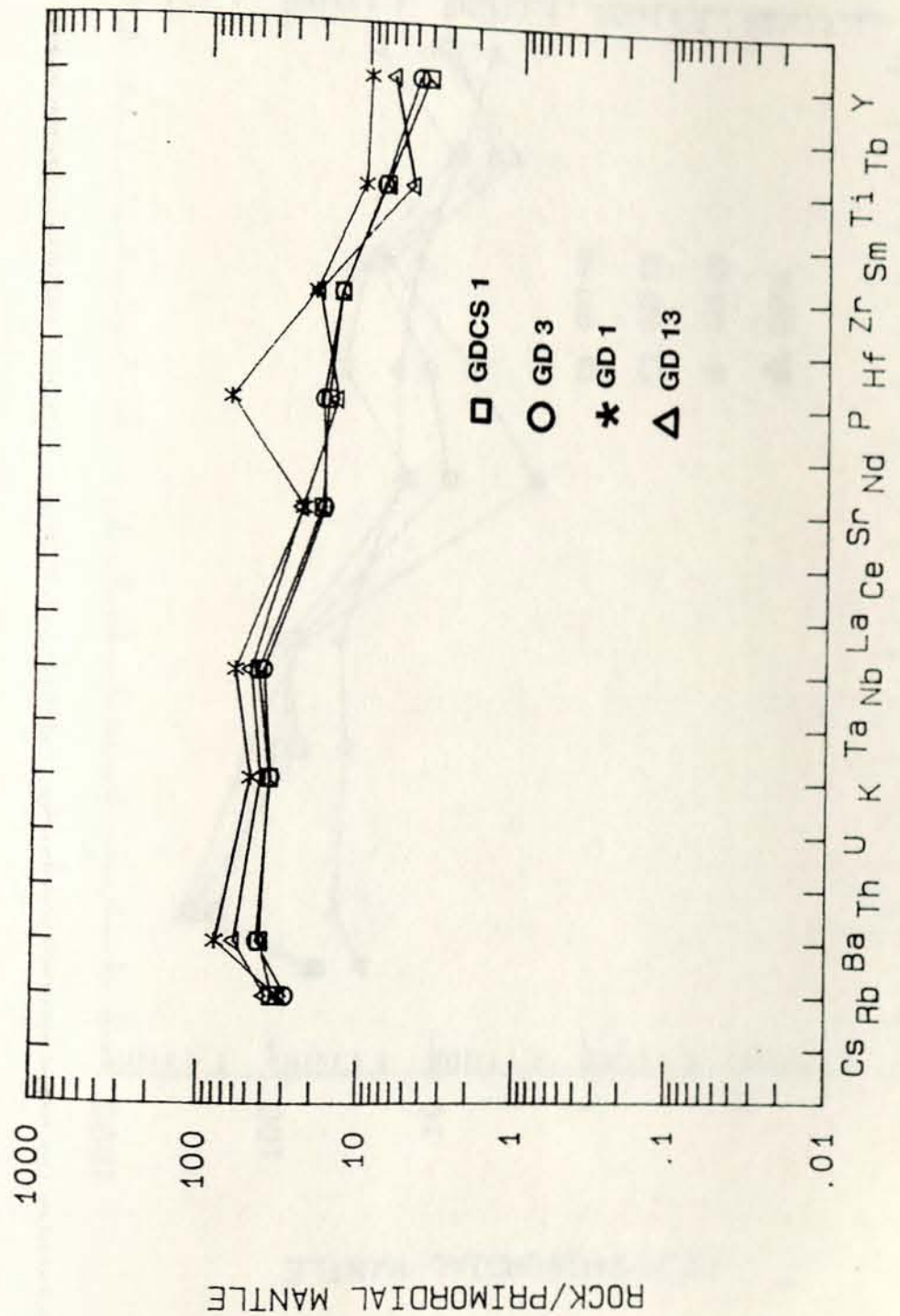

Fig.10.2.

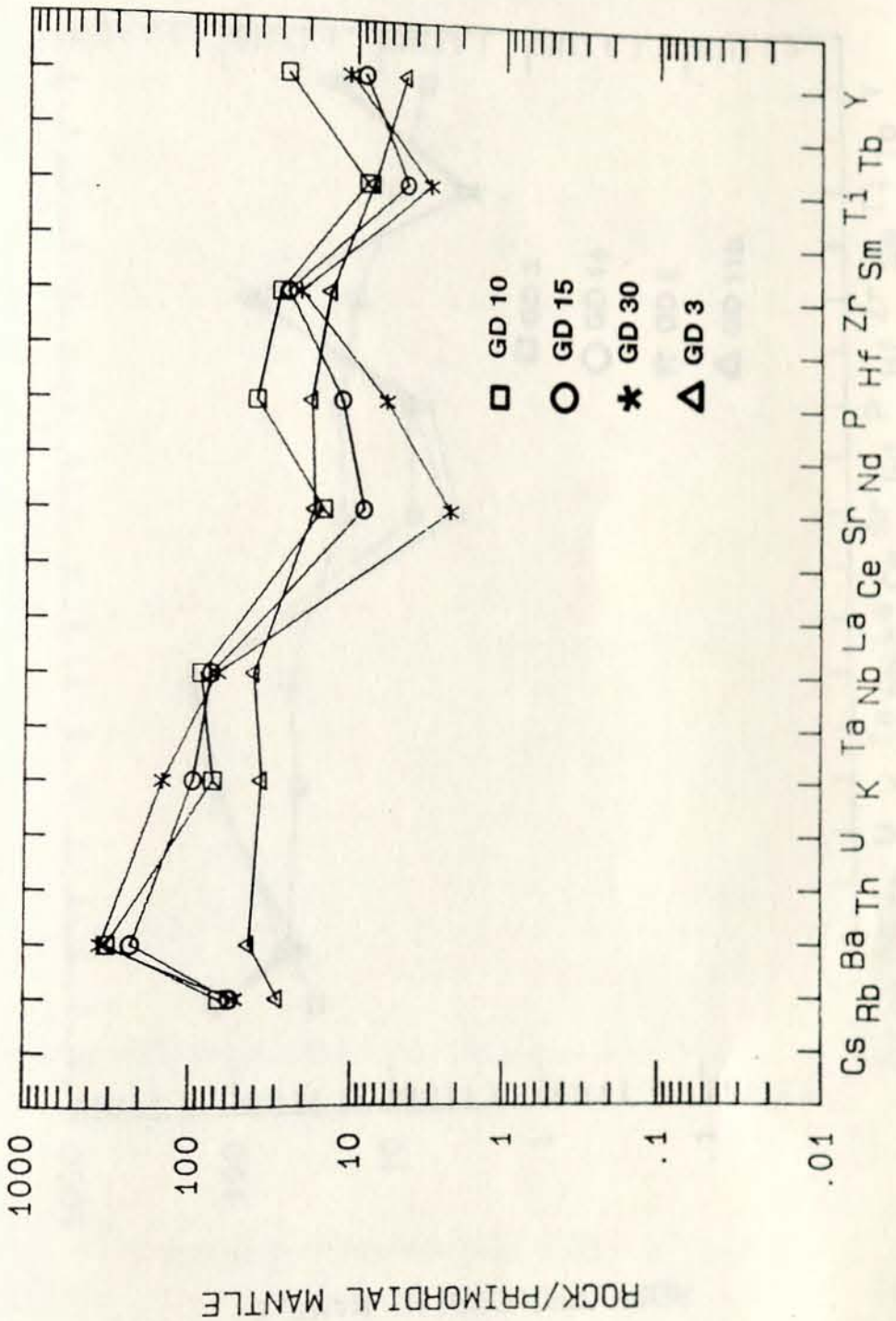
ROCK/PRIMORDIAL MANTLE
1000
100
10
1
.1
.01
Cs Rb Ba Th U K Ta Nb La Ce Sr Nd P Hf Zr Sm Ti Tb Y
GD 10
GD 15
GD 30
GD 3

Fig.10.3.

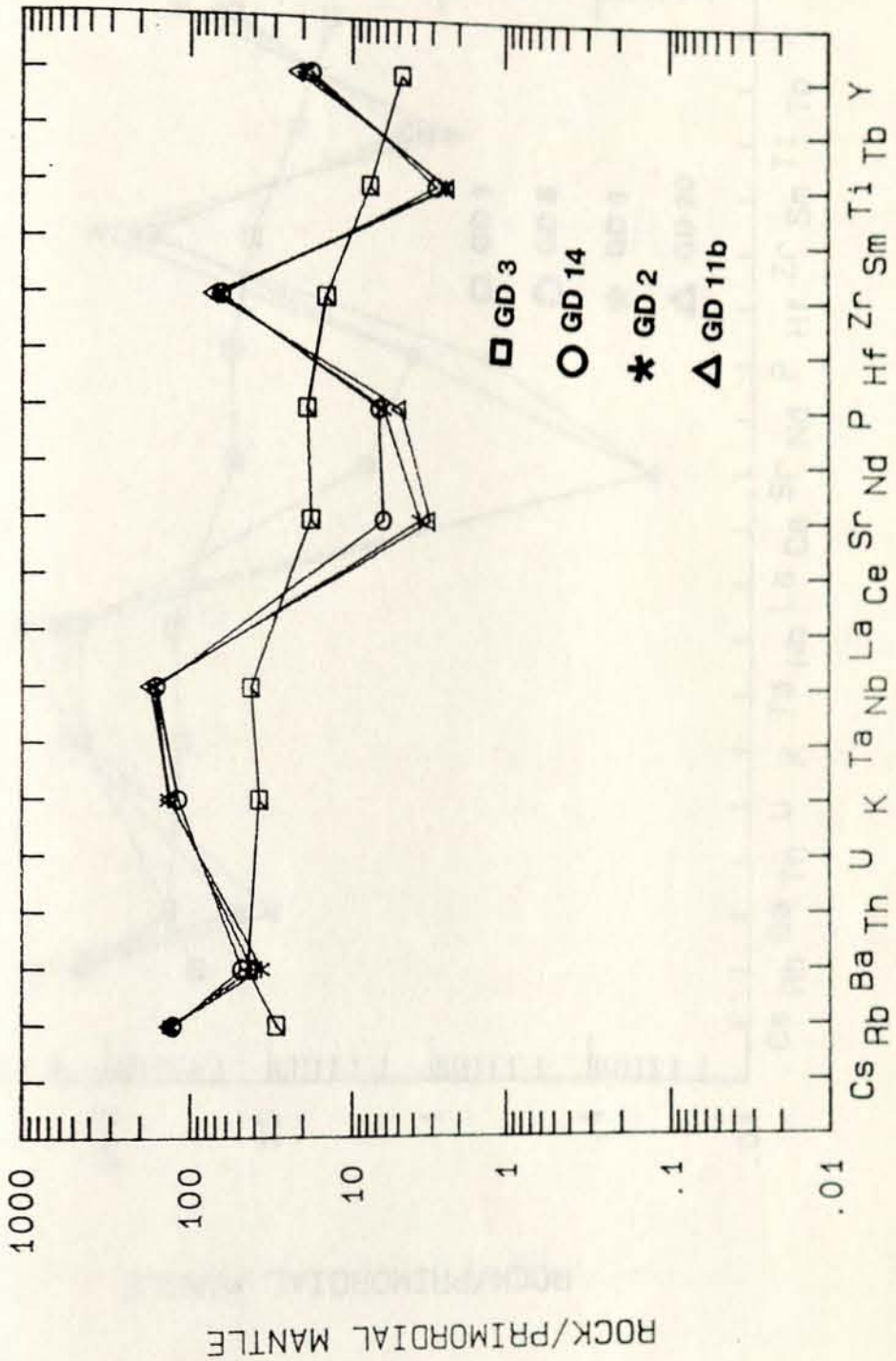
ROCK/PRIMORDIAL MANTLE
1000
100
10
1
.1
.01
Cs Rb Ba Th U K Ta Nb La Ce Sr Nd P Hf Zr Sm Ti Tb Y
GD 3
GD 14
GD 2
GD 11b

Fig.10.4.

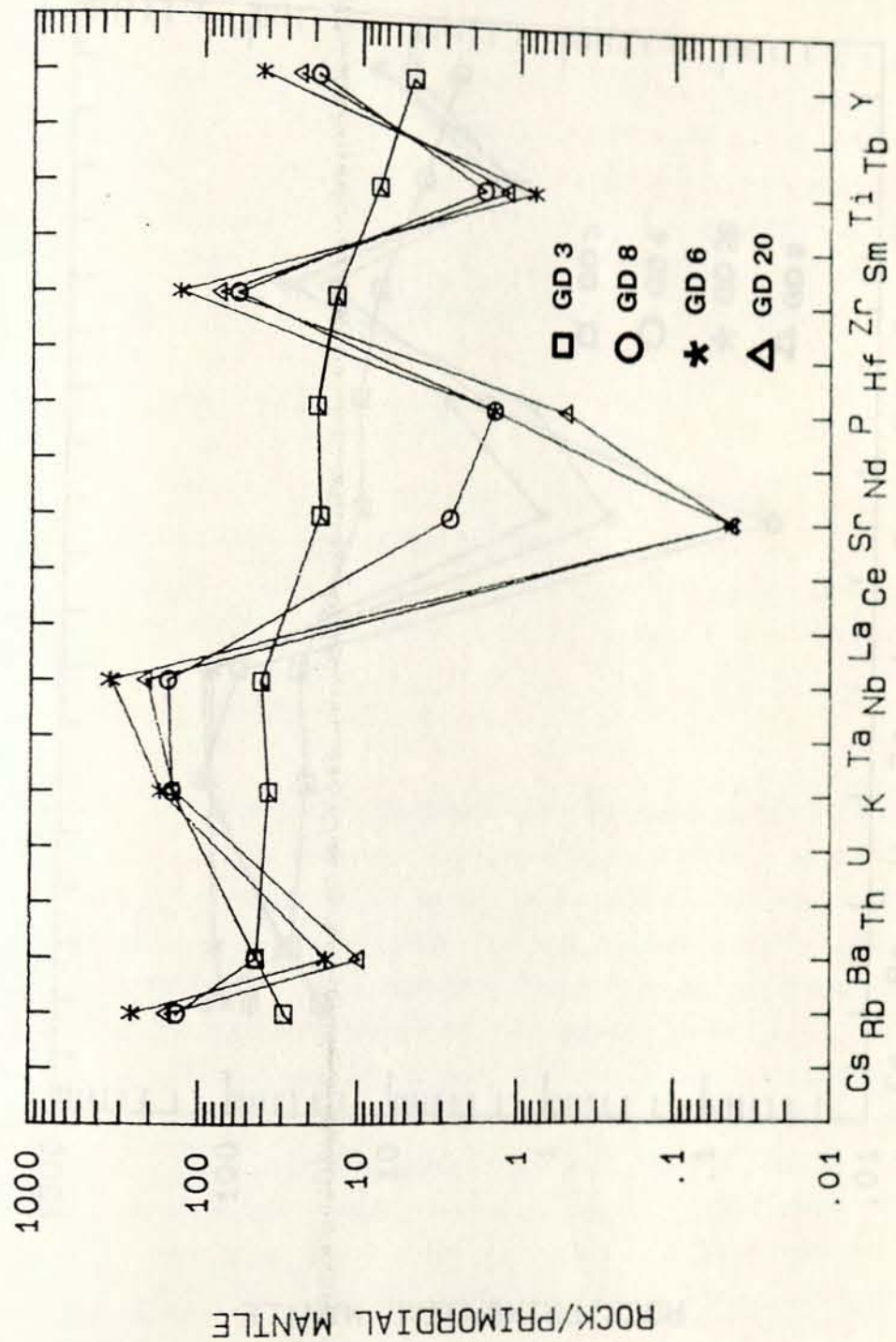
ROCK/PRIMORDIAL MANTLE
1000
100
10
1
.1
.01
Cs Rb Ba Th U K Ta Nb La Ce Sr Nd P Hf Zr Sm Ti Tb Y
GD 3
GD 8
GD 6
GD 20

Fig. 10.5.

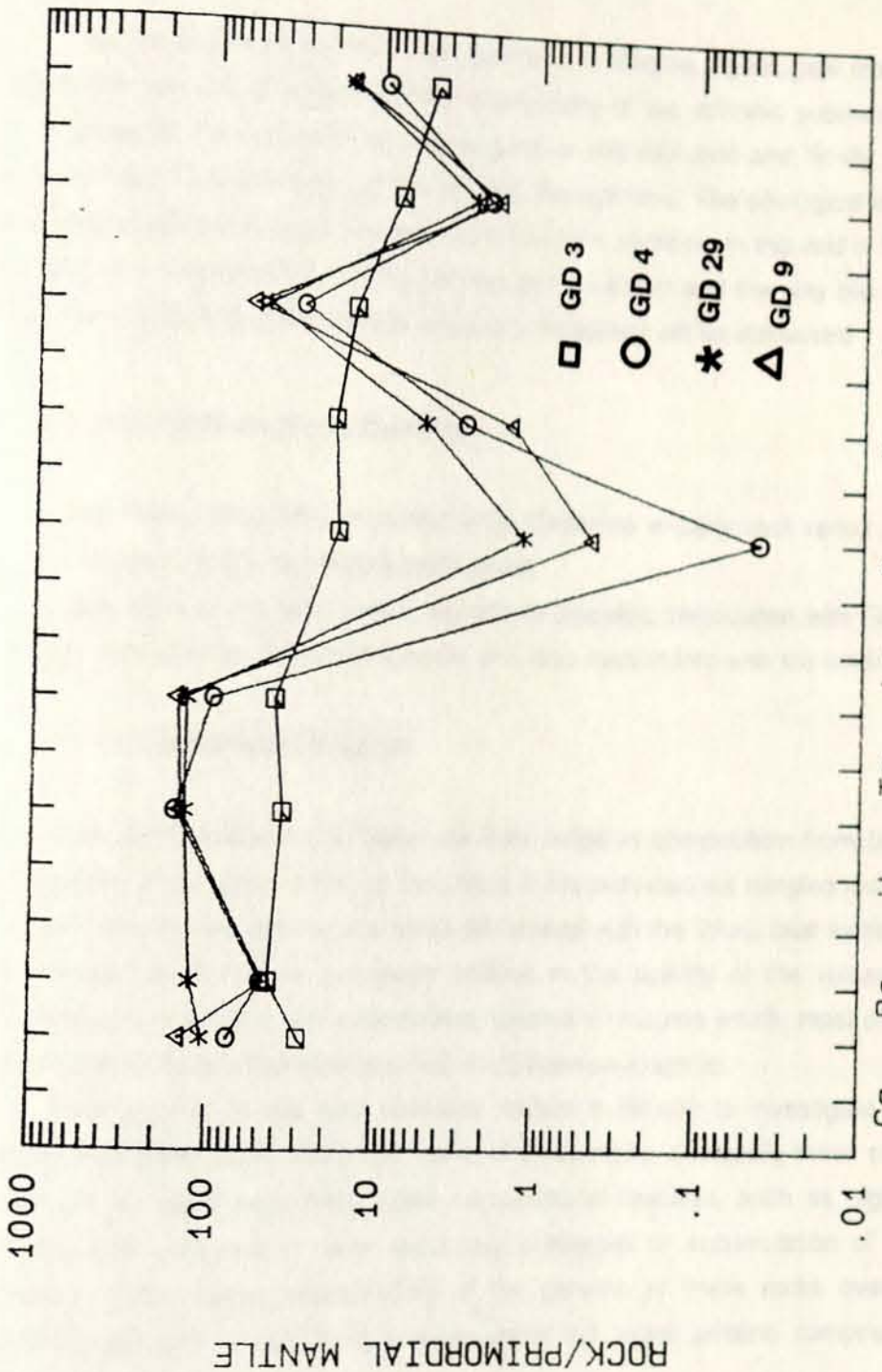
GD 3
GD 4
GD 29
GD 9
1000
100
10
1
.1
.01
Cs Rb Ba Th U K Ta Nb La Ce Sr Nd P Hf Zr Sm Ti Tb Y
ROCK/PRIMORDIAL MANTLE

6. DISCUSSION

The present thesis had the main objectives to compile a geological map of the Gedemsa volcano, to reconstruct the stratigraphy of the volcanic successions, to investigate on the processes of magma genesis and evolution and, finally, to work out a model for the evolution of the volcano through time. The geological map and the stratigraphy have been reported in the previous sections. In this and in the next chapter the processes of magma genesis and evolution and the way the volcano has been behaving during various phases of its activity will be discussed.

6.1 Magma Genesis and Evolution

The main petrogenetic problems of the Gedemsa volcanic rock series are:

1. the origin of the peralkaline silicic rocks.
2. the origin of the mafic rocks, basaltic to hawaiitic, associated with Gedemsa activity and with the Wonji fault system, and their relationship with the acidic rocks.

6.1.1 Origin of Mafic Magmas

The mafic rocks in the Gedemsa area range in composition from basalt to mugearite. They occur either as inclusions in the post-caldera mingled lavas or as surges, strombolian scorias and lavas associated with the Wonji fault system. The first lavas are somehow genetically related to the activity of the volcano. The second group of lavas are independent batches of magma which, most probably, have little or no direct relationship with the Gedemsa magmas.

The scarcity of the data available makes it difficult to investigate on the genesis of mafic rocks. Moreover, some of these rocks, especially those collected from the mingled lavas have some compositional features, such as high F, Y, Al_2O_3 which are due to either secondary processes or accumulation of mineral phases. This makes understanding of the genesis of these rocks even more difficult, since it is very hard to understand the exact pristine composition of magmas.

However, inspection of the magmatophyle element patterns (Fig.10) indicates that sample GD13, belonging to mingled intracalderic lavas, has a similar

incompatible element abundances and ratios as the basalts connected to the Wonji fault system. The main difference is that GD13 has lower TiO_2 than the Wonji basalts. However, this is easily explained by the fact that GD13 is more evolved than the other basalts and the lower Ti could be due to some fractionation of Fe-Ti oxides. Accordingly, the data available indicate that the Gedemsa mafic magmas had a similar composition as those erupted along the Wonji faults and both could be generated in an astenospheric mantle (Woldegabriel, 1987).

6.1.2 Origin of Acid Magmas

The high abundance of acidic rocks is the main petrological feature of the Gedemsa volcano. Such a characteristics is observed in many other volcanoes along the rift (e.g. Kampunzu and Mohr, 1991) . Accordingly, the understanding of the processes which generated acidic magmas is important not only to understand Gedemsa volcano but to shed light on a first order magmatologic process of regional importance.

Several genetic hypotheses have been so far proposed in order to explain the geochemistry of the peralkaline silicic rocks of the Gedemsa caldera. Damte (1990) largely on the basis of the huge volumes of acidic products, has proposed a genesis by melting of lower crust. Similar hypotheses have been suggested by several authors for explaining the genesis of huge volumes of acid volcanics in distensive tectonic environments (see Davies and MacDonald, 1987, and references therein). EIGS and Elc (1987) on major element basis showed that the different products of Gedemsa have a common parental magma and they are linked by differentiation processes through fractional crystallization. Di Paola (1972) proposed a model for the close association of peralkaline silicic rocks with the basalts of transitional nature by fractionation processes.

The data obtained in the present study allow to put some constraints on the genesis of acid rocks at Gedemsa. This will be done by calculating quantitative melting and fractional crystallization models to see which one of the two fit better the geochemical data obtained in this thesis.

6.1.2.1 *Partial Melting Models*

The main problem in the calculation of models of partial melting is that of

chosing a composition for the source rock. In the case of crustal melting, the problem is even more difficult, given the large compositional variation of crustal rocks. However, as far as Gedemsa is concerned, Sr isotopic ratios determined by Mazzuoli (personal communication) on some rhyolites gave values around 0.705. These ratios are much lower than those typical of upper crustal rocks (e.g. Taylor and McLennan, 1985). Accordingly, if the Gedemsa acid magmas have been formed by partial melting within the crust, the source rocks can only be represented by lower crustal material.

Fig. 11 shows calculated melting models of lower crustal rocks (Shaw, 1970; Hanson, 1978). The trace element abundances of lower crust have been taken from Taylor and McLennan (1985). The trends of partial melting have been calculated for both compatible (e.g. Sr) and incompatible elements (e.g. Rb, Zr and Y). The models show that the incompatible element abundances increase with decreasing degrees of partial melting, i.e. with decreasing F%. On the contrary, Sr abundances decrease with decreasing F%. However, it can be observed that the incompatible elements rarely reach the high concentrations which are observed in the Gedemsa acidic rocks. For instance, Y and Zr reach concentration of about 100 ppm and 700 ppm, respectively, only when the degrees of partial melting is around a few percent. Both these values are much lower than those observed in some Gedemsa rhyolites. Moreover, it is well known that magma formed by a few percent partial melting of crustal rocks are unable to separate from the source rocks; the high viscosity of crustal melts, in fact, requires that melting must be higher than 30% in order to allow separation of magma from the residue. If this requirement is not fulfilled, migmatitic rocks are formed rather than separated bodies of acid magmas. Accordingly, the most realistic composition of acid crustal magma are those of melts formed by about 30-50% crustal melting. These show much lower values of incompatible element abundances than those observed in the Gedemsa rhyolites.

With regard to concentration of compatible elements such as Sr (Arth, 1976), it can be noticed that partial melting is unable to give liquids with extremely low abundances of this element. For instance, in the case reported in Fig. 11, melts with Sr lower than a few tens ppm are not obtained, even if high values of $D_{S/l}$ are assumed during partial melting.

All these models agree in suggesting that it is unlikely that the studied rhyolitic

Fig. 11. Partial melting models for an average lower continental crust. Vertical axis reports compositions of anatectic liquids normalyzed to the composition of the parent rock (C_l/C_0) which expresses the degree of element enrichment or depletion of the anatectic liquids with respect to the source. F% indicated degree of partial melting. For Sr, different values of bulk partition coefficient (D) have been tested.

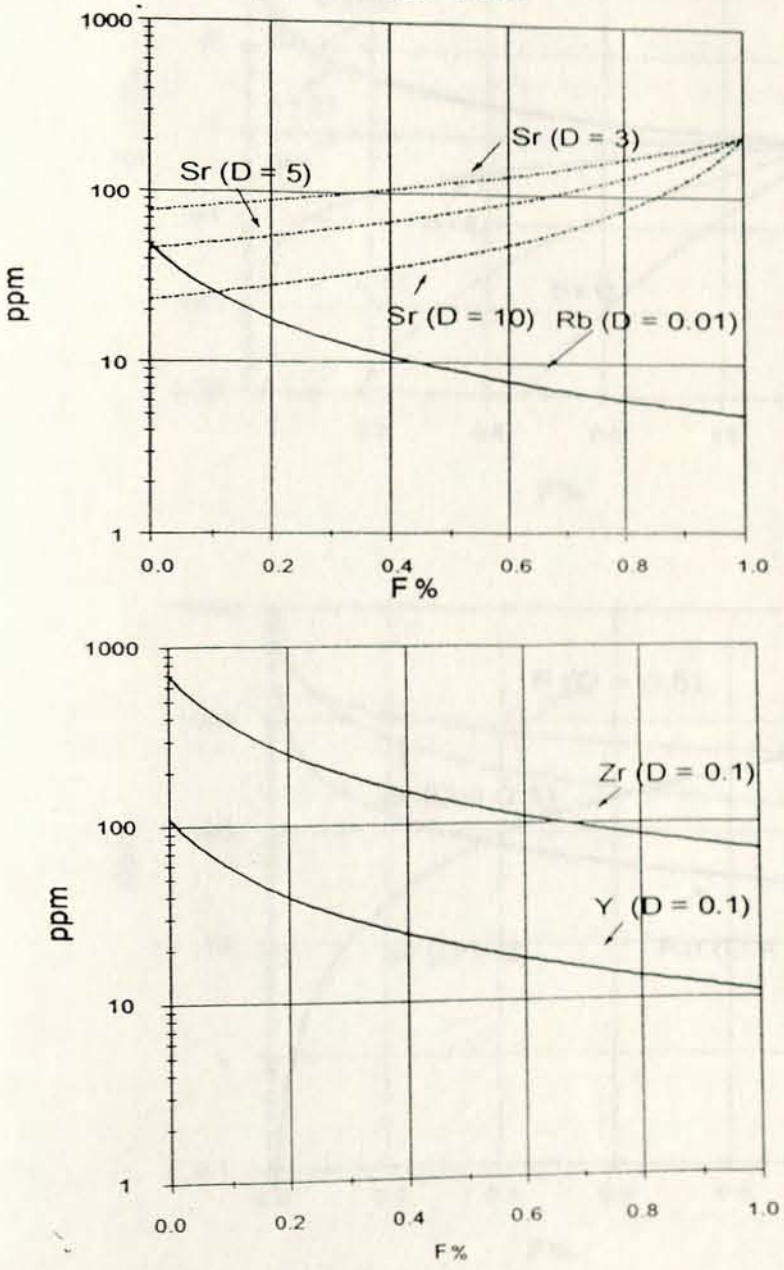

Fig. 12. Fractional crystallization models for the most primitive Gedemsa basalt. Vertical axis gives absolute abundances of residual liquids in ppm. F% indicates weight fraction of residual liquid.

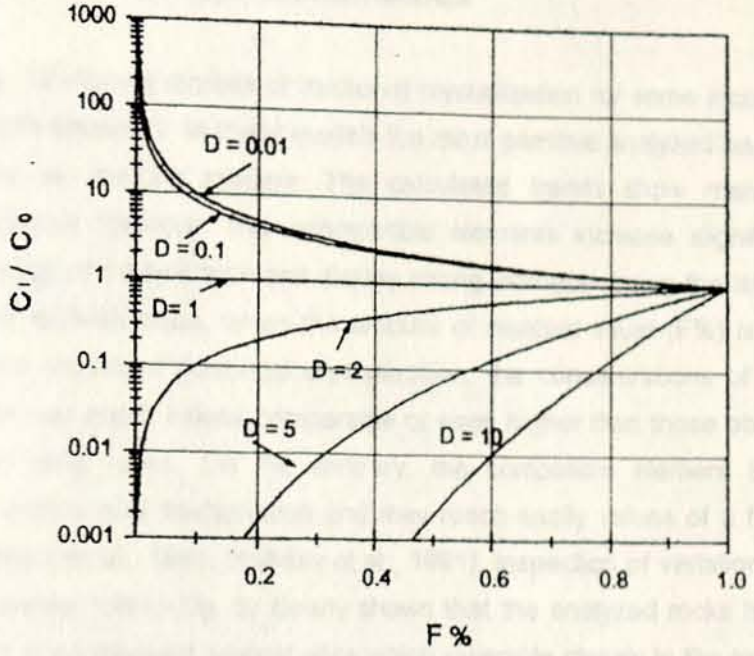

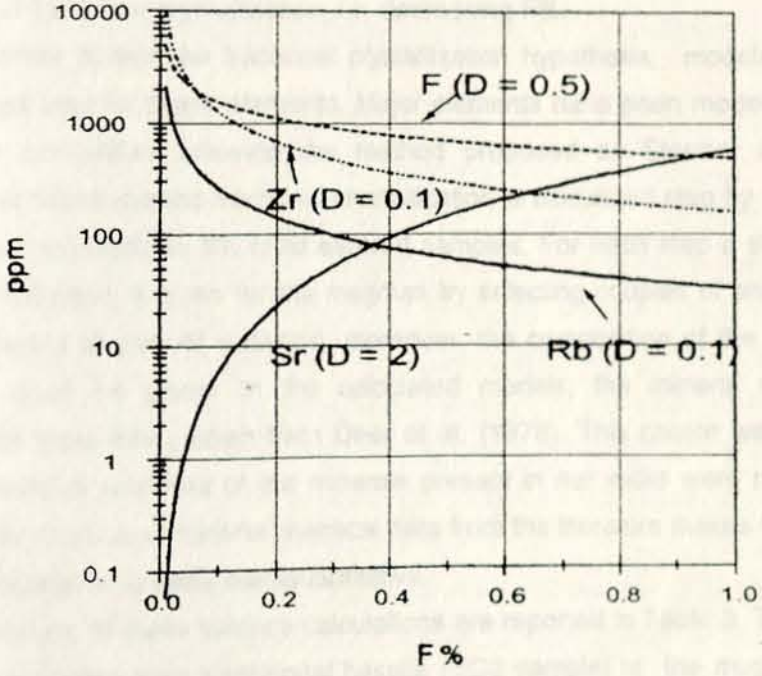

magmas were formed by the melting of crustal rocks.

6.1.2.2 *Fractional Crystallization Models*

Fig. 12 reports models of fractional crystallization for some incompatible and compatible elements. In these models the most primitive analyzed basalt has been assumed as starting magma. The calculated trends show many interesting compositional features. The incompatible elements increase slightly during the early stages of fractionation and display strong increase during the latest stages of fractional crystallization, when the amount of residual liquid (F%) is low. At very advanced stages of fractional crystallization, the concentrations of incompatible elements can reach values comparable or even higher than those observed in the analysed acid rocks. On the contrary, the compatible element Sr decreases sharply with crystal fractionation and may reach easily values of a few ppm (see also Bellieni et al., 1981; Halliday et al., 1991). Inspection of variation diagrams of the Gedemsa rocks (Fig. 9) clearly shows that the analyzed rocks have variation trends of trace element against silica which resemble closely to the trends reported in Fig. 12. It must be recalled that increasing silica contents means increasing degree of fractional crystallization, i.e. decreasing F%.

In order to test the fractional crystallization hypothesis, models have been calculated also for major elements. Major elements have been modelled by mass balance calculation following the method proposed by Stormer and Nicholls (1978). In these models fractional crystallization is calculated step by step passing from the most mafic to the most evolved samples. For each step a starting and a final composition is given for the magmas by selecting couples of analysed rocks with different degree of evolution; moreover, the composition of the fractionating phases must be given. In the calculated models, the mineral compositions employed have been taken from Deer et al. (1978). This choice was necessary since chemical analyses of the minerals present in our rocks were not available. Obviously, the use of mineral chemical data from the literature makes the results to be considered as broadly semiquantitative.

The results of mass balance calculations are reported in Table 3. They indicate that the evolution from transitional basalts (GD3 sample) to the mugearite GD13 can be modelled by about 30% fractional crystallization of mafic minerals. The transition from mugearite GD13 to the benmoreite GD10 requires about 40%

fractional crystallization of mafic minerals and plagioclase. The transition from benmoreite to trachyte GD14 is possible after 50% fractional crystallization dominated by plagioclase and clinopyroxene. Finally, rhyolites can be obtained after about 20% of fractional crystallization of plagioclase, clinopyroxene and sanidine starting from trachytic magmas. The model provides reasonable fits between the observed and calculated compositions of daughter magmas, as expressed by the sum of the squares of the residuals (r^2).

6.2 Role of magma mixing

Field and petrographic evidence indicated that magma mixing has been an important process during the evolution of the Gedemsa volcano. This process appears to have been working especially during the latest stages of the post-caldera activity. This is suggested by the widespread occurrence of mingled salic-mafic lavas and pyroclastics in the latest products of Gedemsa.

Geochemical data allow to evaluate the importance of mixing processes during the formation of magmatic suites. It is well known that mixing processes between compositionally diverse magmas give straight trends on inter-element variation diagrams. Instead, fractional crystallization processes give typically curved trends.

This derives from the fact that different types of mineral assemblages separate from the magma during fractional crystallization thus making the partition coefficients for major and trace elements to change. Variation of partition coefficents for major and trace elements makes the various elements to behave differently during fractional crystallization. It must be reminded, however, that if two elments do not show changes in the solid/liqid partition coefficient during fractionation, they also show linear trends when plotted on inter-element variation diagrams. For instance, if two elements are perfectly incompatible during the all fractional crystallization process, they show perfectly linear trends on inter element variation diagrams.

Variation diagrams of major and trace elements against silica (Fig. 8,9) have shown typically fractional crystallization trends. In fact, almost all major and trace elements show changes in the rate of variation from mafic to intermediate to salic rocks. In some cases, such as in the Sr and Ba vs. SiO_2, positive trends change to

Table 3. Results of mass balance calculations for major elements

STEP 1: from GD3 to GD13	Solid frac.% = 30.00		$r^2 = 1.5$	
	GD3	GD13	Calc. comp.	Diff. real-calc
SiO_2	49.89	53.43	52.78	0.66
TiO_2	1.98	1.31	2.16	-0.85
Al_2O_3	14.75	20.19	20.23	-0.04
FeO_t	10.47	6.97	7.05	-0.08
MnO	0.19	0.15	0.01	0.14
MgO	8.82	3.22	2.98	0.24
CaO	9.51	9.65	9.27	0.38
Na_2O	2.84	3.45	3.72	-0.27
K_2O	1.14	1.33	1.49	-0.16
P_2O_5	0.39	0.32	0.49	-0.17
	olivine	clinopyroxene		
SiO_2	39.87	46.61		
TiO_2	0.03	1.18		
Al_2O_3	0.00	3.47		
FeO_t	14.06	21.08		
MnO	0.22	1.11		
MgO	45.38	7.27		
CaO	0.25	17.24		
Na_2O	0.04	1.04		
K_2O	0.01	0.27		
P_2O_5	---	---		
Phase frac.%	-40.00	-60.00		
STEP 2: from GD13 to GD10	Solid frac.% = 40.00		$r^2 = 0.41$	
	GD13	GD10	Calc. comp.	Diff. real-calc.
SiO_2	53.43	56.84	57.22	-0.37
TiO_2	1.31	2.22	2.25	-0.03
Al_2O_3	20.19	13.90	13.98	-0.08
FeO_t	6.97	10.23	10.20	-0.07
MnO	0.15	0.28	0.23	0.05
MgO	3.22	2.64	2.77	-0.13
CaO	9.65	5.58	5.70	-0.12
Na_2O	3.45	5.16	4.72	0.44
K_2O	1.33	2.28	2.26	0.02
P_2O_5	0.32	0.88	0.71	0.17
	olivine	plagioclase	clinopyroxene	
SiO_2	39.87	49.06	46.61	
TiO_2	0.03	0.00	1.18	
Al_2O_3	0.00	32.14	3.47	
FeO_t	0.86	0.27	21.08	
MnO	0.22	0.00	1.11	
MgO	45.38	0.20	7.27	
CaO	0.25	15.38	17.24	
Na_2O	0.04	2.57	1.04	
K_2O	0.01	0.17	0.27	
P_2O_5	----	----	----	
Phase frac.%	-7.00	-86.00	-7.00	

STEP3: from GD10 to GD14		Solid frac.% = 47.02	r^2= 1.6	
	GD10	GD14	Calc. comp.	Diff. real-calc.
SiO_2	56.84	67.69	67.51	0.18
TiO_2	2.22	0.74	0.53	0.21
Al_2O_3	13.90	12.38	11.78	0.60
FeO_t	10.23	6.18	5.97	0.21
MnO	0.28	0.21	0.20	0.01
MgO	2.64	1.04	0.82	0.22
CaO	5.58	2.44	3.01	-0.57
Na_2O	5.16	5.50	5.29	0.21
K_2O	2.28	3.68	3.94	-0.26
P_2O_5	0.88	0.14	0.95	-0.81
	olivine	plagioclase	clinopyroxene	Ti-Fe oxide
SiO_2	39.87	49.06	51.92	0.51
TiO_2	0.03	—	0.77	50.02
Al_2O_3	0.00	32.14	1.85	—
FeO_t	14.06	0.27	32.19	46.37
MnO	0.22	—	—	1.44
MgO	45.38	0.20	—	0.46
CaO	0.25	15.38	—	0.71
Na_2O	0.04	2.57	12.86	—
K_2O	0.01	0.17	0.19	—
P_2O_5	—	—	—	—
Phase frac.%	-10.52	-50.80	-30.51	-8.19
STEP 4: From GD14 to GD 8		Solid frac.% = 19.0	r^2= 0.90	
	GD14	GD8	Calc. comp.	Diff. real-calc.
SiO_2	67.69	70.37	70.34	0.04
TiO_2	0.74	0.44	0.80	-0.36
Al_2O_3	12.38	10.59	10.59	-0.00
FeO_t	6.18	6.06	6.54	-0.48
MnO	0.21	0.29	0.24	0.05
MgO	1.04	0.10	-0.09	0.19
CaO	2.44	1.31	1.29	0.02
Na_2	5.50	6.24	5.87	0.37
K_2O	3.68	4.58	4.27	0.31
P_2O_5	0.14	0.03	0.14	-0.11
	plagioclase	clinopyroxene	sanidine	
SiO_2	64.1	48.9	67.27	
TiO_2	—	0.12	—	
Al_2O_3	26.44	3.87	18.34	
FeO_t	0.19	30.0	0.92	
MnO	—	0.51	—	
MgO	—	6.87	—	
CaO	7.84	7.96	0.15	
Na_2O	6.48	0.58	6.45	
K_2O	1.1	0.2	7.05	
P_2O_5	—	—	—	
Phase frac.%	-70.9	-26.37	-2.65	

negative ones with ongoing evolution.

Variation diagrams of trace elements vs. Rb also show typical fractional crystallization trends (Fig. 13). For instance Ba and Sr increase from basic to intermediate rock and then decrease with typical curved trends going to acid compositions. Only Zr, Nb and Y show linear trends with Rb. Howover, this does not contraddict fractional crystallization but simply means that all these elements have been incompatible all through the fractionation process. Fluorine also shows some linear increase with Rb, but with some scattering probably due to the volatility of F, as it will be discussed later.In conclusion, geochemical evidence clearly suggests that fractional crystallization has been the most important evolutionary process. Mixing did also occur, as indicated by petrographic and field evidence, but its role was minor and did not offset the trends generated by fractional crystallization processes. Speculatively, it can be envisaged that also crustal assimilation had a role during magma evolution, but this need isotopic studies in order to be constrained.

It seems difficult to admit that fractional fractionation of basalt magma may give origin to huge volumes of peralkaline silicic volcanics. However, the presence of strong Bouguer anomalies, recently discovered by Baker et al (1972), along the rift axis and interpreted as an evidence of shallow intrusion of a basic igneous body related to magma chambers may support fractional crystallization hypothesis. In fact, fractionaltion in huge magma chambers are able to give large volume acid products. Similar conclusions have been reached for other silicic central volcanoes along the Ethiopian rift margins (e.g. Gasparon et al., 1993).

The gravity values for Gedemsa area are markedly negative (Dakin, 1975). The Gedemsa volcano has a gravity value of approximatly -190 mgal, suggesting that the continental crust beneath the volcano is somehow attenuated. These arguments are in favour of the presence of large magma chamber beneath the volcano, in which extensive fractional crystalization produced large volumes of acid liquids.

Fig. 13 Variation diagrams of trace elements (ppm) vs. Rb (ppm) and F (ppm). Symbols as in Fig. 7.

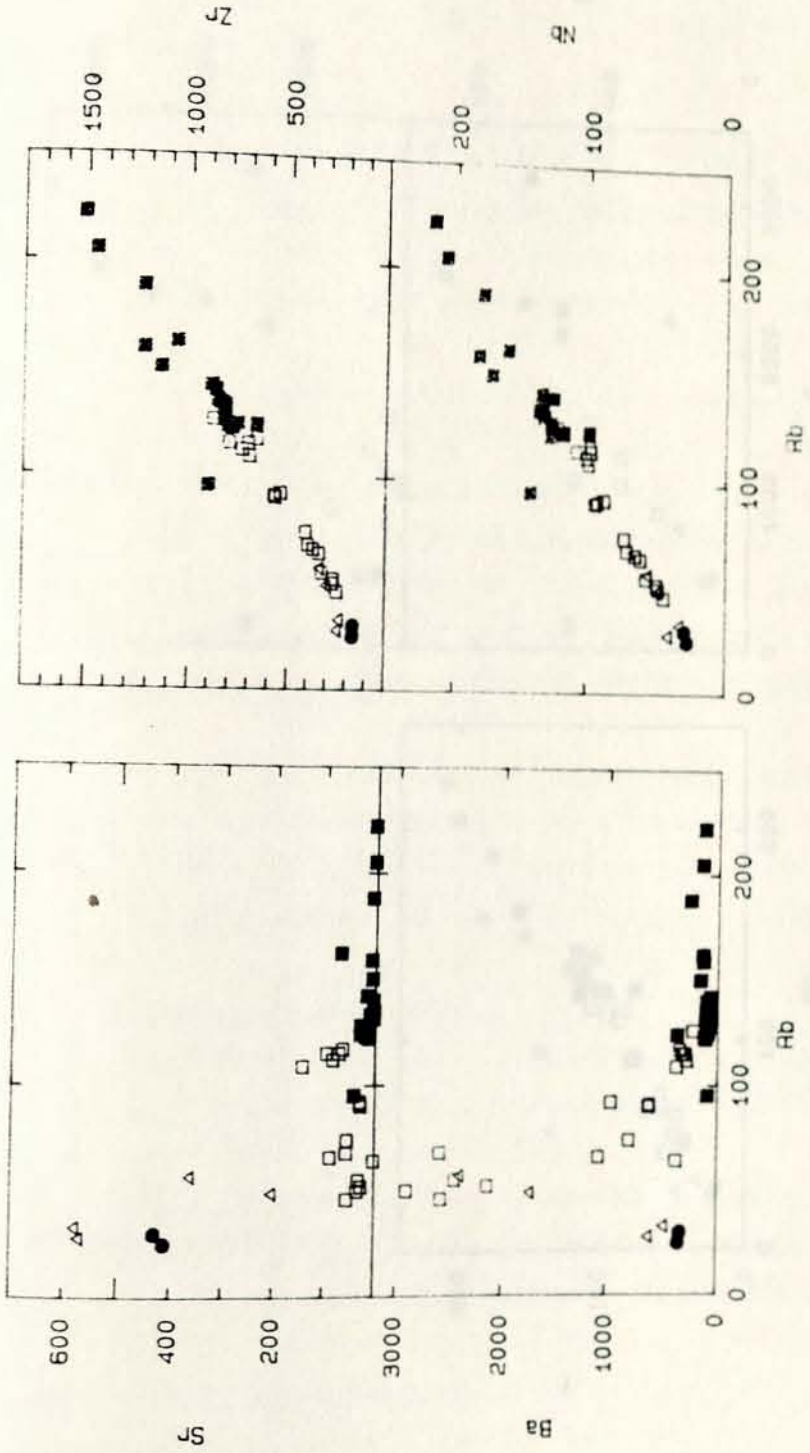

Fig.13. (continued)

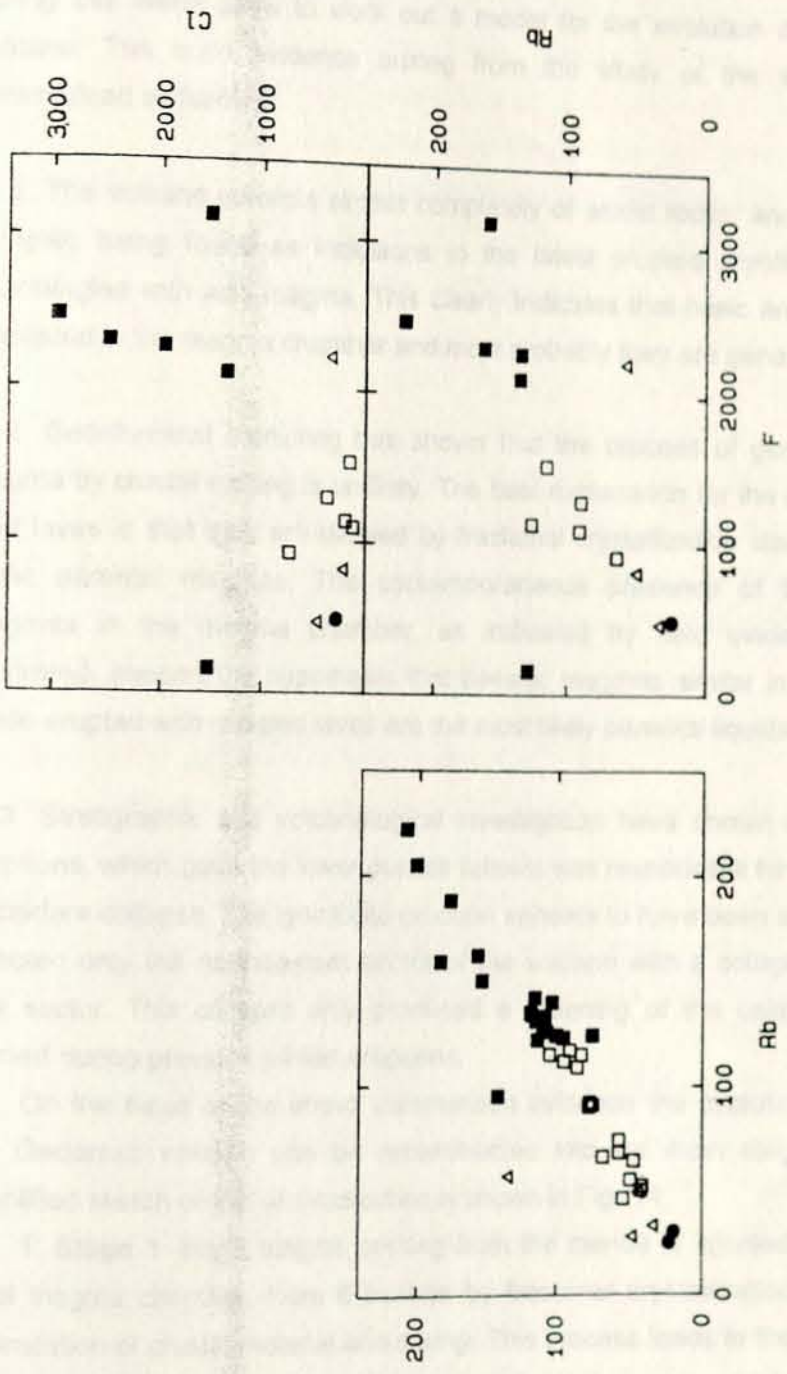

7.MODEL FOR THE EVOLUTION OF GEDEMSA VOLCANO

The volcanological, stratigraphic, petrological and geochemical data obtained during this thesis allow to work out a model for the evolution of the Gedemsa volcano. The main evidence arising from the study of the volcano can be summarized as follows:

1. The volcano consists almost completely of acidic rocks, and the only mafic samples being found as inclusions in the latest erupted rhyolites, are closely intermingled with acid magma. This clearly indicates that basic and acid magmas coexisted in the magma chamber and most probably they are genetically related.

2. Geochemical modelling has shown that the process of generation of acid magma by crustal melting is unlikely. The best explanation for the geochemistry of acid lavas is that they are derived by fractional crystallization starting from more mafic parental magmas. The contemporaneous presence of basic and acid magmas in the magma chamber, as indicated by field evidence previously illustrated, support the hypothesis that basaltic magmas similar in composition to those erupted with mingled lavas are the most likely parental liquids.

3. Stratigraphic and volcanological investigation have shown that the plinian eruptions, which gave the lower pumice fallouts was responsible for the main stage of caldera collapse. The ignimbrite eruption appears to have been a minor one and affected only the northeastern sector of the volcano with a collapse restricted to that sector. This collapse only produced a widening of the caldera depression formed during previous plinian eruptions.

On the basis of the above summarized evidence the evolutionary history of the Gedemsa volcano can be reconstructed into six main stages. A pictorial simplified sketch of this reconstruction is shown in Fig. 14.

1. **Stage 1**. Basic magma coming from the mantle is injected into a shallow level magma chamber. Here it evolves by fractional crystallization, possibly with assimilation of crustal material and mixing. This process leads to the formation of a zoned magma chamber formed by a convecting lower zone and by a stable acid upper zone. The mafic magma ponding at the bottom of the chamber undergoes convective stirring due to its low viscosity. Mixing with newly injected magmas

coming from the mantle keeps the composition of the convecting magma approximately constant and basic. In the upper part only fractional crystallization takes place with no convective stirring, since the acid magma is much more viscous. This process brings to the formation of a bimodal (basic and acid) distribution of magmas in the chamber with scarce intermediate liquids. Note that during this stage the mafic magma cannot be erupted to the surface because the less dense acid liquid staying at the top of the chamber acts as a density filter. It is possible that mafic magmas were erupted during previous stages, but no evidence has been found for this in the field. This stage ends with the eruption of acid magmas rich in volatiles lying at the top of the chamber.

2. **Stage 2.** The plinian eruption produced emission of large volumes of magmas and the collapse of the central part of the volcano with the formation of the caldera. This collapse generates a decrease in the volume of the magma chamber. Also cooling of magmas along the interface with wall rocks contributes to decreasing volume of the magma chamber. However, fractional crystallization processes, convective stirring and all the proceses which occurred previously also take place in this reduced chamber which is still zoned.

3. **Stage 3.** Accumulation of gaseous phases at the top of the chamber generates an ignimbritic explosion. Probably, this explosion was triggered by an injection of mafic magma coming from the source. This is suggested by the presence of some mafic material mingled with juvenile acid component of the ignimbrite. Before the ignimbrite eruption some small volume, mostly effusive eruption produced the emplacement of acid domes and flows.

4. **Stage 4.** The ignimbrite eruption produces an additional but minor collapse. This is the cause of a further reduction of the magma chamber. At the same time further cooling of the magma causes a very strong reduction of the reservoir which, at this stage, most probably consisted of a small zoned reservoir still undergoing fractionation.

5. **Stage 5.** Low energy explosions or effusive eruptions characterize the post-ignimbrite stage of the volcano. The magma emission is concentrated in the central part of the caldera, probably along the fractures connected with the

collapse generated by the ignimbrite eruption. The main characteristics of the emitted magmas is that they all contain mingled mafic material. This is due to the fact that the volume of the magma chamber is very reduced and in all occasions the eruption tapped the upper acid part and the interface between the mafic and salic layer.

6. **Stage 6.** During the latest activity of the Gedemsa volcano new magma is injected along crustal fissures connected to the main stages of rift opening. Some of these injection accidentally cut through the Gedemsa system. The pathways and the evolutionary history of these magmas are completely independent on those which fed the Gedemsa activity. The few geochemical data available on mafic magmas suggest that, most probably, the composition of these late basalts was not much different from those involved in the Gedemsa volcano.

Fig. 14 Pictorial view of the evolution of the Gedemsa volcano as inferred from volcanological and geochemical study. For explanation see text.

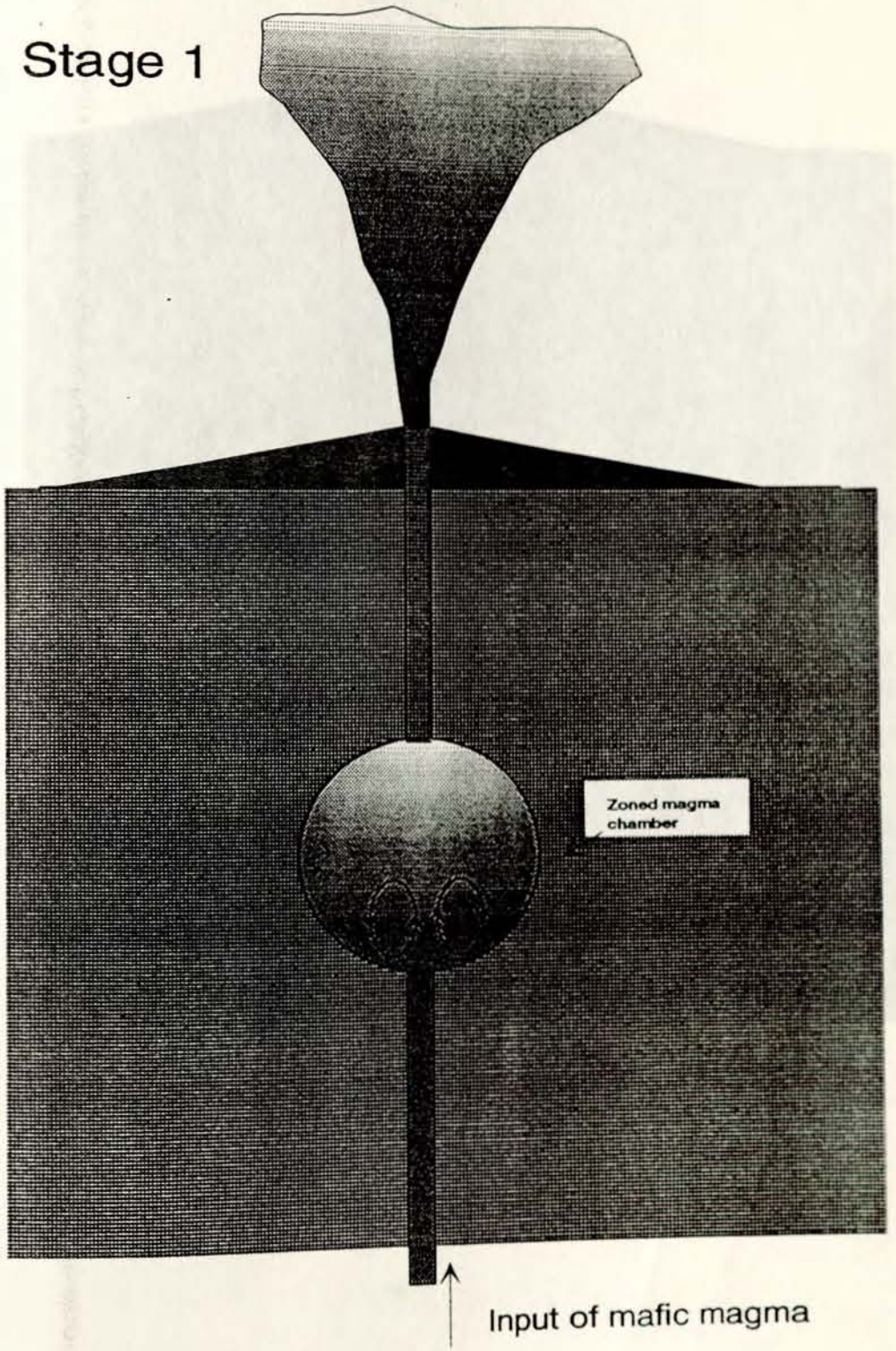

Stage 2

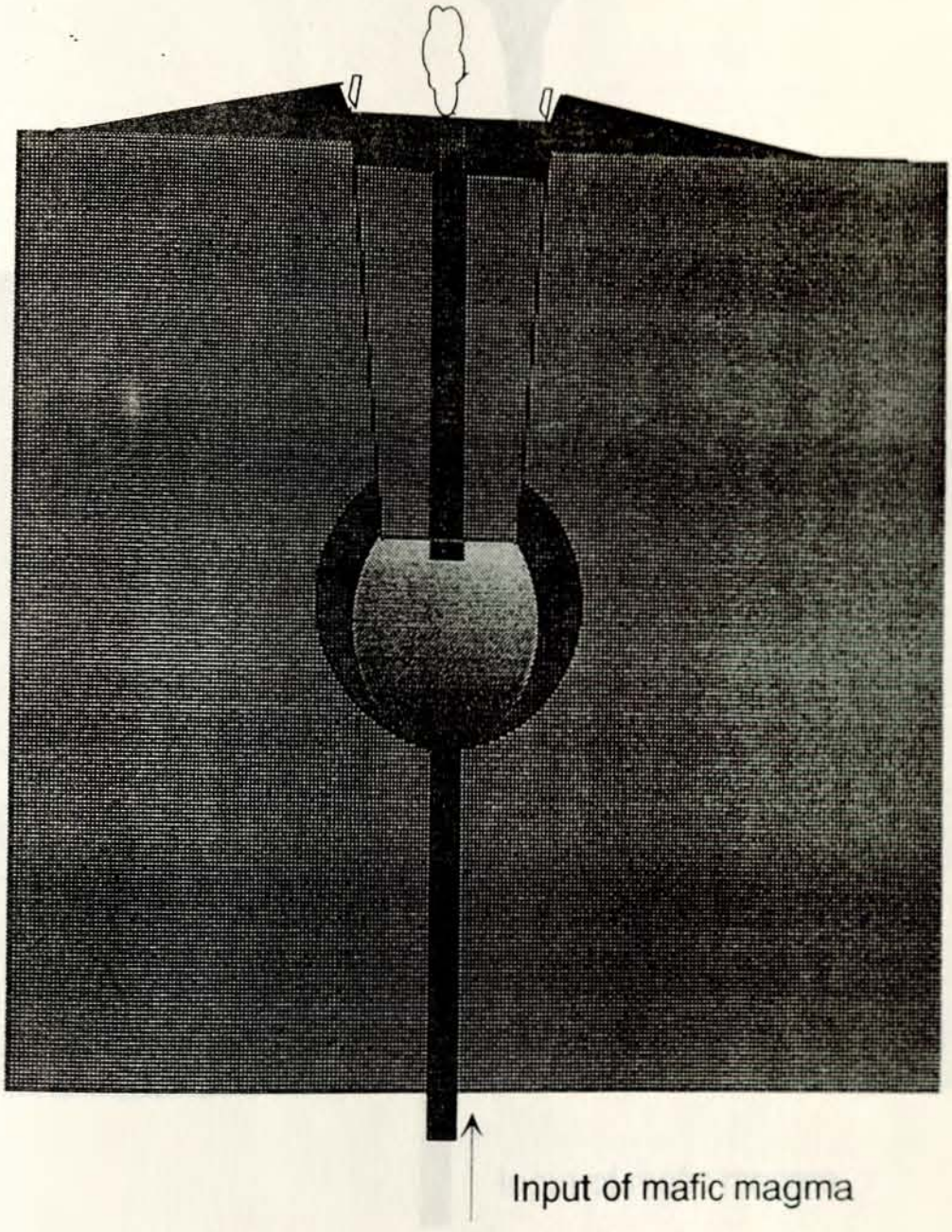

Stage 3

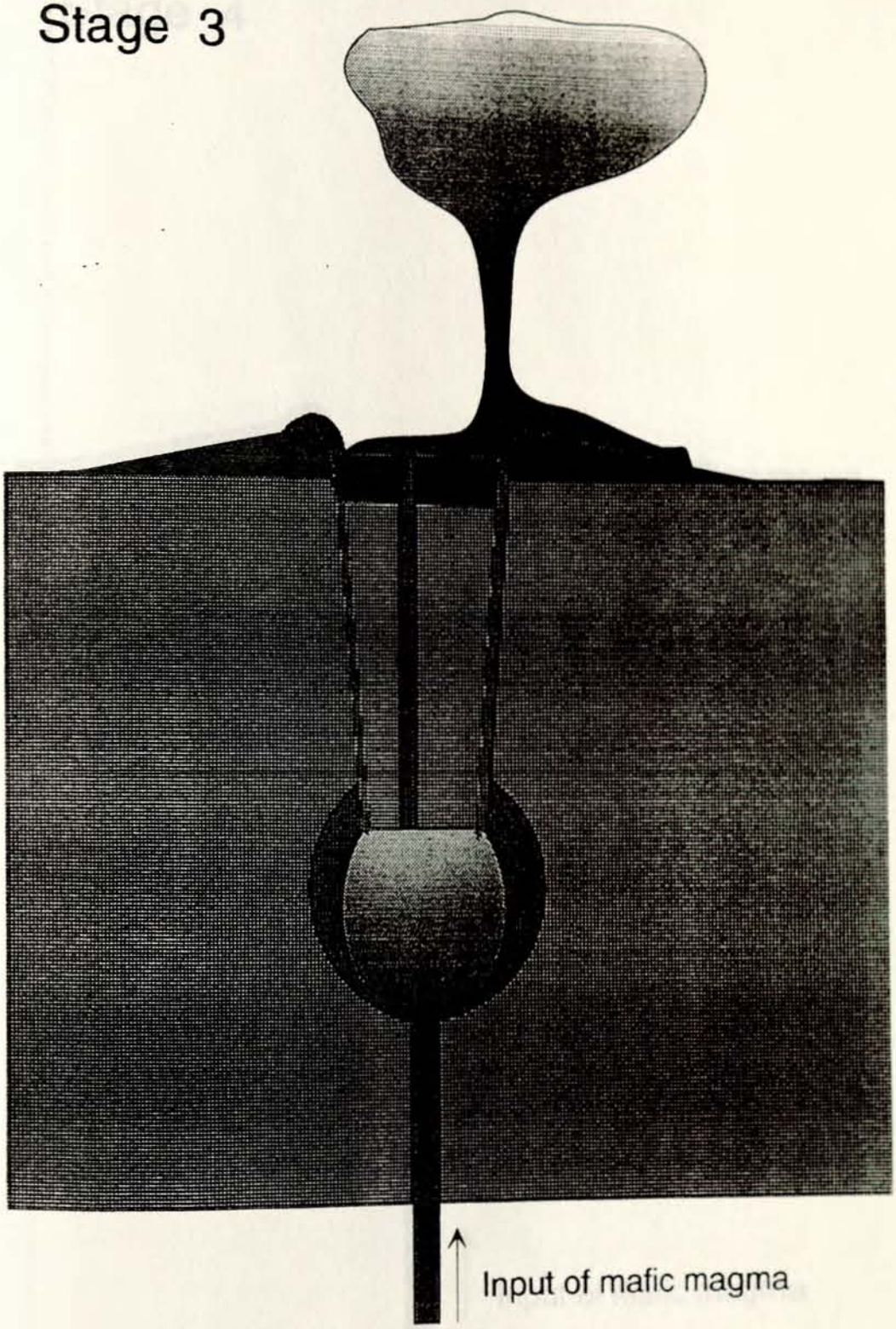

Stage 4

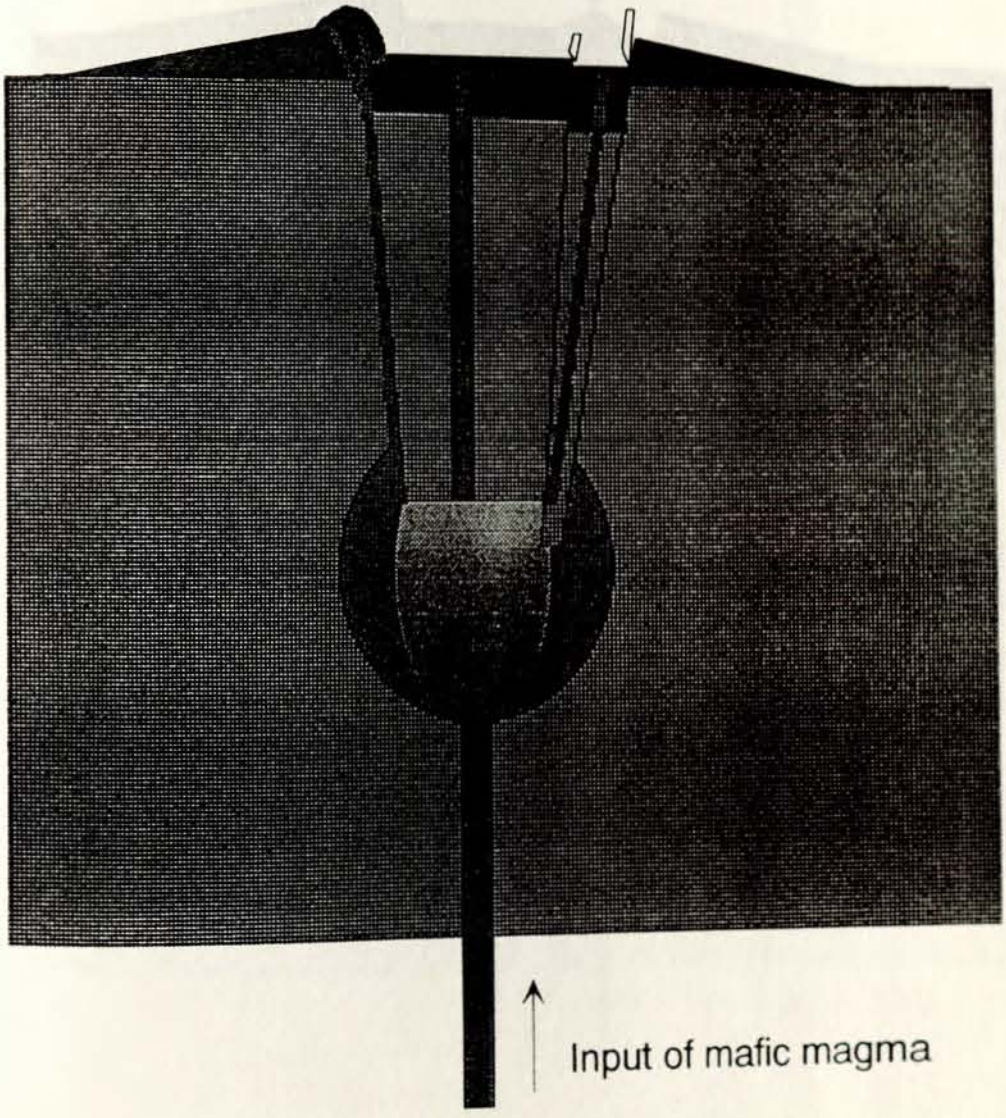

Stage 5

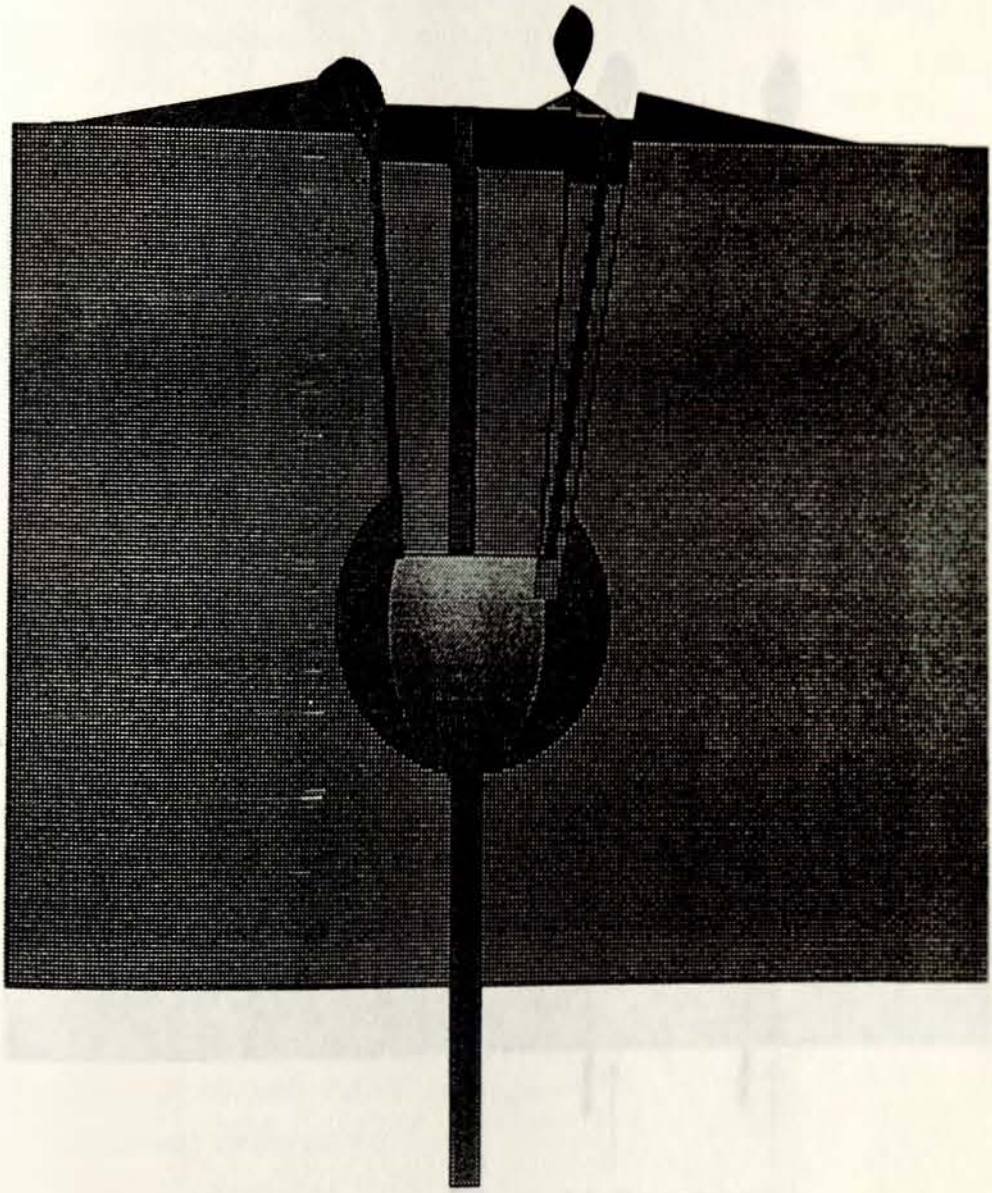

Stage 6

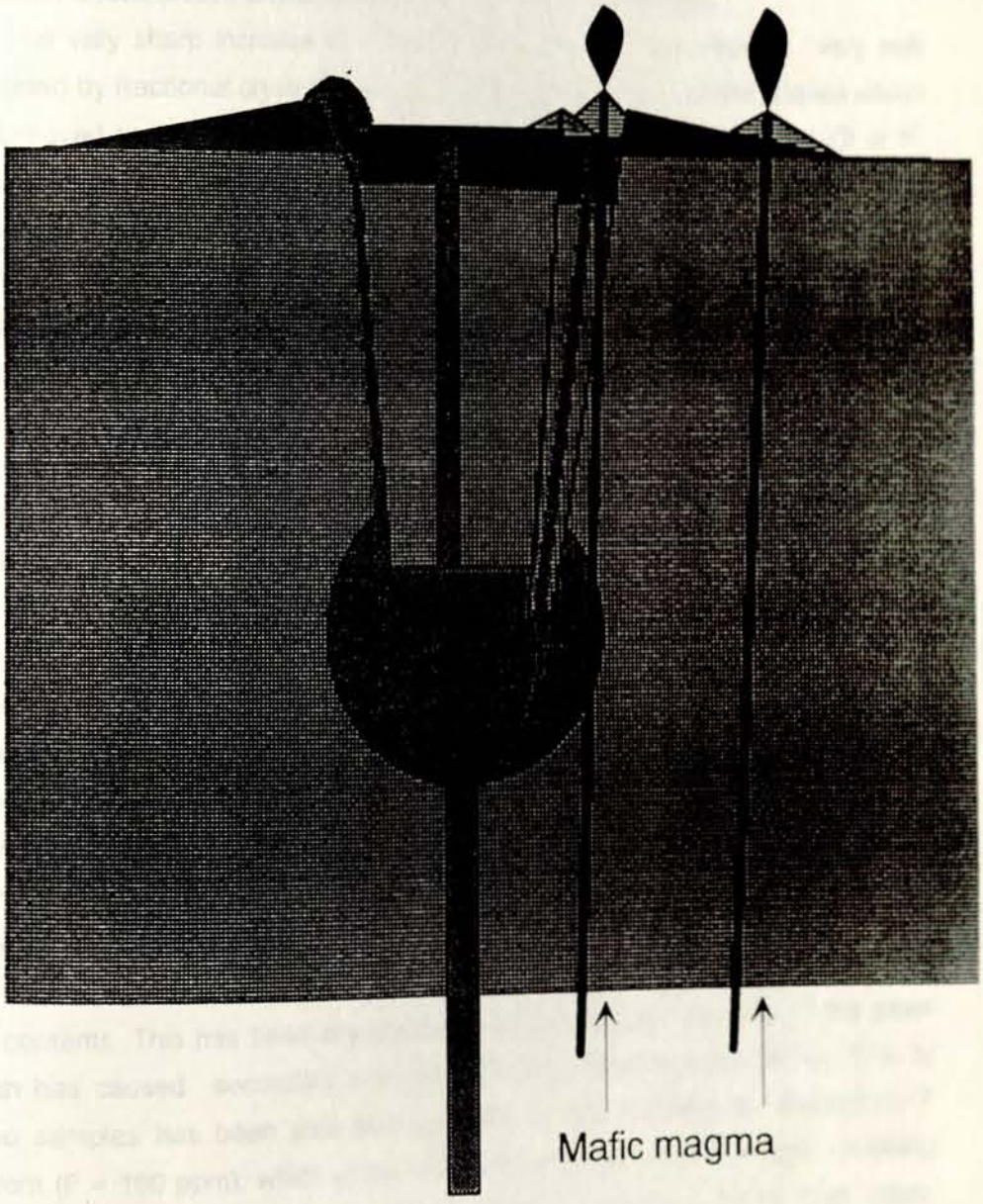

8. BEHAVIOUR OF VOLATILE ELEMENTS DURING MAGMA EVOLUTION: The fluorine problem

One of the most striking characteristics of the Gedemsa acid rocks is their very high concentration in fluorine and chlorine. Both these elements show rather low values in the basalts, which are believed to represent the parent of all the Gedemsa series. Although only a few data on F and Cl are available, some interesting conclusion can be drawn on the behaviour of these elements during fractional crystallization and after emplacement of volcanic rocks.

The very sharp increase in F and Cl from mafic to salic rocks is very well explained by fractional crystallization processes. In fact, none of the phases which are believed to have fractionated during magma evolution contain either Cl or F. Accordingly, these elements behave incompatibly and increase in the most acid products. The increase in F is much more regular than the increase in Cl. This is due to the fact that F has a much lower affinity for gaseous phase than Cl. In other words, F prefers to remain in the liquid more strongly than Cl during fractional crystallization. Only when magma is very rich in F, a F-rich gas phase can separate from the magma. This happens in the latest stages of magma crystallization. According to this slightly different behaviours, F behaves almost as other non-volatile incompatible trace elements, whereas Cl is more scattered because it is lost by the magma in the gaseous phase.

Sample GD10 represents an exception in that it has an intermediate major element composition but a high F abundance, comparable to those of some rhyolites. As mentioned, this sample contains fluorite filling some vesicles. Thus the most obvious explanation for the high F is that this sample has undergone post-depositional enrichment in fluorite most probably by some type of fumarolic activity. The interesting feature of this rock is that it is also anomalously enriched in Y which indicates that the fumarolic gases were also able to bring Y in solution and to cause anomalous enrichments in the rocks with which they come into contact.

Some rhyolitic samples, generally pumices, have shown low Na_2O and high LOI contents. This has been interpreted as an evidence of alteration of the glass which has caused secondary enrichment in H_2O and depletion in Na. One of these samples has been also analayzed for F and revelead an anomalous F content (F = 160 ppm), which is lower than in any other analyzed rock, including basic and intermediate ones. On the contrary, Cl shows a rather high value,

comparable to that of other acid samples. The obvious implication of these data is that some pumices have interacted with ground waters undergoing chemical changes. Na and F were lost very heavily, whereas Cl and other elements did not suffer any significant modification. It is also obvious that the elements lost by the rocks were transferred to the ground water.

Several studies carried out on the ground and lake water from the Nazret and surroundng areas have revealed high contents in F. In several cases the F contents reach 30-40 mg/l (Tamiru Alemayehu, personal communication). Since the maximum acceptable value for F in drinking water is F = 1.5 mg/l, it is obvious that the presence of high F makes these water of little use for drinking and cooking purposes. Use of this high-F waters has caused and is still causing severe health problems in the Gedemsa population which often shows clear symptoms of fluorosis, such as dark stained teeths, slim and fragile bones etc.

The data obtained in the present study suggests that the source of fluorine is the interaction between pumiceous rocks and ground waters. Since also fumarolic gases are rich in fluorine, fumarolic activity can contribute in some cases to fluorine enrichment of water. The F enrichment in fumaroles and acid rocks is the extreme products of fractional crystallization. Accordingly, the Gedemsa case history provides a very compelling evidence of how magmatic processes may have important bearing on life quality for human beings.

9. CONCLUSIONS

Volcanological, petrologic and geochemical data on volcanic products from Gedemsa are used to establish the following conclusions:

1) The Gedemsa volcano consist, almost totally of acid trachytic and rhyolitic alkaline and peralkaline rocks. Mafic volcanics are very scarce and occur as enclaves in the latest erupted lavas and pyroclastics. The younger basalts which gave surge deposits, strombolian cones and some lava flows are not connected to the Gedemsa system but arose from the source along crustal fractures of the Wonji Fault System.

2) A large central caldera is the main volcanological feature of Gedemsa. Its collapse has been correlated with the plinian eruptions which formed huge pumice fall deposit. However, the shape and the size of the caldera have been modified during the following ignimbrite eruption.

3) The central part of the caldera is occupied by post caldera cones and domes and there is no evidence for the occurrence of resurgent structures.

4) The main process involved in the genesis of the Gedemsa peralkaline silicic rocks is fractional crystallization of transitional basaltic magmas at shallow depth. This process occurred in a zoned magma chamber where only the low density rhyolitic and trachytic magmas staying in the upper part had the possibility to be erupted at the surface.

5) Magma mixing processes also played a role, although minor, during the late stage of the evolution of the volcano.

REFERENCES

Arth, J.G., 1976. Behaviour of trace elements during magmatic processes: a summary of theoretical models and their applications. J. Res. US Geol. Survey, V. 4, p. 41-47.

Baker, B.H., Mohr, P.A., and Williams, L.A., 1972. Geology of the Eastern Rift System of Africa. Geol. Soc. Am., Spec. Pap., 136, p. 67.

Barberi, F., Ferrara, G., Santacroce, R., and Varet, J., 1975. Structural evolution of the Afar triple junction. West Germany, Schweizerbart. p. 38-54.

Barberi, F., Civetta, L., and Varet, J., 1980. Strontium isotopic composition of Afar volcanics and its implication for mantle evolution. Earth and Planetary Science Letters. V. 50, p. 247-259.

Barberi, F., Santacroce, R., and Varet, J., 1982. Chemical aspects of magmatism in continental and oceanic rifts. American Geophys. Union and Geol. Soc. of America, Washington, D.C., V. 8, pp 223-258.

Bellieni, G., Peccerillo A., and Poli, G., 1981. The Vedrette di Ries plutonic complex: petrological and geochemical data bearing on its genesis. Contrib. Miner. Petrol., V. 78, p. 145-156.

Betton, P.J., and Civetta, L., 1984. Stronzium and neodymium isotopic evidence for the hetrogeneous nature and development of the mantle beneath Afar (Ethiopia). Earth Planet. Sci. Letters. V. 71, p. 59-70.

Bigazzi, G., Bonadonna, F.P., Di Paola, G.M. and Giuliani, A., 1981. New K-Ar and Fission track ages of the last volcanotectonic phase in the Ethiopian Rift Valley. (Tullu-Moye area). Proceedings of the First International Symposium on Crustal Movements in Africa. Wassef, A.M. (edit.) p. 141-159.

Cinque, A., Ferri, M. and Rolandi, G., 1991. The caldera of Gedemsa (Ethiopia). International Conference on Active Volcanoes and Risk Mitigation. Napoli, September, 1991, Italy.

Dakin, M., Wood, A. and Norton, H., 1975. Gravity survey of Gedemsa caldera. Addis Ababa Univ., Internal Report.

Damte, A., 1990. Neotectonic of Nazret-Dera area. M. Sc. Thesis, Addis Ababa Univ.

Davies, J.R., and MacDonald, R., 1987. Crustal influence in the petrogenesis of the Naivasha basalt-comendite complex: combined trace element and Sr-Nd-Pb isotope constraints. J. Petrol., V. 28, p. 1009-1031.

Deer, W.A., Howie, R.A. and Zussman, J., 1978. An introduction to rock-forming minerals. Longman, London, p. 528.

Di Paola, G.M., 1972. The Ethiopian Rift Valley (between 7.00' and 8.40' lat. North). Bull. Volcan., V. 36 p. 317-560.

EIGS (Ethiopian Institute of Geological Surveys) and Elc (Electroconsult, Milano, Italy, and Geotermica Italiana, Pisa), 1987. Geothermal reconaissance study of selected sites of the Ethiopian rift system. Geothermal report, p. 5-1-5-34.

Gasparon, M., Innocenti, F., Manetti, P., Peccerillo, A., and Tsegaye, A., 1993. Genesis of the Pliocene to Recent bimodal mafic-felsic volcanism in the Debre Zeit area, Central Ethiopia: volcanological and geochemical constraints. African J. Earth Sci., V. 17, p. 145- 165.

Gibson, I.L., 1974. A review of the Geology, Petrology and Geochemistry of the Volcano Fantale. Bull. Volcan., V. 38, p. 791-802.

Gibson, I.L. and Tazieff, H., 1970. The structure of the Afar and the northern part of the Ethiopian Rift. Phil. Trans. Roy. Soc. London. (A). V. 267, p. 331-338.

Halliday, A.N., Davidson, J.P., Hildreth, W., and Holden, P., 1991. Modelling the petrogenesis of high Rb/Sr silicic magmas. Chem. Geol., V. 91, p. 107-114.

Hanson, G.N., 1978. The application of trace elements to the petrogenesis of igneous rocks of granitic composition. Earth Planet. Sci. Letters, V. 38, p. 26-43.

Hart, W.K., WoldeGabriel, G., Walter, R.C. and Mertzman, S.A., 1989. Basaltic volcanism in Ethiopia: Constraints on continental rifting and mantle interaction. J. Geophys. Res., V. 94, No. B6, p. 7731-7748.

Justin-Visentin, E., Nicoletti, M., Tolomeo, L. and Zanettin, B., 1974. Miocene-Piocene volcanic rocks of the Addis Ababa-Debre Berhan area (Ethiopia). Geopetrographic and radiometric study. Bull. Volcan., V. 38, p. 2-17.

Kampunzu, A.B., and Mohr, P., 1991. Magmatic evolution and petrogenesis in the East Africa Rift system. In: Magmatism in extensional stuctural settings (Edited by A.B. Kampunzu and R.T. Lubala), p 85-136, Springer, Berlin.

Kazmin, V., 1979. Stratigraphy and correlation of volcanic rocks in Ethiopia. E.I.G.S. No. 106, p. 1-26.

Kazmin, V., Berhe, S.M., Nicoletti, M. and Petrucciani, C., 1980. Evolution of the northern part of the Ethiopian Rift. Rome, Italy. Accademia Nazionale dei Lincei. V. 47, p. 275-292.

Kebede, S., 1988. Results of shallow wells drilling at Gedemsa, geothermal prospect, Ethiopia. Geother. Project of Ethiopian Ministry of Mines.

Kunz, K., Krewzer, H. and Muller, P., 1975. K/Ar determination of the Trap basalts of the southeastern part of the Afar Rift. In: Pilger. A. and Rosler, A. (edits.), Afar Depression of Ethiopia, Stuttgart, p. 370-374.

Le Bas, M.J., Le Maitre, R.W., Streckeisen, A. and Zanettin, B., 1986. A chemical classification of volcanic rocks based on the total alkali-silica diagram. J. Petrol., V.27, p. 745-750.

MacDonald, R., and Bailey, D.K., 1972. The chemistry of peralkaline oversaturated obsidians. U.S. Geol. Survey Prof. Paper n. 440-N, part 1.

Makris, I. and Ginzburg, A., 1987. The Afar Depression: transition between continental rifting sea floor spreading. Tectonophysics, V. 141, p. 199-214.

Merla, G., Abatte, E., Azzaroli, A., Bumi, P., Fazzouli, M., Sagri, M. and Tacconi, P., 1979. Comments and a geological map of Ethiopia and Somalia. Scale 1:2,000,000. Frienze, Italy, Consiglio Nazionale delle Ricerche, 89 p.

Meteorological Map of Ethiopia. Call No. Qc857. E8, 1981. Ref

Miller, J.A. and Mohr, P.A., 1966. Age of the Wachacha trachyte-carbonatite volcanic center. Bull. Geophys. Obs., Addis Ababa, V. 9, p. 1-6.

Mohr, P.A., 1960. Report on a geological excursion through southern Ethiopia. Bull. Geophys. Obs., V. 3, p. 9-20.

Mohr, P. A., 1961. Notes on the geology, structure and origin of the Bishoftu explosion craters. Bull. Geophys. Obs. Addis Ababa, V. 4, p. 1-9.

Mohr, P.A., 1967. The Ethiopian Rift System. Bull. Geophys. Obs., V. 11, p. 1-65.

Mohr, P.A., 1968. The Cenozoic Volcanic Succession in Ethiopia. Bull. Volcan., V 32, p. 5-14.

Mohr, P.A., 1970. Volcanic composition in relation to tectonics in the Ethiopian rift system: apreliminary investigation. Bull. Volcan. V. 34, p. 141-157.

Moor, J.M. and Davidson, A., 1978. Rift structure in southern Ethiopia. Tectonophysics, V. 46, p. 159-173.

Morbidelli, L., Nicoletti, M., Petrucciani, C. and Piccirillo, E.M., 1975. Ethiopian southeastern plateau and related escarpment: K-Ar ages of the main volcanic events (MER 8°10' to 9°00' lat. N). In: Pilger, A. and Rosler, A. (edits.), Afar Depression of Ethiopia. Stuttgart, p. 362-369.

Morton, W.H., Mitchell, J.G. and Mohr, P.A., 1979. Riftward younging of volcanic units in the Addis Ababa region, Ethiopian rift valley. Nature, V. 280, p. 284-288.

Piccirillo, E.M., Justin-Visentin, E., Zanettin, B., Joron, J.K. and Treuil, M., 1979. Geodynamic evolution from plateau to rift: Major and trace element geochemistry of the central eastern Ethiopian plateau volcanics. Neues Jahrbuch fur Geologie und Palaontologie, V. 258, p. 139-179.

Shaw, D.M., 1970. Trace element fractionation during anatexis. Geochim. Cosmochim. Acta, V. 34, p. 237-243.

Streckeisen, A., 1976. To each plutonic rock its proper name. Earth Sci. Rev., v. 12, 1-33.

Taylor, S.R., McLennan, S.M., 1985. The continental crust: its composition and evolution. Blackwell, London, 323 p.

Thrall, R., 1973. Gedemsa caldera, Ethiopia. Center for Astrophysics, Darthmouth College, USA, Reprint Ser. n. 280, p. 71-80.

WoldeGabriel, G., 1987. Volcanotectonic history of the central sector of the Main Ethiopian Rift: A geochronological,geochemical and petrological approach. Ph. D. thesis, Case Western Reserve Univ., 410p.

WoldeGabriel, G., 1990. Geology, geochronology and rift basin development in the central sector of the Main Ethiopia Rift. Bull. Geol. Soc. Am., V. 102, p. 439-458.

Zanettin, B. and Justin-Visentin, E., 1975. Tectonical and volcanological evolution of the western Afar margin (Ethiopia). In: Pilger, A. and Rosler, A. (edits.), Afar Depression of Ethiopia. Stuttgart, p. 300-309.

Zanettin, B., Nicoletti, M. and Petrucciani, C., 1978. The evolution of the Checha Escarpment and the Ganjuli Graben (Lake Abaya) in the southren Ethiopian rift. Neues Jahrbuch fur Geologie und Palaonotologie, V. 8, p. 473-490.

Plate 1

A: Lower pumice fall deposit (Bogra)

B : Spatter agglutinate at the base of multiple ignimbrite (Bogra)

Plate 2

A: Lithic breccia at the base of the ignimbrite (Bogra)

B: Plinian fallout of the ignimbrite (Jemute)

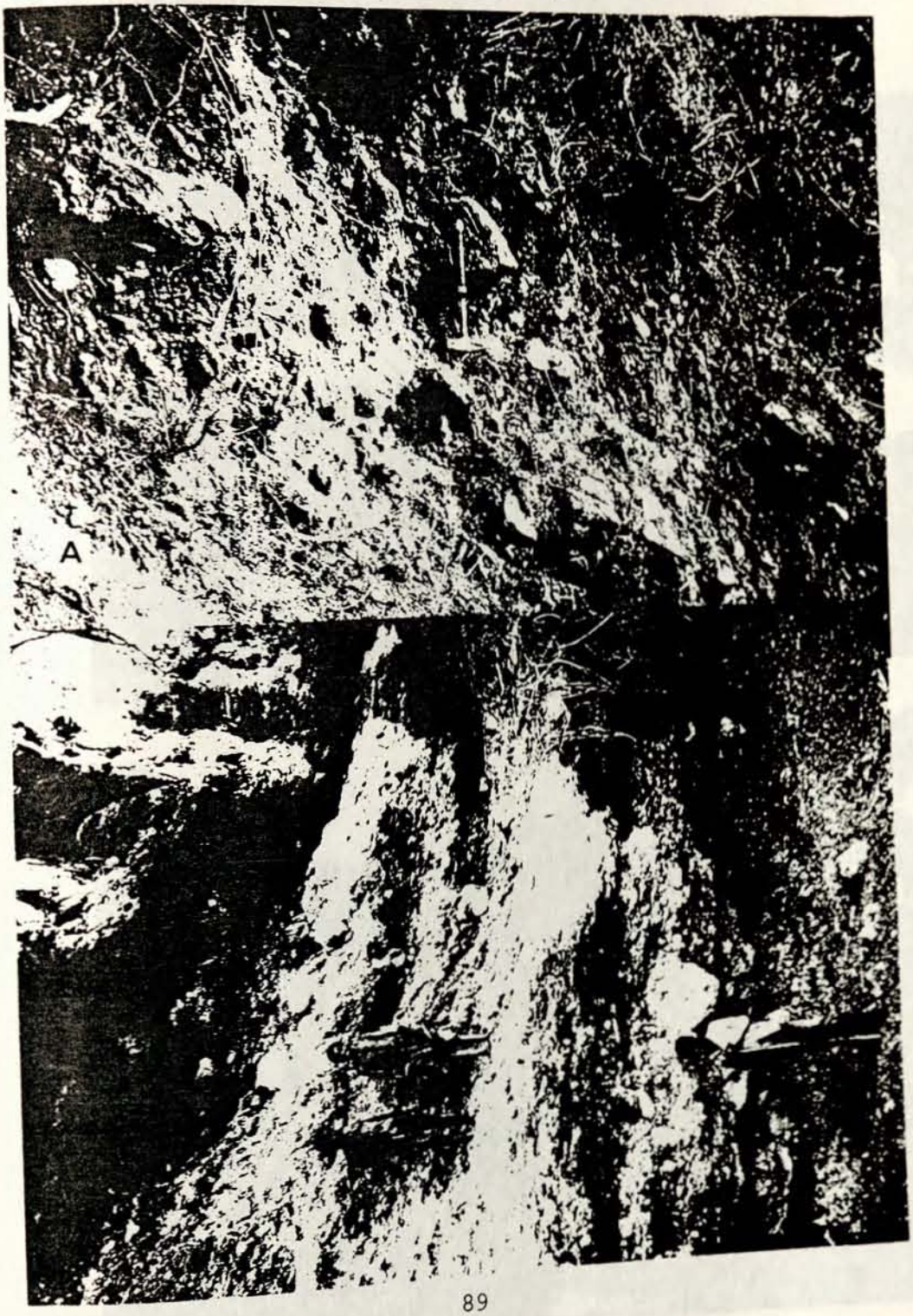

Plate 3

A, B: Intracalderic centers

Plate 4

A, B: Mesoscopic textures of intracalderic mingled lavas (Kore)

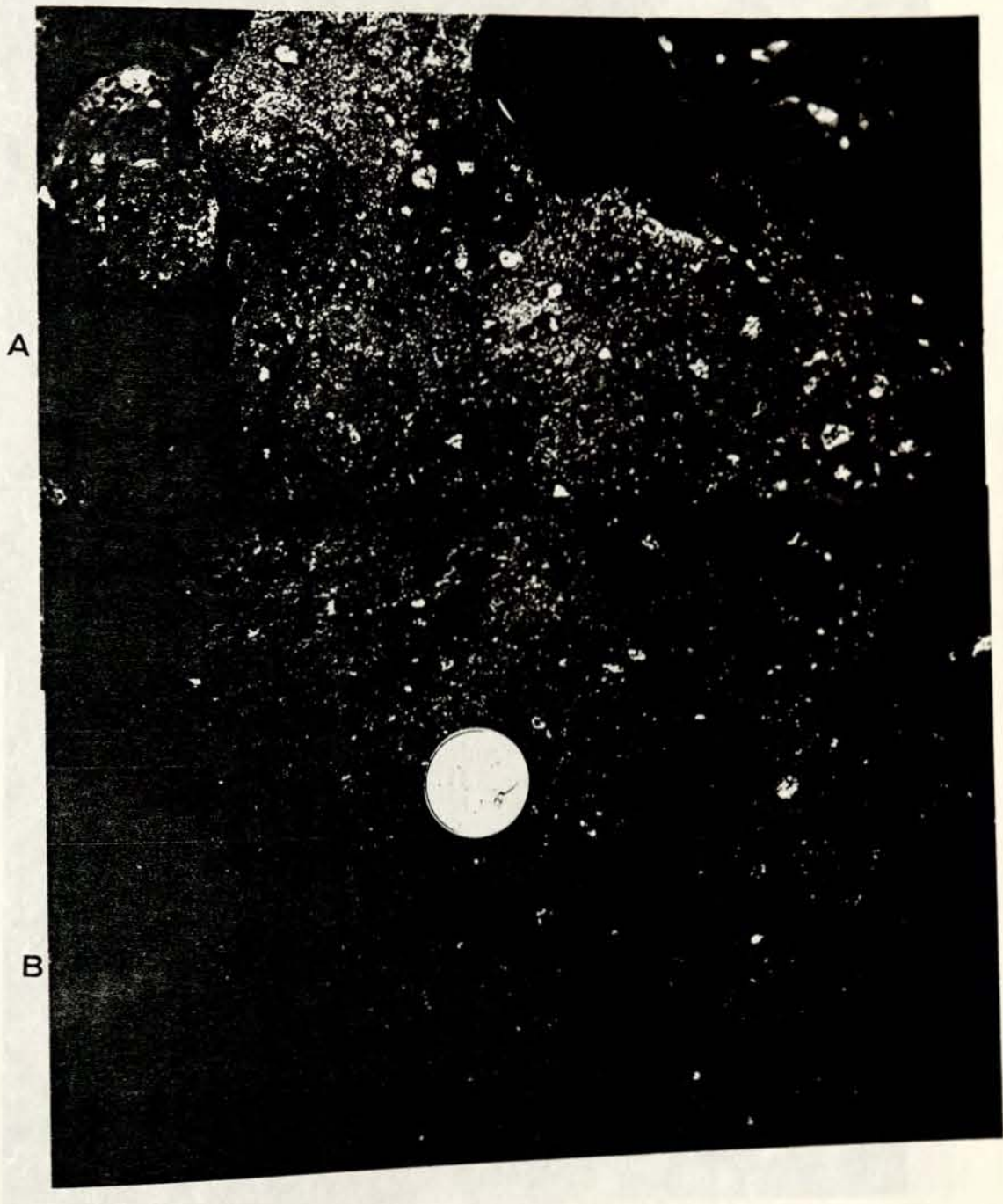

Plate 5

A, B: Mingled mafic scoriae and rhyolites at Kelo

Plate 6

A: Stratified surge deposits (Bogra)

B: Surge deposits along the caldera walls (Bogra)

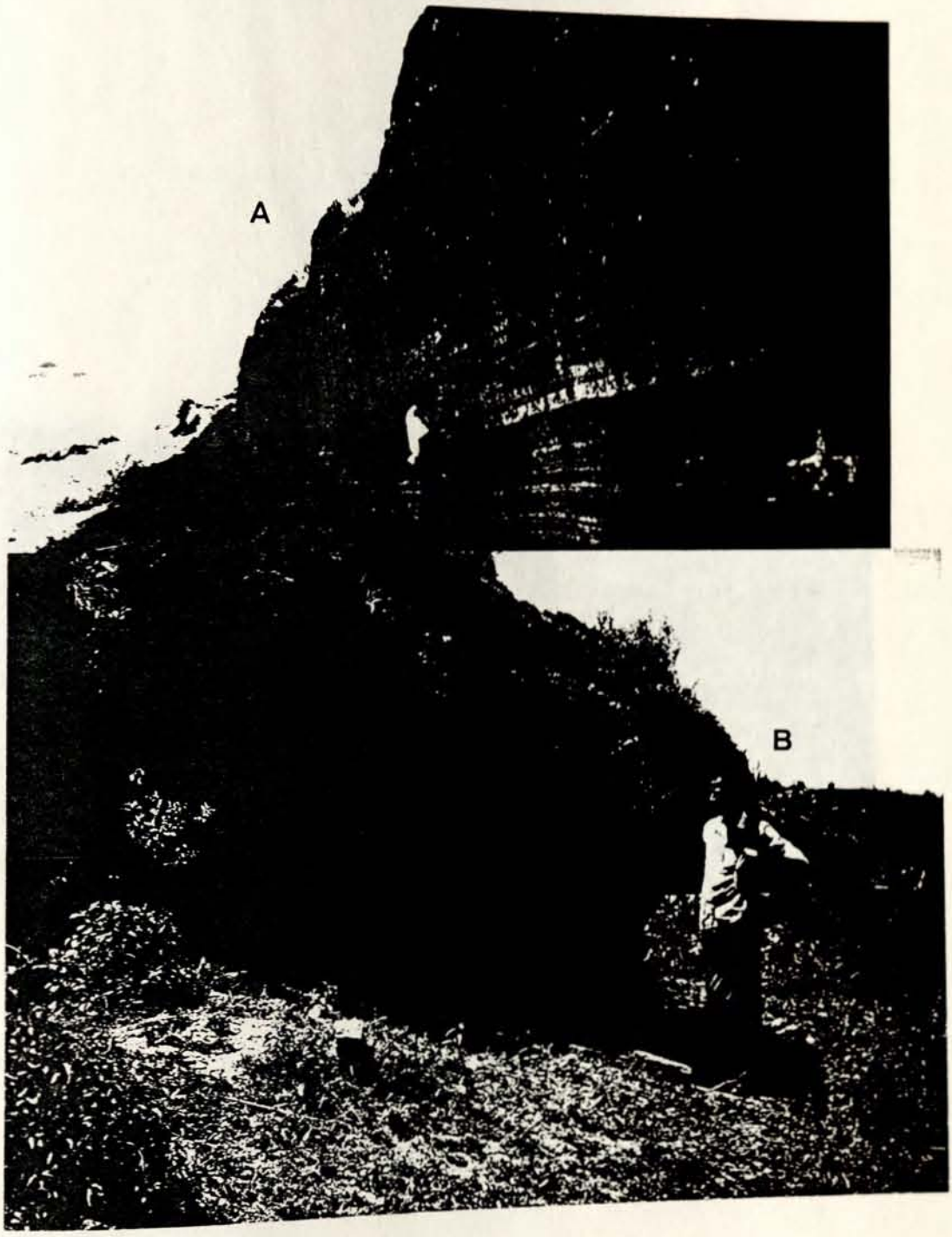

Plate 7

Young cinder cone cut by a fault (Bogra). In the background: intracalderic cones and the southern rim of the caldera.

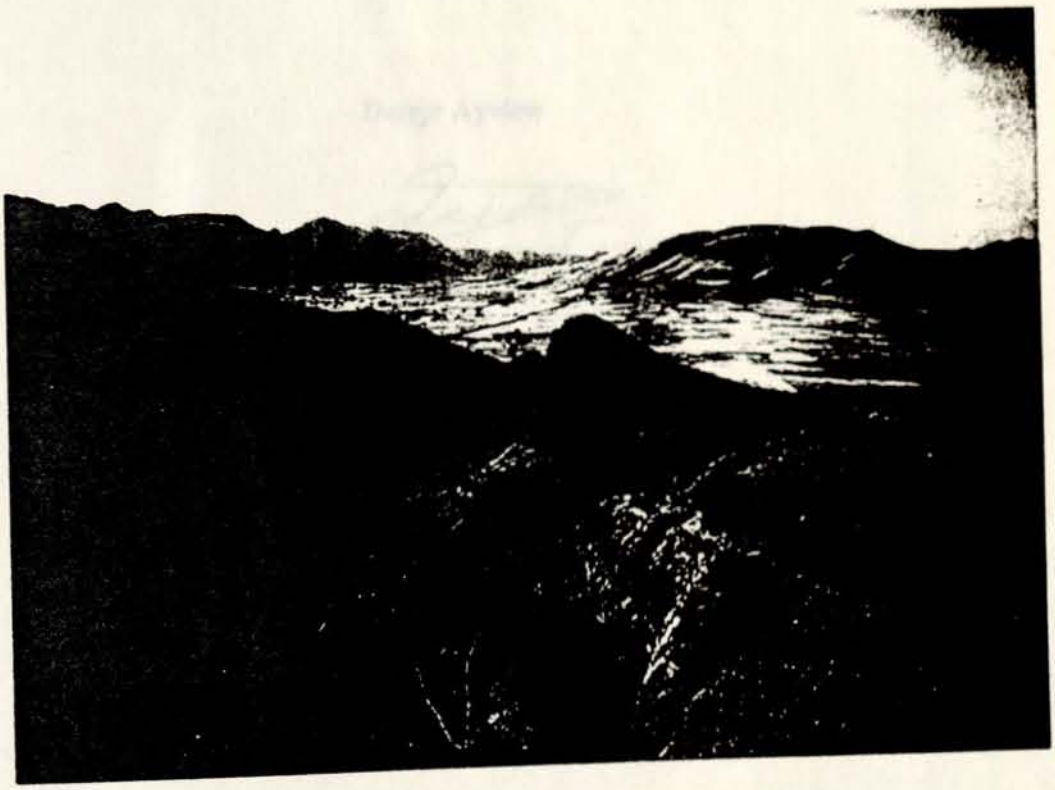

DECLARATION

I, the undersigned, declare that this thesis is my work and that all sources of material used for the thesis have been duly acknowledged.

Dereje Ayalew

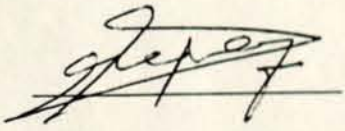

Addis Ababa, January 1994